Modeling and Control of Hydraulic Linear and Free-Piston Engines

by

Kevin Michael Zaseck

A dissertation submitted in partial fulfillment
of the requirements for the degree of
Doctor of Philosophy
(Mechanical Engineering)
in The University of Michigan
2013

Doctoral Committee:

      Professor Dionissios N. Assanis, Stony Brook University, Co-Chair
      Professor Zoran S. Filipi, Clemson University, Co-Chair
      Professor Ilya Vladimir Kolmanovsky, Co-Chair
      Aristotelis Babajimopoulos, Volvo
      Professor Andre Boehman
      Matthew J. Brusstar, US Environmental Protection Agency
      Professor Jing Sun
      Associate Professor Angela Violi

To my family

ACKNOWLEDGEMENTS

I would like to thank my advisors and committee co-chairs, without whom this dissertation would not be possible: Professor Zoran Filipi, Professor Dennis Assanis, and Professor Ilya Kolmanovsky. Professor Filipi invited me to the W.E. Lay Automotive Lab and provided me the opportunity to work on compelling research with some of the most intelligent and friendly people I have ever known. His technical guidance and direction were instrumental to the completion of this work. Professor Assanis was the patriarch of the Autolab. His barbeques kept moral high and he made sure everyone was taken care of. Professor Kolmanovksy was a tremendous source of inspiration and guidance. He helped me find direction, graduate, and even find a job. His weekly advice kept my research on track and gave me a myriad of ideas to explore. I am extremely grateful to have worked with Professor Kolmanovksy, and look forward to doing so in the future.

Two additional committee members were crucial to my progress. I was fortunate to work with Matthew Brusstar at the EPA. Matt was a fantastic mentor who always found time to help me out. Aristotelis Babajimopoulos was enormous help in the modeling effort. I would also like to recognize and express my sincere appreciation to my other committee members, Professor Angela Violi, Professor Andre Boehman, and Professor Jing Sun, for stepping in with short notice.

I am appreciative to the EPA for funding my research. The staff of the National Vehicle and Fuel Emissions Laboratory was extremely valuable for their advice, support, and expertise. I would specifically like to acknowledge David Haugen and

TABLE OF CONTENTS

LIST OF FIGURES

Figure

LIST OF ABBREVIATIONS

BDC bottom dead center

BMEP brake mean effective pressure

BSFC brake specific fuel consumption

CAD crank angle degrees

CFD computation fluid dynamics

CIDI compression-ignition direct-injection

EGR exhaust gas recirculation

EPA Environmental Protection Agency

ES extremum seeking

FMEP friction mean effective pressure

FPE free-piston engine

GM General Motors

HCCI homogeneous charge compression ignition

HEV hybrid electric vehicle

HHV hydraulic hybrid vehicle

HP high pressure

HLE hydraulic linear engine

ICE internal combustion engine

IMEP indicated mean effective pressure

LA linear alternator

LP low pressure

MEP mean effective pressure

NVFEL National Vehicle and Fuel Emissions Laboratory

NVH noise, vibration, and harshness

OPOC opposed-piston opposed-cylinder

PEFD persistently exciting finite difference

PFM position feedback modulation

PID proportional-integral-derivative

P/M pump / motor

PNGV Partnership for a New Generation of Vehicles

PPM pulse-pause modulation

PV pressure volume

PX power extraction

RPM revolutions per minute

SI spark-ignition

SOI start of injection

SIGMA Société Industrielle Générale de Mécanique Appliquée

SPSA simultaneous perturbation stochastic approximation

TDC top dead center

ABSTRACT

Modeling and Control of Hydraulic Linear and Free-Piston Engines

by

Kevin Michael Zaseck

Co-Chairs: Ilya Kolmanovsky, Zoran Filipi, and Dennis Assanis

The United States Environmental Protection Agency has developed a free-piston engine (FPE) and a Hydraulic Linear Engine (HLE) for application as hydraulic power plants in a hydraulic hybrid vehicle. Both engines extract power from the oscillatory motion of the pistons using a linear hydraulic pump. The HLE uses a single crank as a safety and timing mechanism. However, the FPE does not possess a crank and therefore has a variable compression ratio and lower friction than a conventional internal combustion engine (ICE). This dissertation's objective is to compare HLE and FPE performance trends though modeling while developing control tools necessary to enable reliable operation.

A physics-based engine model is necessary to evaluate performance trends and assist with controls development. We combine dynamics, thermodynamics, and hydraulics modules to predict the instantaneous behavior of each engine. Phenomenological friction models capture the major differences in engine performance. Preliminary results show that asymmetrical piston behavior causes discrepancies in HLE efficiency from cylinder-to-cylinder (C-2-C). Variations in C-2-C HLE performance necessitate a cylinder balancing control structure.

An adaptive control scheme estimates and adjusts for HLE cylinder performance discrepancies. By leveraging an energy balance and an estimate of rotational kinetic energy sampled at the turnaround points, we construct a discrete control-oriented model to capture HLE behavior. State feedback control ensures the HLE tracks a set point and a recursive least squares algorithm estimates periodic differences in HLE response. The proposed controller successfully reduces C-2-C variations in sampled engine speed when applied to a physics-based HLE model developed as a part of this work. Additionally, the adaptive algorithm allows the HLE to operate with a different load or combustion scheme for each cylinder. An extremum seeking algorithm exploits the adaptive scheme to optimize injection timing of each cylinder individually.

Precise control of piston turnaround location is paramount to reliable FPE operation. Combining an energy balance and the Otto cycle, a discrete, control-oriented model implicitly describes FPE clearance height behavior. A linearization of the control-oriented model shows open-loop unstable operating conditions at high load. State feedback, using dynamic inversion, stabilizes the FPE system and Smith predictor compensates for a single time step delay. A Newton's method solver estimates current FPE piston position in order to facilitate the Smith predictor. The physics-based FPE model demonstrates stable operation and set point transitions using the proposed controller. However, step changes in hydraulic load disturb the piston motion beyond safe positions. In order to constrain piston motion, a reference governor manages load changes. The reference governor uses Newton's method to forecast the control-oriented FPE model forward in time. Based on the prediction and a bisection search algorithm, the reference governor chooses the maximum constant hydraulic load which satisfies all constraints for all future time steps. Additional robustness techniques adjust for uncertainty by tightening constraints using model sensitivity. When implemented on the physics-based model, the reference governor successfully enforces a position constraint of ± 0.5 mm during a load change.

Using the proposed control and modeling methods, a series of physics-based simulations explore HLE, FPE, and ICE performance under similar conditions with identical geometry. The primary difference in engine performance is friction. In the absence of a crank, the FPE exhibits the lowest frictional losses and the highest relative hydraulic conversion efficiency. The HLE outperforms the ICE with respects to friction at most operating conditions. However, inertial forces resulting from a large oscillating mass increase HLE bearing loads and friction at high engine speeds. While each engine experiences a similar magnitude of heat loss, the FPE shows only a marginal improvement in indicated efficiency at high compression ratios due heat transfer. As a result, best FPE brake specific fuel consumption at a specified power level is not necessarily at the highest compression ratio. Further, the FPE suffers from a restricted power range compared to the HLE and ICE due to engine speed limitations.

The presented research illustrates that with the appropriate control strategies, the HLE and FPE have promise as hydraulic power plants compared to a conventional engine because of reduced friction. Further hardware iterations and modeling efforts can improve HLE and FPE understanding and make the engines even more competitive.

CHAPTER I

Introduction

1.1 Motivations

The American transportation sector is highly dependent on both foreign and domestic supplies of petroleum. In 2010, the United States alone consumed 19.1 million barrels of oil a day, accounting for 37% of total worldwide energy usage. That same year, two-thirds of U.S. oil went to the transportation sector. Additionally, the Energy Information Administration projects that the transportation sector will employ oil-based fuels beyond the next two decades. To compound these issues, oil prices will likely increase in the coming years [3]. The United States government recognizes that petroleum usage is not sustainable and is working with automakers to establish practical steps and objectives targeted at producing more efficient and cost effective vehicles. Further, improved fuel economy will reduce greenhouse gas production by decreasing CO_2 emissions.

1.2 Background

A myriad of factors impact the fuel economy of automobiles. Each vehicle subsystem operates with its own efficiency and best operating conditions. How the different components interact over changing a drive cycle determines the fuel economy. For

instance, some components may operate best at low speed and other at high speed. Hybridization offers a unique pathway for fuel economy improvement in certain vehicle classes by offsetting component demand so that the subsystems can operate with mutually more efficient conditions. As an added benefit, most hybrid vehicles offer a means of recovering brake energy that would be otherwise lost during deceleration.

1.2.1 Partnership for a New Generation of Vehicles

To better understand the influence of hybridization and vehicle design on fuel economy, President Clinton launched the Partnership for a New Generation of Vehicles (PNGV) in the September of 1993. The program united the federal government and US automakers in a joint research effort centered around three primary goals:

- "Goal 1: Significantly improve competitiveness in manufacturing for future generations of vehicles.

- Goal 2: Implement commercially viable innovations from ongoing research on conventional vehicles.

- Goal 3: Develop vehicles to achieve up to three times the fuel efficiency of a comparable 1994 family sedan." [77]

As an embodiment of the aforementioned goals, the PNGV culminated in a combined effort to produce an 80 mpg passenger vehicle while maintaining the utility and cost of existing commercial automobiles. Although automakers to-date have been unable to achieve the target in their commercial product line, PNGV findings highlight the importance of hybrid power trains.

1.2.2 Hybrid Vehicles

To be classified as a hybrid vehicle, an automobile must utilize two or more different energy sources for propulsion and energy storage. Generally, hybridization re-

quires the addition of an energy storage mechanism and a supplementary, reversible drive motor that when used correctly increase overall efficiency. Hybrid technology increases vehicle efficiency through two core mechanisms: a storage device captures energy otherwise lost during braking and the multiple motors offset load to ensure they mutually run in more efficient ranges. The most common hybrid today is the hybrid electric vehicle (HEV), popularized by the Toyota Prius. In one possible HEV configuration, an electric motor-generator slows the vehicle while charging an on-board battery for brake energy recovery. Furthermore, the battery can drive a motor to compensate for the low load efficiency of a conventional gasoline engine.

1.2.3   Environmental Protection Agency

Founded in December, 1970, the United States Environmental Protection Agency (EPA) creates and enforces regulations intended to preserve environmental and public health, including but not limited to automotive emissions and fuel economy. Scientific research is one of many tools at the EPA's disposal. The EPA primarily conducts research at the National Vehicle and Fuel Emissions Laboratory (NVFEL) in Ann Arbor, Michigan. The NVFEL investigates technologies to help achieve and inform future regulations while also promoting industry advancement.

1.2.4   Hydraulic Hybrid

Having a vested interest in technology development for clean vehicles, the EPA was a major participant in the PNGV. Through the NVFEL, the EPA contributed innovative advancements in hydraulic hybrid technology. One major outcome of the PNGV was the EPAs development of an 80 mpg prototype hydraulic hybrid approximately the size of a Ford Taurus, shown in Figure 1.1.

A hydraulic hybrid vehicle (HHV) stores energy via the compression of gas in a hydraulic accumulator. The resulting high power density storage is capable of captur-

Figure 1.1: Prototype series hydraulic hybrid vehicle developed by the EPA.

ing approximately 70% brake energy as opposed to around 30% brake energy recovery attainable by batteries in an HEV. Conversely, accumulators have an inherently low energy density, translating to less energy storage capacity and packaging constraints. A fully charged battery may last for tens of miles, whereas an accumulator may deplete within one acceleration event. These traits make an HHV ideal for frequent stop and go operation, particularly when used with larger vehicles that may already employ onboard hydraulics, such as delivery trucks, garbage trucks, and busses. Consumer vehicles can also benefit from HHV technology, especially in dense stop-and-go city traffic.

The HHVs designed by the EPA operate in a series configuration, as depicted in Figure 1.2. A series hybrid uses a conventional engine to add energy to a storage mechanism while an additional drive apparatus draws energy from the storage to propel the vehicle. An HHV transmits hydraulic power to the accumulator with a pump/motor mechanism [35] coupled either rigidly or through a transmission to a conventional engine. This process pressurizes nitrogen gas separated from the oil by a flexible bladder. As a consequence of the series configuration, the engine is effectively decoupled from road and only experiences hydraulic accumulator and pump/motor loads. For launching or locomotion, another pump-motor located on the drive axle

4

draws high pressure fluid from the accumulator and effectively adds energy from storage to the rear wheels to move the vehicle. In addition to increased efficiency, the projected costs of upgrading to HHV are relatively small [4].
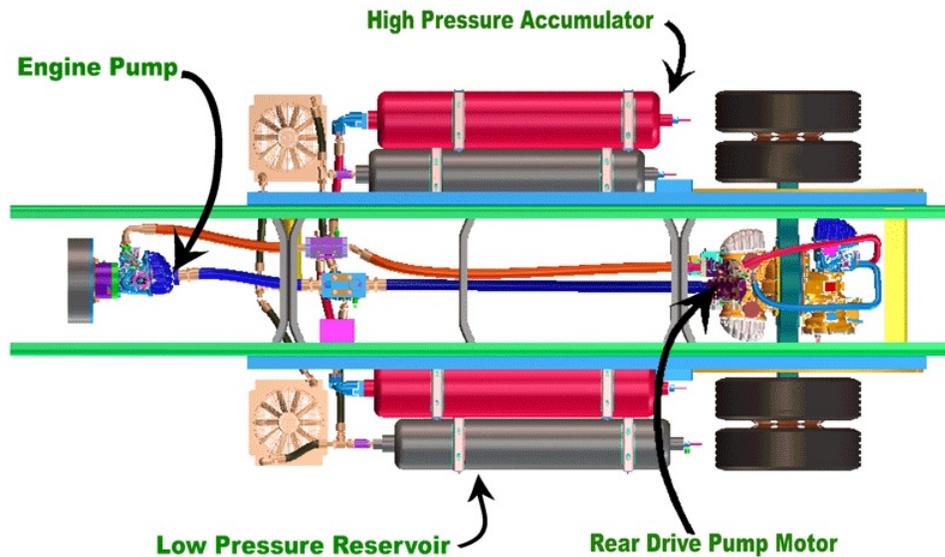
Figure 1.2: Schematic of a hydraulic hybrid urban delivery vehicle developed by the EPA.

As an extension of their HHV research, the EPA is investigating new hydraulic power plants based on free-piston engine (FPE) concepts.

1.3   Free-Piston Engine

A number of institutions are currently investigating the free-piston engine for its potentially low cost and highly efficient power delivery. In a conventional engine, the crank is a large source of friction. Cranks posses a many moving parts that require bearings a lubrication. Generally, as the number of moving parts rise, friction worsens. Crank dynamics also apply appreciable side-loads on the piston that further increase friction. An FPE eliminates the crank entirely and instead transmits work utilizing the translational piston motion.

Without a crank to constrain FPE piston motion, geometric compression ratio and

displacement can change from stroke-to-stroke and may be optimized for a wide variety of fuel types and combustion strategies. Additionally, an FPE has fewer moving parts than a conventional engine, theoretically reducing overall friction, complexity, and production scale costs. The absence of slider-crank dynamics also decreases normal forces contributing to friction, alleviates wear, and permits the use of low-friction piston rings [12, 68].

When continuous operation is achieved, FPE piston behavior resembles a mass oscillating between two air springs [68]. As illustrated in Figure 1.3, the piston assembly travels with near constant velocity between each turnaround point; high accelerations ensure the piston spends little time in close proximity to the cylinder head. In contrast, the crank dynamics in a conventional engine impose an asymmetric, 'egg-shaped' relationship between piston velocity and position. Note that in Figure 1.3, comparatively higher speeds at top dead center (TDC) and lower speeds at bottom dead center (BDC) signify that the cylinder operates for a shorter duration at low volume and a longer duration at high volume.

Free-piston engines exist in three common configurations: single-piston, dual-piston, and opposed-piston. A single-piston FPE, popular in design for its simplicity, contains a solitary combustion cylinder [2, 53, 111, 118]. Shown in Figure 1.4, a single-piston arrangement is dynamically unbalanced and requires either an air bounce chamber for rebounding or an additional work element to compress the charge. By utilizing a bounce chamber, a single-piston FPE can oscillate continuously. Alternatively, some single-piston FPEs allow the piston to rest after each stroke and, following a short pause, use an external load to initiate piston motion for the subsequent stroke [2]. Single-piston FPEs predominately use stationary gas exchange ports for two-stroke operation, although the Nanjing University of Science and Technology introduced a single-piston FPE with fully-flexible valve timing and a mechanical rebound spring to enable four-stroke operation [111]. The most cited single-piston FPE
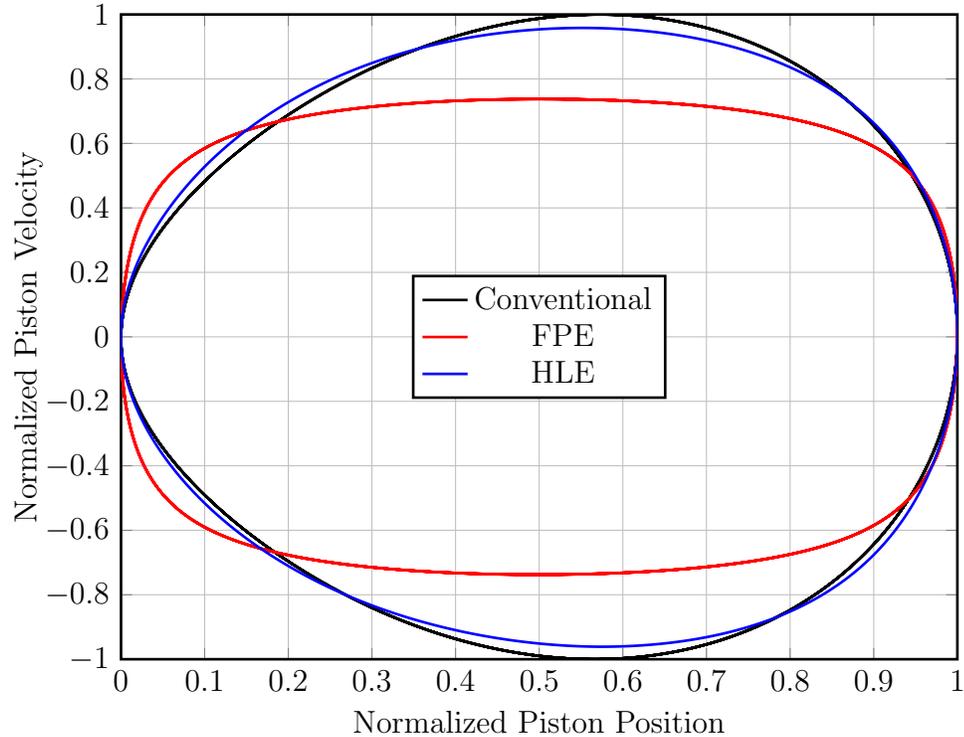
Figure 1.3: Phase diagram showing piston velocity as a function of position. The piston position is normalized by stroke length such that zero corresponds to BDC and one corresponds to TDC. Velocity is normalized using the maximum velocity of the conventional engine, where a positive value signifies the piston is traveling toward TDC.

is the diesel Chiron engine developed by Dutch company Innas BV as an alternative to conventional hydraulic power plants [2].

Figure 1.4: Illustration of a single-piston, hydraulic FPE.

As depicted in Figure 1.5, a dual-piston FPE consists of two combustion chambers and two pistons rigidly coupled back-to-back. A number of institutions use the dual-piston configuration because combustion and expansion in one chamber compresses the other chamber's charge, facilitating continuous oscillation [12, 96, 102]. Like the single-piston design, most dual-piston configurations are dynamically unbalanced a

7

operate with a two-stroke cycle using static intake and exhaust ports. The EPA combined three dual-piston assemblies with fully-flexible electro-hydraulic gas exchange valves to construct a dynamically balanced, four-stroke FPE [12, 32, 33].
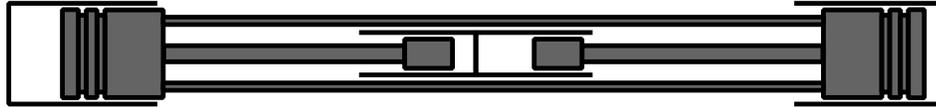
Figure 1.5: Illustration of a dual-piston, hydraulic FPE.

Figure 1.6 demonstrates a third approach: the opposed-piston FPE. With an opposed-piston architecture, two pistons share the same combustion chamber. Both pistons race toward each other to compress a charge, then travel apart during expansion. This symmetric motion dynamically balances the assembly. Opposed-piston designs often boast higher power density but are difficult to synchronize without additional components or control. Hibi and Ito of Toyohashi University have presented an opposed-piston, two-stroke design, hydraulic FPE capable of 31% hydraulic conversion efficiency [43].
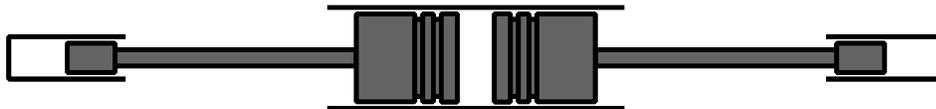
Figure 1.6: Illustration of an opposed-piston, hydraulic FPE

In conventional automotive applications, the engine transmits power through a rotating crank shaft to the wheels or load. Alternatively, an FPE extracts energy directly from the linear motion of the pistons via one of two mechanisms: electric or hydraulic power take-off. For electrical power generation an FPE requires a linear alternator (LA). A permanent magnet fixed to the oscillating piston travels through and induces current in copper wire coiled around the magnet's path. Sandia National Laboratories is developing an electric FPE and have reported thermal efficiencies as high as 56% when evaluating the concept with a rapid compression and expansion machine [102]. Alternatively, Xu and Chang have developed a four-stroke concept

with 32% electrical generation efficiency [111].

A hydraulic FPE uses the linear piston motion as a reciprocating pump [43, 90, 96]. Hydraulic energy from the FPE is available to actuate a hydraulic motor or for storage in a high-pressure hydraulic accumulator. Netherlands based company Innas BV has created a single-cylinder, two-stroke, hydraulic FPE capable of indicated efficiencies up to 50% [90].

1.3.1 EPA Free-Piston Engine Design

As part of a hydraulic hybrid development program, the EPA designed and produced two prototype hydraulic FPEs [12, 32, 33]. A smaller, two-stroke configuration was constructed as a first step and proof of concept for a larger, six-cylinder design capable of four-stroke operation.

1.3.1.1 Two-Cylinder, Two-Stroke FPE

As shown in Figure 1.7, the two-cylinder arrangement contains a dual-piston assembly coupled to counterbalance rods through a rack and pinion mechanism. The counterbalance devices oscillate 180 degrees out of phase with the main piston assembly to reduce engine vibration. Fixed geometry intake and exhaust ports scavenge air during gas exchange. The EPA designed the engine for compression ratios of up to 30:1. Fuel volume control maintains a constant engine speed while actively managed check valves adjust load and power to a nominal value. Low pressure check valve can open for a portion of the power stroke to decrease load and power, and consequently fuel. Experimentally, the two-stroke configuration reached a hydraulic output of 18kW per liter of displacement [12].
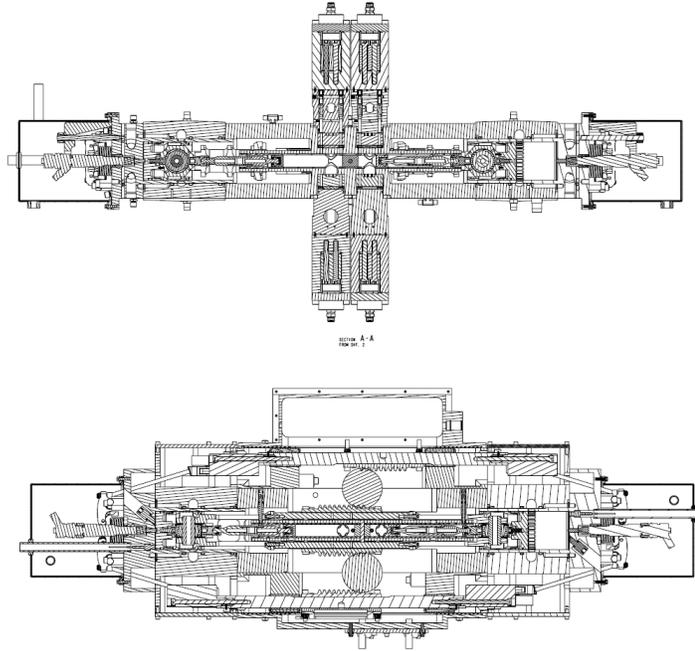
Figure 1.7: Prototype two-cylinder FPE developed by the EPA.

1.3.1.2 Six-Cylinder, Four-Stroke Design

The larger EPA FPE concept, shown in Figure 1.8, consists of three dual-piston assemblies rigidly coupled by a rack and pinion mechanism. Essentially, the additional piston assemblies replace the counterbalance devices used on the two-stroke engine in Figure 1.7. The six-cylinder geometry and fully flexible, electro-hydraulic valve train enable a four-stroke cycle. Because both the outer assemblies move together 180 degrees out of phase with the main assembly, there are 4 distinct combustion events. To accomplish balanced operation, cylinders 3_a and 3_b compress and ignite simultaneously and are considered a single cylinder, i.e. cylinder 3. Ideally, the combined displacement of cylinders 3_a and 3_b is equivalent to the displacement of one of the center cylinders (1 or 2). As a result, cylinders 3_a and 3_b have a smaller diameter than cylinders 1 and 2. Likewise, cylinders 4_a and 4_b are considered a single cylinder and also possess the smaller diameter.

The center piston assembly acts as reciprocating pump for hydraulic power take-

10
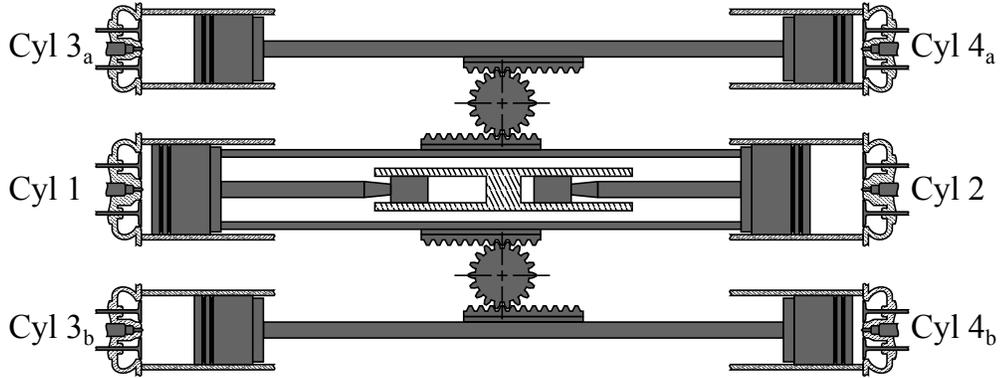
Figure 1.8: Prototype six-cylinder FPE developed by the EPA.

off. As highlighted in Figure 1.9, the engine draws hydraulic fluid from a low pressure (LP) reservoir or pumps hydraulic fluid into a high pressure (HP) accumulator that stores energy in the form of compressed nitrogen gas, while check valves passively control flow. With passive check valves and constant HP accumulator pressure, the amount of hydraulic work produced from a nominal stroke length is fixed. Consequently, the power range of an FPE is limited because the operating frequency is fairly constant [1, 68]. In order to adjust power output, the EPA designed the FPE with a circuit to bypass the LP check valves. During a specified fraction of each stroke, the bypass valves open to allow hydraulic fluid a path to low pressure and to prevent pumping to high pressure. While represented as a distinct path in Figure 1.9, a set of actuating rods physically force open the check valves to accomplish a bypass. The current design requires the bypass valves to open at the beginning of the stroke, before the hydraulic chamber is pressurized.

The intake and exhaust valves are a hydraulically-actuated, variable valve timing system. The fully-flexible valve train allows for further customization and optimization of in-cylinder conditions, but creates a large hydraulic accessory load compared to conventional valve actuation. The FPE operates with compression-ignition direct-injection (CIDI) diesel combustion using a vertically-oriented, hydraulically intensified, HEUI-type injector. A magnetostrictive absolute position sensor monitors the
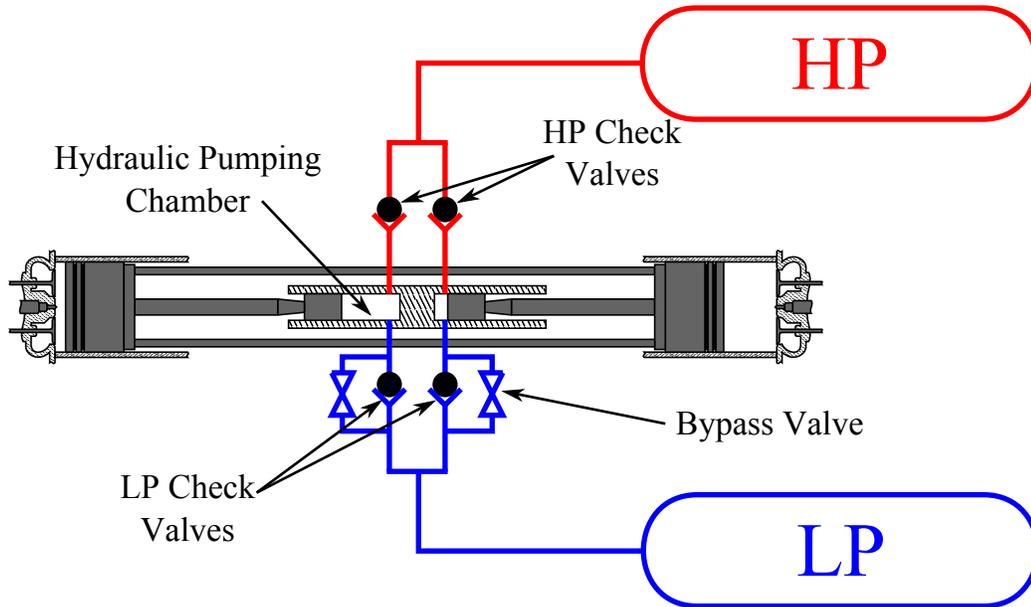
Figure 1.9: Schematic of hydraulic circuit in the EPA FPE.

linear piston location with 0.06 mm resolution and a hydraulic motoring circuit performs start-up.

Without any optimization, the six-cylinder FPE achieves between 30% and 40% hydraulic conversion efficiency, consistent with the conventional alternative, an optimized diesel engine utilizing a high-efficiency rotational pump [12]. Additionally, the prototype was able to reach full operating speed within one stroke, potentially reducing startup transients and making the engine ideal for on / off operation.

1.3.2   FPE History

Internationally and for over a century, numerous institutions have been investigating the free-piston engine for its potentially low cost and highly efficient power delivery. In fact, linear engine concepts are intertwined in external combustion designs of 18th century steam engines and 19th century Sterling engines [98, 99].

As early as 1912, the German company Junkers began exploring the internal combustion free-piston engine for application as an air compressor [5]. However, Argentinean inventor Raúl Pateras Pescara filed for the patent of an SI free-piston

air compressor in 1925, as what would become the first documented free-piston engine. A CI free-piston air compressor soon followed in 1928 [79]. Junkers introduced their FPE compressor in the 1930's which employed a rack and pinion mechanism for timing control [5]. Both the Pescara and Junkers engines utilized an opposed-piston design. Notably, a number of German submarines used the Junkers engine as an air compressor for torpedo launchers during WWII [5].

Free-piston engine research gained momentum in the 1930's in an attempt to create a gas generator for turbine power. Pescara developed and patented the concept, later selling the rights to Swiss company Société d'Etudes et de Participations. French affiliates Société d'Etudes Méchaniques et Energétiques and Société Industrielle Générale de Mécanique Appliquée (SIGMA) then manufactured and cultivated the concept. In this application, the FPE acts as a multi-stage compressor, finally delivering its exhaust gasses under pressure to an expansion turbine that extracts shaft work. Overall, the device was less expensive to manufacture and provided higher thermal efficiencies than axial turbine combuster alternatives as a consequence of more constant volume combustion. Further, the two-stroke scavenging process diluted exhaust gases and lowered turbine intake temperatures permitting the use of lower cost turbine materials [5].

After the limited success of SIGMA's GS-34 type free-piston gas-turbine, General Motors (GM) collaborated with SIGMA in the 1950's to assess the FPE-gasifier design. Out of the partnership, GM developed the GM-14 gasifier. Further, GMs FPE gas-turbine research in the 1950's resulted in the GM XP-500, a GM concept car powered by the Hyprex 250 hp free-piston gasifier-turbine engine [5, 100]. Ford also explored FPE gas-turbine power: in the 1950's Ford developed the 'Typhoon' tractor powered by an FPE gas-turbine.

While a handful of other companies investigated the FPE-gasifier combo in the 1950's, the concept was fundamentally flawed. Turbines best operate with a continu-

ous input flow of hot gases, but performance suffered when supplied by the positive-displacement, pulsating flow from an FPE [5, 68]. As competing technologies evolved in the early 1960's, interest in the FPE as a gasifier dwindled. However, the FPE resurfaced as an air compressor in the 1970's, developed by Braun of Tectonics Research Inc. The engine was a two-stroke, spark-ignition (SI) with counterweights for balancing. Braun reported 15000 hours of successful operation [11].

1.3.3 Recent FPE Research By Institution

With the exception of a handful of free-piston air compressors, large-scale FPE development nearly disappeared until the 1980s. Renewed interest in hybrid propulsion and the advent of enabling technology incentivized the exploration of free-piston linear electric generator and hydraulic FPE concepts. Prior to the 1980s, active high-speed control and accurate FPE measurements had been impossible. However, modern advancements in computational technology have enabled automatic, feedback control of free-piston engines. As a result, both experimental and simulation-based FPE research is growing in popularity. Here we present a comprehensive literature review of contemporary free-piston engine research organized alphabetically by institution.

1.3.3.1 Beijing Institute of Technology

Zhao et al. introduce a single-cylinder, two-stroke, hydraulic FPE with diesel combustion [118]. The researchers describe a model to capture engine behavior built on basic first law principle. Although the authors do not comment on mass transfer, it appears to be included in the resulting plots. The model employs a Wiebe function to capture combustion and uses hydraulic flow expressions similar to the material in Chapter II. For speed and power control, the authors apply the pulse pause modulation technique proposed by engineers at Innas BV [2]. With calibration-based fueling, the FPE has a maximum operating frequency of 30 Hz. Yuan et al. [112] present

the same process and results as Zhao et al. [118], but also introduce accumulator dynamics. The researchers also talk more in-depth regarding pulse-pause modulation and the necessity for fast sensor response.

In 2011, Hu et al. [49] expand the previous FPE model developed by Zhao et al. [118] and Yuan et al. [112] to include mass exchange and heat transfer using common correlations. The researchers also consider hydraulic valve dynamics. After introducing a physical prototype, the authors compare experimental results with the model behavior. By and large both have satisfactory agreement. However, Hu et al. seem to claim that oscillations in hydraulic pressure in the pumping chamber are the result of valve dynamics [49]. More likely, the pressure oscillations are the result of a standing wave in the hydraulic fluid resulting from the water hammer effect [106]. Hu et al. also suggests that it is necessary to manage valve lag to reduce the impacts of valve dynamics on chamber pressure. Similar to the experimental work of Hibi and Hu [42], the model predicts hydraulic rebounding that must be managed. To achieve an Atkinson cycle [41], the researchers suggest exploiting variable FPE stroke length to achieve a longer expansion stroke than compression stroke whenever possible.

Guo et al. [39] consider the same FPE system presented by Zhao et al. [118] but focus on experimental contributions. In agreement with Mikalsen and Roskilly [70], the majority of FPE fuel burns during the pre-mixed combustion phase resulting in a high rate of heat release and pressure gradients approximately two fold higher than a conventional engine. More accurately, the researchers estimate a 1.14 ms combustion duration. Heat transfer losses are low due to rapid expansion away from TDC. Ultimately, Guo et al. report roughly 37% efficiency. The primary losses are associated with combustion and lag in hydraulic suction valves.

A 2011 study by Guo et al. investigates a control strategy for the previously proposed FPE. Rather than adjusting speed and power with the common pulse-pause modulation method created by Innas BV [2], the researchers introduce piston position

feedback modulation control. Piston position feedback modulation is essentially a more intelligent pulse-pause modulation strategy that takes into account the dynamics of certain valves relative to the piston position. Because valve flow is critical, hydraulic leakage must be accounted for. Additionally, if the frequency control valve pulse width command is too long, the piston will continue to bounce and oscillations will become unstable [37]. In a supplementary publication, Guo et al. expand the FPE control strategy with a feedback proportional-integral-derivative (PID) structure as a mechanism to reduce variation in BDC position. Using a measurement of BDC deviation from a nominal set point, the controller adjusts injection timing to minimize error [38]. Typically injection timing acts as either an optimization or emissions actuator: it may therefore be unwise to modify injection timing as a method of piston position control. Hu et al. expands the piston position feedback modulation analysis by comparing its performance directly to pulse-pause modulation. The researchers claim position feedback modulation is superior in that it is immune to cyclic variations in BDC position [48].

Zhao et al. [117] present more experimental FPE results in a 2012 investigation, reporting an increase in indicated efficiency to 41%. Top dead center position is controlled by hydraulics, bottom dead center position is controlled by fuel mass. The authors are not clear on control, but the engine includes misfire detection based on a prediction of piston speed. Consistent with their previous work [39], the researchers again observe a predominately premixed phase burn, in this instance witnessing 130 bar peak pressure. Zhao et al. conjecture that piston velocities around TDC produce better mixing, resulting in a more premixed burn. As an additional study, Zhao et al. [116] address concerns regarding the impacts of cyclic variations on FPE stability. The authors introduce cycle-to-cycle variations and note that BDC position is the function of an energy balance across the expansion stroke. Ultimately, the researchers considered BDC and TDC control stable, although the positions did

fluctuate approximately 3% and 1.4%, respectively.

In an alternative approach, Tian et al. investigate the dynamics and control of a single cylinder, two-stroke, spark-ignition FPE with a linear alternator for electrical energy generation and a mechanical spring for rebounding [94, 95]. The researchers use the basic principles presented by Tikannen et al. [97] to achieve step change load following. However, the engine only maintains stability for roughly three sequential cycles. The authors also present a simplified model-based study assuming ideal gas behavior and isentropic compression. By linearizing the system, Tian et al. present an explicit relation to predict FPE frequency. In contradiction with other studies [7, 67, 98], the researchers note an increase in frequency as piston mass grow because they do not actively control piston position: the frequency increases because the amplitude of oscillations decrease as mass increases.

1.3.3.2   Chalmers

Researchers at the Chalmers University of Technology in Sweden have been investigating a two-stroke, dual-piston FPE with a linear alternator for application in HEV. Chalmers considers both diesel and HCCI-like combustion in a series of primarily model-based studies, using both computation fluid dynamics (CFD) and dynamics simulations.

Fredriksson and Denbratt use BOOST and SENKIN to investigate engine performance for multiple fuels. The authors create a dynamic model of the FPE to predict piston motion and frequency. Commercial software BOOST simulates gas exchange by solving gas dynamics equations and SENKIN captures detailed chemical kinetics for roughly 60-100 species depending on the fuel. As cetane number decreases, the authors show that the FPE requires higher compression ratios to achieve that appropriate ignition timing. Generally, increasing compression ratio produces higher engine speed, power, and efficiency. However, high heat loss also increases with compres-

sion ratio, reducing potential benefits. Despite fast combustion, the paper reported relatively low temperatures due to a brief duration at TDC and rapid expansion of combustion gasses. Low temperatures suggest low NOx and potentially high hydrocarbon and carbon monoxide levels, although the simulations ran at low load, dilute, HCCI-like combustion conditions [22].

Further studies at Chalmers utilized KIVA-3V CFD code in tandem with piston motion control modeled in MATLAB / Simulink. The researchers first integrate a diesel surrogate model to capture HCCI-type combustion conditions [9]. Additionally, Chalmers personnel leverage the KIVA model to investigate injection timing by incorporating autoignition integrals and Wiebe burn rate functions [21]. The authors find that during startup-like conditions, bad mixing of cool intake air and hot combustion products during scavenging results in late and incomplete combustion. In order to achieve sufficient combustion, the authors propose retarding injection timing and suggest that real FPE hardware may share similar issues [21].

1.3.3.3 Ford

Ford has developed the unique opposed-piston opposed-cylinder (OPOC) free-piston engine for hydraulic power generation [15, 45, 46]. The OPOC combines dual-piston and opposed-piston designs to create a naturally balanced engine with supposedly improved scavenging characteristics. The OPOC configuration contains two opposed-piston combustion chambers. Both combustion chambers interact via two sets of rigidly coupled dual-piston assemblies: an inner dual-piston assembly with outward facing pistons and an outer piston assembly with inward facing pistons. The engine does not possess a cylinder head in that each opposed-piston chamber consists of one outer-piston and one inner piston. As combustion occurs in one chamber and the pistons are forced apart, the pistons are thrust together in the other chamber. The dual-piston assemblies are also rigidly joined to hydraulic pumping mechanism.

Some hydraulic chambers function as a power extraction mechanism while others utilize a Lee valve to control and maintain piston synchronization [66]. Although no significant results have been published and the concept has been abandoned by Ford, the OPOC continues to endure. Ford has donated the prototype OCOP engine to University of Minnesota as a partner for academic research [63, 64, 65, 66]. Additionally, Michigan-based company EcoMotors International has reworked the original OPOC design as a single crank, 2-stroke device [44]. The crank constrained OPOC is currently seeking major investors.

1.3.3.4 French Institute of Petroleum (IFP)

Researchers at the French Institute of Petroleum investigated the optimization of a two-stroke, uniflow scavenging, FPE-linear alternator for series hybrid vehicles. The engine is a dual-piston design. Kleemann et al. prescribe a piston motion profile generated using 0D and 1D models, and supply the path to a 3D CFD simulation. Using the CFD, the authors determine optimal intake port, exhaust port, and injection characteristics. The researchers project high indicated efficiencies, over 50%, along with low soot and NOx emissions if including EGR and HCCI at higher compression ratios. The authors also report that scavenging efficiency is relatively constant regardless of port shape. An investigation into the effects of injection timing and spray cone for HCCI-type conditions found that later injection causes higher peak pressure and better efficiency [59].

1.3.3.5 Innas BV

Arguably the most recognized FPE, the Chiron shown in Figure 1.10 is a single-cylinder, two-stroke, hydraulic engine. Innas BV developed and is marketing the FPE as a highly efficient hydraulic power plant for forklifts and other construction equipment. Several publications describe the engine [2, 90]. After preliminary designs were

validated, Innas BV shifted focus to studying and optimizing the combustion system [90]. By design, the Chiron FPE requires stored energy to actuate the compression stroke. A dedicated, one liter, bladder-type hydraulic accumulator stores compression energy throughout each power stroke to launch the subsequent compression event. A series of fast-acting hydraulic valves control timing and fluid flow. Depending on power demand, the piston can rest between strokes in a method dubbed by Innas researchers as pulse-pause modulation [2].
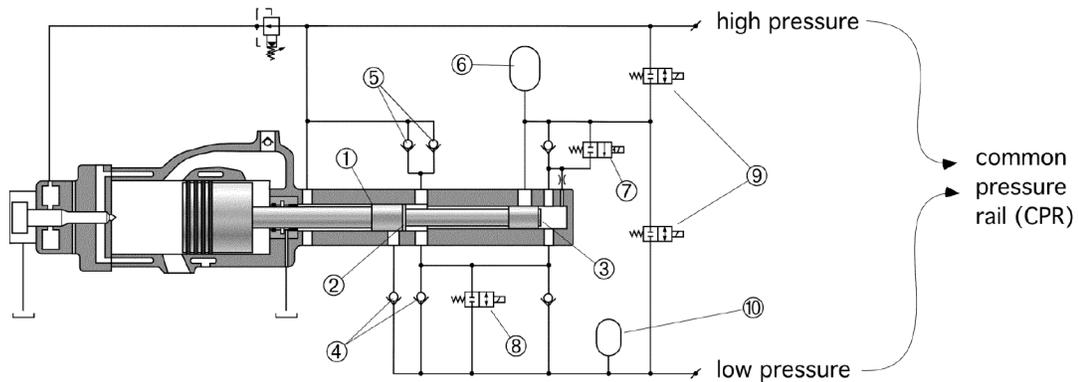
Figure 1.10: Diagram of Chrion FPE from [2]

As noted by Achten, the FPE behaves similar to a gas spring [1]. The experimental engine reportedly achieves up to 50% indicated efficiency [90]. Somhorst and Achten also note high heat release rates consistent with a pressure rise rate 2 to 5 fold faster than a conventional engine, and combustion durations as brief as 1 millisecond.

1.3.3.6 University of Minnessota

The University of Minnesota is responsible for two distinct avenues of FPE research. Doctor Hans Aichlmayr performed the initial FPE research at the University of Minnesota regarding micro-scale, HCCI combustion in a miniature FPE air compressor. The FPE considered is a single-cylinder, two-stroke design utilizing an air bounce chamber for rebounding. Simplified chemical kinetics and an FPE motion model assisted with hardware design, leading to single shot experiments. Aichlmayr

demonstrate that HCCI-type combustion is possible in spaces 3mm diameter and 0.3 mm long. At such a minute scale, blow-by became the biggest issue [5, 5].

Some years later, Professor Zongxuan Sun's Automotive Propulsion Control Laboratory at the University of Minnesota began publishing additional FPE research. The first publication proposes a dual-piston FPE operating with HCCI combustion and utilizing both a linear alternator and a linear hydraulic pump to take advantage of a battery's energy density and a hydraulic accumulator's power density. For reliable operation, the engine is dependent on a fully-flexible valve train. The authors primarily focus a model-based study of the proposed design. Fairly standard models describe engine behavior. Newton's second law force balance captures piston dynamics as a function of cylinder pressure, hydraulic pressure, friction, and electric load. An auto-ignition integral expresses ignition delay and feeds into a mean value model for HCCI combustion. The researchers approximate gas exchange as compressible flow through an orifice and use a mean value mass balance and a first law balance to track thermodynamic behavior with an ideal gas assumption. The primary findings are somewhat trivial, that FPE performance is sensitive to valve timing and fuel injection [64].

Apparently following the work published in 2010 [64], Ford donated their OPOC hydraulic FPE to Professor Sun's lab and partnered with the University of Minnesota for research. The initial OPOC publication is a model-based study of the engine. Li and Sun specify that the OPOC engine relies on a Moog servo valve to vary hydraulic chamber pressure rather than a binary on-off valve. Variable pumping pressure provides the researchers with improved control over piston motion characteristics. In one case, the authors exploit the Moog valve to delay combustion and even hold the piston near TDC to temporarily wait for the start of combustion. Li and Sun claim the waiting behavior increases efficiency by 5%. However, the FPE experiences potentially damaging pressures in the combustion chamber in excess of 200 bar if combustion oc-

curs too early at high compression ratios. A simple PID control structure maintains a desired compression ratio by managing fuel quantity [65].

University of Minnesota researchers published two FPE papers in the proceedings of the ASME 2011 Dynamic Systems and Control Conference [66, 85]. Li and Sun attempt to analyze the stability of a hydraulic FPE with HCCI combustion [66]. The authors start with the same basic model presented previously [65], but simplify assuming isentropic compression and expansion. A linearization, based on a 1st order Taylor expansion, reduces the model to six states but does not appear to contain the piston behavior. The description is somewhat unclear. Assembling the states, the solution to a series of nonlinear equations provides equilibrium. By evaluating the eigenvalues of the linear model, Li and Sun determine the system is unstable at a single operating point. The authors fail to expand their analysis to other equilibrium and do not comment on overall FPE stability. Further, the authors do not offer a physical explanation or interpretation for the apparent instability. Li and Sun conclude by validating the simplified model by showing an unstable operating condition with the physics-based model described previously by Li and Sun [65]. At the same conference, Sadighi et al. [85] of the University of Minnesota presented a second study comparing the hydraulic OPOC engine donated by Ford to a potential electric OPOC design. Using the modeling architecture described by Li et al. [65], the authors apply closed-loop, PI fuel control to achieve stable operation of both design concepts. However, the plants responds with rather large fluctuations to a step command. Evidently, it is more difficult to control engine load with a linear alternator than a hydraulic valve due to a fixed magnetic flux field. Additionally, the FPE LA magnet increases the oscillating mass of the piston assembly and produces greater overshoot during a transient. While the authors noted that the hydraulic FPE has a higher power density, they failed to comment on energy density. However, Sadighi et al. did conjecture that the LA may be more robust to disturbances or sudden changes in

operating condition because alternator load is proportional to piston speed and that it is capable of passive piston synchronization.

The most recent study by Li et al. investigates active piston motion control of the OPOC FPE [63]. The authors utilize a robust repetitive-type controller to follow a prescribed path with the piston. A Moog valve permits adjustable hydraulic chamber pressure and enables active motion control. As a preliminary measure, Li et al. apply motoring motion control to the FPE in simulation. Expanding on the modeling results, the repetitive controller demonstrates successful control of piston motion on the experimental engine with the cylinder heads removed, i.e. no gas dynamics or pressure forces. Finally, the authors reattach the cylinder head and show active piston motion control for a motoring state including compression and expansion. Although the method presented is potentially useful for startup, the researchers do not extend the results to any firing conditions. Additionally, this method relies heavily on the prescribed path, which must be feasible and similar to the actual dynamics. If the piston diverges too much, the controller performance may break down, and therefore, the prescribed path must change with load and compression ratio. For this reason, the controller proposed by Li et al. may not be robust to disturbances of combustion variation.

1.3.3.7 Nanjing University of Science and Technology

Researchers at Nanjing University of Science and Technology have developed and fabricated an interesting FPE concept similar to the engine presented by Tian et al. [94, 95], albeit two years earlier and much more effectively [86, 111]. The FPE is a single-cylinder, spark-ignition design that utilizes a linear alternator to produce electric power. A mechanical spring kickback mechanism rebounds the piston every stroke and enables four-stroke operation by assisting with the intake and exhaust strokes. During the expansion stroke, a portion of the combustion work compresses

and stores energy in the spring. In turn, the compacted spring drives the piston toward TDC to perform the exhaust stroke. Upon entering the intake stroke, the linear generator applies an additional load to compress the kickback device and achieve the desired BDC position. It is unclear how or if the spring is preloaded or at what length the spring is unloaded. The researchers have complete control over valve timing and electric generator load. By design, the intake and exhaust stroke are not as long as the compression or expansion stroke, creating a natural Atkinson cycle. Conventional engines achieve an Atkinson cycle by altering the effective compression ratio with valve timing [41], whereas an FPE can accomplish the same cycle by physically modifying the stroke length and geometric compression ratio. Preliminary tests show 32% efficiency with 2.2 kW output [111]. The researchers expect to improve these numbers as simulations have yielded 42% efficiency. Shi and Chang present much of the same information, but include a more insight into control and modeling [86]. Overall, it is a very simple and effective design, although NVH may be issues.

Huang uses the same basic principles as the single-cylinder engine described in previous Nanjing University publications, and proposes assembling two of the devices in an opposed-piston configuration. However, rather than utilizing springs to achieve four-stroke operation, the author's preliminary investigation models a two-stroke design. The simulation predicts 15 kW power output with 42.5% efficiency [50].

1.3.3.8 Newcastle University

Mikalsen and Roskilly from the Sir Joseph Swan Institute for Energy Research at Newcastle University in the United Kingdom are responsible for some of the most cited research regarding free-piston engines. They predominately use models to describe behavior of the FPE and assist with control development.

In 2007, Mikalsen and Roskilly released an excellent review of FPE history, detailing a number of different applications and FPE configurations. The authors point

out that while many institutions claim the FPE is a viable alternative to conventional engine technology, further research is necessary to highlight and confirm value in a practical application. The biggest issue is robust piston motion control. Further, they comment that the greatest developed and currently most promising concept is hydraulic FPE [68].

Mikalsen and Roskilly continue in 2008 with an investigation of the design and modeling of a two-stroke, compression ignition FPE LA. The authors construct a model very similar to the one we discuss in section II, utilizing what appears to be a Watson heat release model and a Hohenberg heat transfer correlation. A first law balance calculates mean temperature and pressure based on bulk properties and friction is constant, assuming a cycle average 120 kPa friction mean effective pressure (FMEP) [69].

The engine utilizes a bounce chamber for rebounding and the authors implement an energy-based control structure similar to [52]. Mikalsen and Roskilly perform some sweeps for a number of parameters such as stroke, bore, exhaust back pressure, stroke to bore ratio, and burn rate. The most interesting result is that lower piston mass leads to lower efficiency but higher power due to higher oscillating speeds. It turns out that lower piston velocities allow more time for scavenging, permit lower port heights, and promote more constant volume combustion. The authors note that optimal compression ratio is between 15 and 25. However, while higher expansion ratios lead to higher efficiencies, they reduce available energy in the exhaust gas and can decrease overall output power at a constant air-to-fuel ratio [69].

In a 2009 study, Mikalsen and Roskilly take modeling a step further and introduce a multidimentional CFD model [71]. The authors later leverage that model to investigate the effects of flow and combustion on efficiency of an FPE [70]. Compared to a conventional engine, the CFD model indicates lower average gas velocities near TDC, but higher average radial velocity due to squish. As a result, the FPE exhibits

lower heat transfer than convention engines with a similar injection and higher radial gas velocities which may potentially lead to decreased hydrocarbon emissions. The researchers claim that heat transfer benefits outweigh the low pressure rise issues associated with faster expansion. Additionally, the engine demonstrates a high rate of heat release but low temperatures and low NO due to rapid expansion [70].

In 2010, the lab released a number of publications regarding the control of a single piston, hydraulic FPE. The first release was a two part study first focusing on a fundamental analysis of the engine to identify key actuators, control objectives, and operating parameters [72] followed by a more in depth description of dynamics and control [73]. Mikalsen and Roskilly determine fuel is the best actuator to control TDC position of their particular FPE, while an air bounce chamber is used to control BDC position. The authors tune a PID controller to accomplish the desired performance objectives, although it fails to manage load changes effectively. Mikalsen and Roskilly do not present any fundamental analysis of stability [72, 73]. Later in 2010, the same authors improved their methods by using a prediction of TDC position for controller feedback rather than a delayed output signal [74]. The prediction is based on a calibrated linear fit of TDC position as a function of piston velocity at half the nominal stroke length. The TDC estimate improves overall performance compared to the delayed output feedback. Further, the investigation models the impact of cylinder-to-cylinder (C2C) variation by introducing a $\pm 2\%$ uniform variation in fuel mass injected from nominal. Mikalsen and Roskilly find the predictive controller less sensitive to C-2-C variations.

1.3.3.9   Norwegian University of Science and Technology

Published primarily under the author Tor Johansen, the FPE research at the Norwegian University of Science and Technology focuses on a single-cylinder, two-stroke, diesel design utilizing an air bounce chamber for rebounding. This work

utilizes the gas-turbine technology abandoned in the 1960's. Their design stacks multiple free-piston engines to deliver the exhaust gas to a power turbine. The FPE setup works with essentially three stages of compression: a turbocharger uses some of the exhaust energy to compress the intake air, the linear movement of the expansion stroke compresses the air further (from 1 to 6 bar), then compression bring the charge from approximately 6 to 45 bar. After combustion, the peak pressure is roughly 125 bar. The turbocharger then uses a portion of the exhaust energy, and finally a power turbine expands the gasses to create shaft work. The apparatus is very similar to earlier Pescara and SIGMA work [5]. Interestingly the team at the Norwegian University of Science and Technology recognize that reliable control is perhaps the most significant barrier to FPE technology [52].

In 2001, Johansen et al. present mostly preliminary work and findings pertaining to both modeling and experimental FPE hardware [51]. The authors create an FPE model to assist with control development and identify basic behavior. The model utilizes standard mass exchange and first law principles, only considering bulk properties. A control structure, derived as an energy balance, monitors the change in energy from a nominal set point. According to Johansen et al., fuel has a stronger influence on TDC position and air cushion mass has a stronger influence on BDC position. Coupling between TDC and BDC position is apparently weak. Using the energy balance, the authors construct a PI controller to adjust the air cushion mass and a PID controller to manage diesel injection, but do not comment on stability and robustness. A set of nonlinear gains expand the potential operating range. Preliminary results appear to validate controller stability and performance, although the feedback law uses a delayed output signal. In 2002, Johansen et al. show the same basic results and process but expand the timing and control to include an estimate of piston behavior based on a best-fit sinusoidal function [52]. The authors note that the air cushion does not consume a large amount of work and introduce an air cush-

ion mass estimator by assuming isentropic compression and ideal gas behavior. An additional injection timing and valve control uses the turnaround estimate to ensure a repeatable combustion process. Once again, the researchers use a cascading PI control structure, but also propose active feedback for synchronization of a multi-cylinder configuration. Similar to the air cushion estimator, an outlet temperature estimator is present and assumes ideal gas and isentropic relations to facilitate set point control. Free-piston engine load is a function of intake and exhaust pressures which are dependent on ambient conditions and output turbine load. Although experimental results support controller performance, the study is not particularly rigorous and does not comment on stability or robustness [53].

1.3.3.10 Pempek

Australian company Pempek Systems proposes constructing FPE 'power packs' by grouping several modular FPE linear generators in order to focus on scalability and compactness. A cluster of Pempek FPEs could produce anywhere from 100 kW to 650 kW for heavy duty applications. Although a limited quantity of information is available pertaining to the operating characteristics, the modules are opposed-cylinder, two-stroke engines with uniflow scavenging. A passive poppet intake valve is located in the piston crown and a fully-flexible electromechanical poppet exhaust valve is located in the cylinder head. In addition to valve locations and air path, the Pempek FPE has a few unique design elements including a scavenging compressor, permanent magnets incorporated into the piston, and ringless carbon pistons. Pempek has constructed a single prototype module as a proof of concept, including tests of linear alternator components, but the development combined 'power pack' depends on future funding and investments [16].

1.3.3.11 Sandia

Sandia National Laboratories is an advocate for free-piston engines as a power plant for series HEVs. Researchers at Sandia have published works regarding a dual-piston FPE coupled to a linear alternator. The primary goal is to achieve HCCI operation, potentially using hydrogen as a fuel. Most Sandia FPE research is simulation-based, considering both diesel and HCCI combustion strategies [29, 30, 102]. However, Sandia researchers also investigate FPE combustion using a rapid compression and expansion machine as an FPE combustion chamber surrogate [102]. Sandia cites research by Caris and Nelson as a major motivation for FPE technology. Caris and Nelson find that compression ratios above 17:1 do not yield significant efficiency benefits due to heat loss and time required to propagate the flame [14]. According to Sandia, the combination of rapid combustion and swift piston reversal enables higher compression ratios [102].

A 1998 Sandia study explores the combustion process in an FPE using a rapid compression and expansion machine to vary the final compression ratio for a variety of fuels: propane, natural gas, hydrogen, methanol, n-pentane, hexane, n-heptane, and isooctane. Van Blarigan et al. record the critical compression ratio at which autoignition occurs for each fuel. The researchers witness high pressure rise rates indicative of fast combustion and near constant volume. The Sandia scientists also note that over compression of in-cylinder gases after autoignition does not seem to affect cycle efficiency, although NOx does increase due to a temperature rise. At peak, Sandia reports thermal efficiencies as high as 56% [102]. This Sandia research emphasizes the FPE's capability to adjust for a variety of fuels by changing the compression ratio, particularly as an HCCI enabling device.

A further investigation in 1999 uses a basic mean value model to investigate FPE operating characteristics. A simplified friction model captures static and viscous friction, although the paper does not provide any details. Goldsborough and Van

Blarigan find that HCCI occurs at near constant volume in an FPE. The researchers note low NOx emissions due to ultra-lean combustion and that scavenging is critical to ensure proper cylinder conditions. Additionally, repeatable piston dynamics are essential to ensuring HCCI actually occurs and that NOx is minimized [29]. The need for consistent piston behavior stresses the importance of a reliable control scheme.

In 2003, Sandia published research regarding optimization of the scavenging process in a two-stroke, dual-piston FPE. Goldsborough and Van Blarigan develop a CFD model to examine conventional loop scavenging, hybrid-loop scavenging, and uniflow scavenging subject to FPE dynamics. The authors determine that conventional loop scavenging and hybrid-loop scavenging are not appropriate for application in an FPE. Rather, uniflow scavenging is ideal. Further, the authors asses that uniflow scavenging appears sufficient for fuel mixing with HCCI [30].

1.3.3.12 Shanghai Jia Tong University

Researchers at the Key Laboratory for Power Machinery and Engineering of Ministry of Education at Shanghai Jia Tong University published two FPE studies in 2010. Li et al. simulate a dual-piston, spark-ignition, two-stroke FPE with linear alternator in MATLAB / Simulink. The authors use basic thermodynamic laws in a single-zone model with a Wiebe heat release correlation to describe combustion and perfect scavenging. Newton's second law force balance describes FPE dynamics with a simplified friction model. The researchers do not add any novel observations, but do corroborate that reducing piston mass increases FPE frequency and power [67]. Xiao et al. consider the same FPE as Li et al., but investigate more in depth. Valuably, the researchers derive an expression to predict the natural frequency of an FPE as a function of length, pressure, and mass. Isentropic relations provide an equivalent mechanical spring stiffness while the damping coefficient is analogous to alternator load. The researchers provide interesting simplifications that are available for a quick anal-

ysis and suggest increasing the damping coefficients to prevent mechanical damage or reduce excitation. Fuel, load, and ignition timing all impact damping coefficient [109].

1.3.3.13 Taijin University

The State Key Laboratory of Engines at Taijin University is responsible for CFD research of an opposed-piston, two-stroke hydraulic FPE with HCCI combustion using dimethyl-ether as fuel. Xu et al. uses single and multi-zone Chemkin models for chemical kinetics in a CFD model to capture heat loss and fluid dynamics. The researchers find that piston dynamics dictate higher scavenging temperatures are required to achieve a desirable combustion phasing. Over-compression of the charge after ignition leads to short burn durations and increases efficiency. However, by including heat transfer, the potential advantages of over-compression decrease. Xu et al. report 51% thermal efficiency with HCCI combustion but note a decrease in peak pressures and thermal efficiency with a decrease in piston mass [110].

1.3.3.14 National Taiwan University of Science and Technology

Staff of the National Taiwan University of Science and Technology partnered with researchers from the Mechanical and Systems Research Laboratories at the Industrial Technology Research Institute in Taiwan to investigate an FPE LA using a model similar to the one we present in Chapter II. Unlike other FPE models, Chiang et al. track composition without CFD using fairly standard practices. The authors investigate HCCI in a dual-piston, two-stroke FPE. They use a Woschni model for heat transfer and a Weibe function for heat release rate. The research does not present anything particularly novel, but does support other FPE related findings. Piston behavior in the FPE exhibited high acceleration rates near dead center and the FPE performed more efficiently with HCCI-type combustion rather than spark

ignited [17].

1.3.3.15   Tampere

The staff at Tampere University of Technology is working on a dual-piston, two-stroke, compression ignition hydraulic FPE. A 2000 SAE Congress study introduces the prototype engine and presents preliminary results. The engine behaves as expected; the FPE exhibits high pressure rise rates indicating rapid heat release with roughly a 2 millisecond combustion duration. TIkkanen et al. observe noticeable cycle-to-cycle variations which they attribute to injection issues, friction changes, leakage, and an asymmetric pump design. Regardless, the FPE is able to run for a short duration without a feedback controller. Early tests show a 11.3 kW power output with approximately 20% efficiency [96].

In 2001, Larmi et al. present a model of the prototype engine calling on standard first law and mass balance principles. The authors also use a one-dimensional model constructed in GT-Power where the piston position and velocity is fixed as a function of crank angle to resemble a free-piston engine. Overall the researchers declare that the modeling results have good agreement with experimental data. However, the 0D model was open-loop unstable at conditions where the experimental data were stable [62]. Friction and other unmolded losses likely account for the difference in stability between the model and the experiment, which we will expand upon in Chapter IV.

An additional study by Tikkanen and Vilenius investigates the FPE control with the assistance of the presented model. Like Johansen [52], the authors take advantage of energy balance principles and apply a PID controller at constant load. Again like Johansen, the description is not particularly rigorous and does not include any consideration for local or global stability. The authors also do not comment whether they feedback a delayed TDC position signal or employ an estimator. With the PID feedback law, the model achieves closed-loop stability and the controller can

somewhat reject small oscillatory disturbances in load [97].

1.3.3.16 Toyohashi University

Staff at Toyohashi University in Japan proposed an opposed-piston FPE in 1984 and in the early1990s [42] constructed fundamental prototypes of different components. The engine is a two-stroke, CIDI design with hydraulic power take-off. Hibi and Hu conclude piston braking is necessary after each stroke because slight compressibility of the hydraulic fluid produces rebounding near BDC. Binary, on / off valves and mechanical springs synchronize the opposed-piston design.

Hibi and Ito return nearly a decade later with a fully constructed engine and preliminary test results [43]. For speed and power control, the researchers utilize the pulse-pause modulation method pioneered by engineers at Innas BV [2]. The report shows roughly 31% hydraulic conversion efficiency. The engine operates between 0.0124 kW and 4.88 kW of hydraulic power without any significant change in efficiency.

1.3.3.17 University of West Virginia

Free-piston engine research at the University of West Virginia focuses mainly on the modeling, development, and refinement of a two-stroke, dual-piston, spark-ignition FPE with a linear alternator for electrical power generation. Clark et al. start in 1998 with a very simple FPE Otto cycle analysis [18]. The authors record high piston velocities near TDC. Decreasing stroke length decreases compression ratio and therefore thermal efficiency, but also reduces frictional losses.

Atkinson et al. continue the FPE research in 1999 by creating a more thorough model based on a first law energy balance and a Wiebe function to describe heat release. However, the researchers still assume perfect scavenging and ignore gas dynamics associated with valve events. Interestingly, the study notes that piston mass

has an inverse relationship with engine frequency such that reducing mass can increase maximum power [7]. In 2002, Shokry et al. add a linear alternator model to the simulation and again point out that lower piston mass can lead to improved output power. The authors also emphasize that compression ratio is sensitive to injection timing and combustion duration [87].

The dissertation by Tóth-Nagy in 2004 agrees that decreasing piston mass increases operating frequency [98]. However, Tóth-Nagy also notes that increased mass and higher compression ratios can assist at stabilizing FPE operation. Because fueling and load both impact frequency as well, the author proposes using frequency as a feedback parameter [98], which may be unwise considering how many other factors play a role. In his dissertation and a helpful 2005 publication, Tóth-Nagy reviews linear engine history and evolution [98, 99].

An additional dissertation by Petreanu [80] in part investigates a four-stroke FPE for electrical power generation. Petreanu uses a model to study the feasibility of converting a pair of two-stroke FPEs to a four-stroke engine. The author proposes joining the two-stroke FPE shuttles side-by-side to drive a large permanent magnet through a linear generator coil. By introducing four cylinders, stored energy is not necessary to drive a gas exchange and compression strokes [80]. However, the design is unbalanced and could lead to excessive noise, vibration, and harshness.

1.3.3.18 University of Wisconsin-Madison

At the SAE World Congress in 1992, researchers from The University of Wisconsin - Madison presented designs for a two-stroke, opposed-piston, diesel FPE with hydraulic power extraction. Intake and exhaust ports in the cylinder walls promote uniflow scavenging. A solenoid-controlled poppet valve supplied by a hydraulic accumulator acts as a hydraulic rebounding mechanism. The authors intend for hydraulic piston synchronization to balance the engine, but note that disparities in engine fric-

tion cause asymmetric piston motion. The researchers also provide useful historical background and perspective, commenting on the strengths and drawbacks of several FPE applications [8].

1.3.3.19 Zhejiang University

In a 2011 study, Ren et al. of the State Key Lab of Fluid Power Transmission and Control at Zhejiang University approximate a single-cylinder, two-stroke, hydraulic FPE utilizing CIDI diesel combustion with a mass-spring-damper system. Free-piston engine frequency is a function of the simplified spring rate. The researchers use a method similar to pulse-pause modulation to actuate the piston. As a result, compression ratio is a function of the hydraulic working pressure [83].

Bizhong Xia of Tsinghua University has collaborated with researchers at Zhejiang University for two studies concerning a dual-piston, two-stroke, hydraulic FPE [107, 108]. In one investigation, Xia et al. examine startup by creating a mass-spring-damper system similar to previous research by Ren et al. [83]. Additional research by Xia et al. analyzes the same FPE configuration with a bipropellant fuel combination: kerosene and peroxide. The combustion process accounts for 55% of total losses, while friction and scavenging losses are roughly the same magnitude.

1.3.4 State of FPE Research

This section is a brief summary of and comments on overall FPE research to-date. Most institutions performing FPE research agree that the linear engine has a great deal of potential with respects to efficiency and flexibility, but requires additional work to overcome practical concerns.

According to most researchers, friction is an important benefit of an FPE over conventional engines. However, there are few if any published experimental or modeling results that support the low FPE friction claim. Intuition appears to be the

main motivation behind the assertion. Unless extra measures are taken, current FPE design precludes four-stroke operation. Only two four-stroke FPEs exist, and both require additional mechanisms that are potential sources of friction [12, 111].

Regarding in-cylinder processing, the consensus is that the FPE exhibits rapid combustion with durations as low as 1 ms. Yet the processes contributing to FPE combustion and heat transfer are not well understood. Some CFD studies scratch the surface, but there is a shortage of experimental data and physical observation from which to build accurate models and classify the processes. For instance, it is common for FPE researchers to point out that an FPE piston experiences high accelerations near TDC, but it is uncommon to consider the thermodynamic impacts of an altered cylinder volume compared to a conventional engine.

The largest hurdle preventing a viable FPE is piston motion control. Nearly all FPE control research uses rudimentary PID control tuned to a specific operating condition and have shown successful implementation on both physical and simulated engines. Nonetheless, few mention stability and none are able to constrain piston motion during a load change. While it is popular to consider electric FPEs in simulation, most experimental FPE hardware utilizes hydraulic loading because it possesses greater control authority.

1.4 Hydraulic Linear Engine

Although current research advocates that FPE concepts hold promise, linear engine design has yet to evolve as a practical alternative to conventional technology. The added flexibility afforded by variable stroke length has numerous advantages, but unconstrained piston motion is also the biggest hurdle preventing a viable engine. Robust piston position control is necessary to maintain consistent and efficient operation while also ensuring that damaging mechanical failures or combustion instabilities do not occur. Excess fuel added to an FPE will drive the piston assembly

36

beyond the desired turnaround location and potentially into the cylinder head. Conversely, an underestimate of fuel will reduce compression ratios and efficiency; in the worst case scenario, the engine can stall entirely. As an additional issue, the EPA's six-cylinder FPE uses a camless, electro-hydraulic valve train that is responsible for substantial parasitic losses.

To address the robustness and control concerns associated with free-piston operation, the EPA has modified their previously reported FPE prototype [34, 113]. In this report, we refer to the new design as a hydraulic linear engine (HLE). As shown in Figure 1.11, EPA engineers have removed and replaced the dual-piston assembly associated with cylinders 3_b and 4_b on the six-cylinder FPE in Figure 1.8 with a crank device mechanically balanced to existing hardware. Unlike a conventional engine, the HLE crank does not deliver power to a load. Instead, the apparatus functions as a safety mechanism to limit piston travel by exerting a force through the rack and pinion. The crank also actuates the intake and exhaust valves. Power take-off remains hydraulic and the bypass valves continue to adjust load, consistent with Figure 1.9. The HLE utilizes CIDI diesel combustion but also possesses the components necessary for port injection. The cylinder firing order is 1-2-4-3. Since the engine is intended to replace the combination of a conventional engine and hydraulic pump-motor for application in an HHV, it is helpful to consider the HLE as an internal combustion engine with an integrated pumping mechanism rather than a substitute for traditional mechanical drives.

While the crank eliminates some flexibility found in an FPE, many of the intended benefits are still present. The rack and pinion mechanism reduces piston side loads and the HLE continues to have fewer moving parts than a conventional four-cylinder engine with pump-motor. Extracting power directly at the piston also reduces crank bearing loads. Additionally, the crank enables a number of traditional engine technologies. A starter motor drives the HLE during start-up and a flywheel is present to
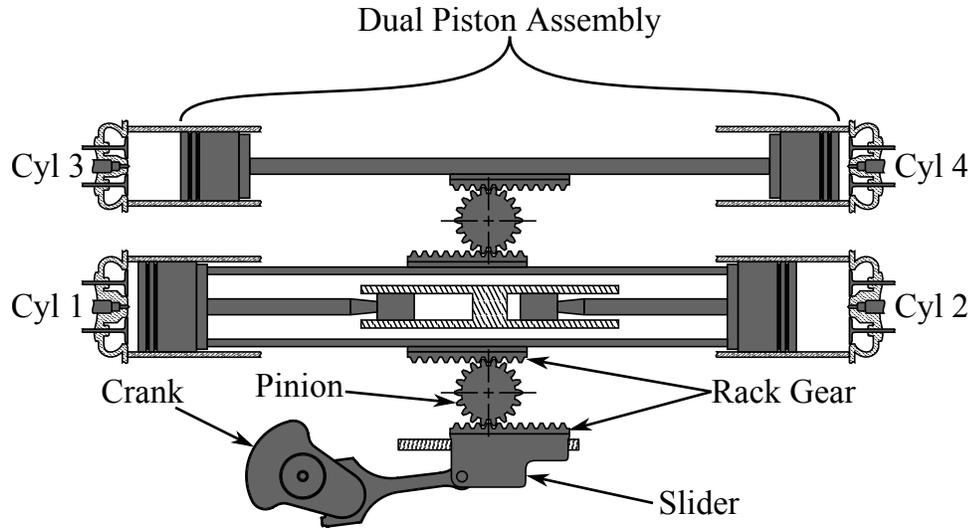
Figure 1.11: Hydraulic linear engine.

ensure sufficient rotational kinetic energy is available to carry the system beyond any given turnaround point. While the magnetostrictive sensor remains to monitor linear piston position, an absolute rotational encoder has been installed to record crank angle. The HLE crank also allows the engine to operate at higher engine speeds than the FPE, increasing the power output range.

Engine geometry requires a novel approach to cam-controlled valve timing. Shown in Figure 1.12, a cam depresses a plunger to pressurize an oil line. On the opposing end, the pressurized oil operates an actuator piston to open the valve. The process is analogous to a 'hydraulic pushrod'.

An HLE piston exhibits velocity characteristics somewhat between the FPE and conventional engine, as shown in Figure 1.3. However, the HLE approaches the behavior of a standard, crank driven piston. Because the HLE operates with a single crank and a small flywheel, the engine has low rotational inertial and experiences rapid transients and a fast start-up. Consequently, the HLE responds to cylinder fueling discrepancies with appreciable engine speed fluctuations. Recall from Section 1.3.1 that engineers designed cylinders 3_a, 3_b, 4_a, and 4_b for the original FPE with a smaller diameter than cylinders 1 and 2. By removing a cylinder pair, the HLE therefore
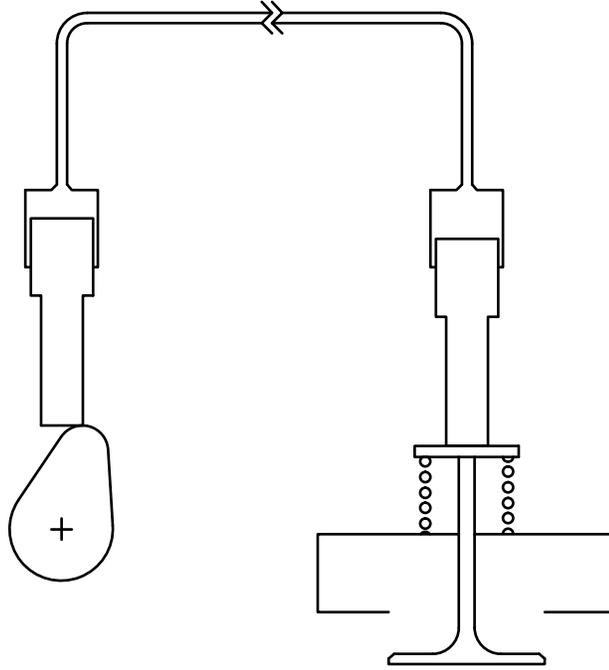
Figure 1.12: HLE hydraulic valve actuation.

possesses inherently unbalanced cylinder displacements. Mismatched displacement leads to varying compression ratios, pumping work, and excessive noise, vibration, and harshness. It is important to keep in mind that the prototype HLE is a proof of concept created by the EPA as a modification of existing hardware as to avoid the high costs of development from scratch. An ideal HLE would likely possess balanced geometry designed specifically for its unique arrangement. Regardless, it is important to actively manage cylinder balancing and engine speed to facilitate prototype HLE operation and adjust for discrepancies in cylinder displacement.

1.5 Objectives

The overarching goal of this dissertation is to enable FPE and HLE technology by addressing controls challenges and to subsequently evaluate the fuel economy potential of the two hydraulic linear engine concepts. Modeling and simulations assist with both objectives by supporting investigations of advanced control algorithms and facilitating

39

evaluation of FPE and HLE performance relative to a conventional ICE baseline. In a synergistic approach, models act as virtual engine platforms that provide the understanding necessary to create reduced-order controller models and ultimately provide a mechanism for demonstration of the control algorithms.

While prototype hardware has provided experimental insight and supports modeling, reliability issues unrelated to this research prevent extensive HLE testing. Therefore, predictive engine simulation, built using original models in MATLAB / Simulink, provide a virtual engine platform invaluable for both control validation and simulation-based comparison of the concepts. In a unique context, the linear engines (both free-piston and constrained piston) incorporate conversion of mechanical energy into hydraulic work, and are therefore promising candidates for direct integration into the hydraulic hybrid powertrain.

Many publications discuss modeling FPE dynamics or thermodynamics [7, 17, 29, 30, 49, 50, 52, 59, 62, 64, 65, 67, 69, 70, 71, 85, 109, 110, 112, 118], but none consider a realistic friction expression and instead opt for a simplified description. Further, only a handful of researchers directly compare FPE behavior to conventional engines; those that do generally constrain dynamics, only consider thermodynamics, or do not use a consistent modeling framework. Therefore, one of the key objectives of this dissertation is to create a modeling architecture that captures all relevant phenomena, thus enabling accurate prediction of trends in performance of an HLE, FPE, and conventional ICE.

The proposed models consider transient engine dynamics. As a result, stable operation of the linear engines is not guaranteed. Accordingly, control challenges were identified, i.e.:

- cylinder-to-cylinder balancing and speed control of the HLE

- FPE clearance height control and stability, including load transients

Active control is necessary to track hydraulic power set points. Because the HLE has a crank to constrain the motion, speed control is similar to that of a conventional engine. However, asymmetric piston velocity profiles create discrepancies in HLE heat transfer across cylinders [113]. Variations in cylinder-to-cylinder performance suggest that for the same quantity of injected fuel, different cylinders will produce different magnitudes of useful, hydraulic work. Therefore, work in this dissertation proposes an adaptive approach for cylinder balancing and speed control of an HLE. Various institutions emphasize the significance of robust and repeatable FPE piston motion control, but no publications take a rigorous approach to defining and stabilizing the system. As a result, these advanced engine concepts have yet to achieve the level of maturity required for practical implementation. The most common FPE control technique entails tuning a PID controller to obtain the desired characteristics [52, 65, 73, 97]. As an additional challenge, load changes can disturb the piston motion of an FPE out of the desired range [73]. The only current, and somewhat ineffective, solution to constrain FPE clearance during a load change is to accelerate the closed-loop system response by introducing a pseudo-derivative controller [73]. However, the authors admit that even the improved controller does not fully satisfy constraints. Hence, this dissertation pursues a novel approach to stabilize and constrain FPE clearance height

Hydraulic linear engine performance has not been previously investigated, and the ultimate goal of this work is to setup a methodology for a fair comparisons of HLE with FPE or conventional ICE technology. This dissertation exercises physics-based models to explore behavior of HLE, FPE, and ICE over a complete operating range, quantify differences, explain observed differences between the three engine concepts, and finally assess the efficiency potential of each.

1.6 Contributions

The unique contributions of this work are as follows:

1. **Physics-based modeling architecture to simulate and analyze FPE and HLE behavior (see Chapter II and [113])**

   - Sections 2.1, 2.2, and 2.3 combine mass balance, energy balance, dynamics, and hydraulics models to simulate instantaneous behavior of a crank or free-piston assembly.

   - Section 2.1.2 develops a model to estimate instantaneous HLE, FPE, and ICE frictional forces.

   - In Section 2.4, a preliminary analysis shows that HLE is inherently unbalanced due to piston behavior regardless of geometry.

2. **Adaptive, energy-based engine speed control of HLE for cylinder balancing (see Chapter III and [114])**

   - Section 3.1 defines a discrete, control-oriented model using an estimate of rotational kinetic energy to describe HLE behavior as a function of fuel injection and load.

   - Section 3.2.1 describes an algorithm for set-point tracking of the control-oriented model using state feedback principles.

   - Section 3.2.1 constructs an adaptive cylinder balancing algorithm using a recursive least squares algorithm to adjust individual cylinder fuel injection commands.

   - The processes in Section 3.2 enable individual cylinder fuel and load control of an HLE.

   - Section 3.2.2 demonstrates stability and effectiveness of control-oriented and physics-based models to the above schemes.

42

- Section 3.3 proposes an individual cylinder injection timing optimization (see also [115]).

3. **Energy-based FPE clearance height control (see Chapter IV)**

   - Section 4.2 presents implicit control-oriented model constructed in discrete-time to describe FPE clearance height behavior and derived from a first law energy balance.

   - Section 4.3 linearizes the control-oriented model over a range of equilibria and evaluates FPE stability and sensitivity.

   - Section 4.3 generates a stabilizing controller for the control-oriented FPE model using dynamic inversion and state feedback.

   - Sections 4.4 and 4.5 express a Smith predictor algorithm using Newton's method to estimate for future FPE conditions.

   - Section 4.6 estimates FPE losses and disturbances using a recursive least squares algorithm.

   - Section 4.8 demonstrates stability and effectiveness of the proposed control structure as applied to both the control-oriented and the physics-based model.

4. **Reference governor for constraint management of FPE piston motion during a load change (see Sections 4.9 and 4.9.3)**

   - Section 4.9 proposes a robust reference governor approach to managing load transitions and enforce constraints on the control-oriented FPE model.

   - Section 4.9 describes a reference governor technique for implicit functions. The scheme uses a Newtons method solver to predict plant behavior and a bisection search to maximize load steps.

- Section 4.9.3 demonstrates the successful application of reference governor techniques to a physics-based FPE model. During a load change, the reference governor constrains piston clearance deviation to ± 0.5 mm of a nominal set point.

5. **Comparative analysis of FPE, HLE, and ICE performance (see Chapter V)**

   - Sections 5.2 - 5.9 compare engines with identical geometry over similar load range using a physics-based simulation, while also investigating FPE compression ratio.

   - Section 5.10 shows that the primary difference in engine behavior is friction. The FPE presents the lowest friction and BSFC and the ICE experiences the highest friction and BSFC.

   - Section 5.9 explains that the FPE suffers from a limited power range that can be expanded by reducing mass or adding a turbocharger.

   - Section 5.9 suggests that due to heat loss and slightly changing speed, best FPE performance at a given power does not necessarily occur at the highest compression ratio.

   - Section 5.4 indicates that large piston assembly mass increases HLE friction significantly at high engine speeds

1.7 Dissertation Overview

The document is structured to first explain the simulation tools we have developed to enable an analysis of each engine architecture. Chapter II discusses the modeling architecture we developed to capture performance of the various designs. We leverage the basic framework to model the prototype HLE and compare the results to limited

experimental data. The dissertation provides a preliminary analysis of the HLE by parametrically altering simulated speed and load and comment on behavior.

Chapter III introduces an adaptive approach to cylinder balancing and engine speed control for the HLE. This dissertation describes a discrete, energy-based, control-oriented HLE model and designs a stabilizing controller with an RLS algorithm to estimate an unknown periodic error. We show response of both a physics-based and control-oriented HLE model. Leveraging the adaptive, cylinder balancing algorithm, we also show an extremum seeking algorithm to optimize injection timing in individual cylinders.

Chapter IV considers clearance height control of a free-piston engine. We start by deriving an explicit, nonlinear, control-oriented function describing piston motion over a stroke. A linearization of the control-oriented model supplies insight on stability and sensitivity of the FPE. Using the linearized system and dynamic inversion, we create a stabilizing control law about an equilibrium. The dissertation shows tracking response of the control-oriented and physics-based models. We also describe and apply a reference governor approach to managing load transitions while maintaining clearance constraints.

In Chapter V, we discuss the performance of each engine across a range of operating conditions by exercising the physics-based models with the control structures discussed in previous chapters. We evaluate trends in heat transfer, friction, and engine efficiency. Further, the dissertation identifies the best BSFC power path and breaks down various losses across that path.

Chapter VI presents concluding remarks and compiles suggestions to improve FPE and HLE design over the current prototype iterations in regards to robustness, efficiency, and power output. Further, we present potential topics for future investigation.

CHAPTER II

Physics-Based Engine Modeling Architecture

The reported engine simulation was developed in MATLAB/Simulink and consists of three basic sub-models: dynamics, thermodynamics, and hydraulics. Figure 2.1 illustrates connections between individual components. The dynamics model uses pressure information to determine the torque acting on the crankshaft and calculates instantaneous engine speed. Gaseous pressure is provided by the thermodynamic subsystem that evaluates in-cylinder conditions and composition of each combustion chamber as a separate control volume. Meanwhile, the hydraulics model takes into account hydraulic compressibility and valve area to estimate pressure and flow in the hydraulic circuit.
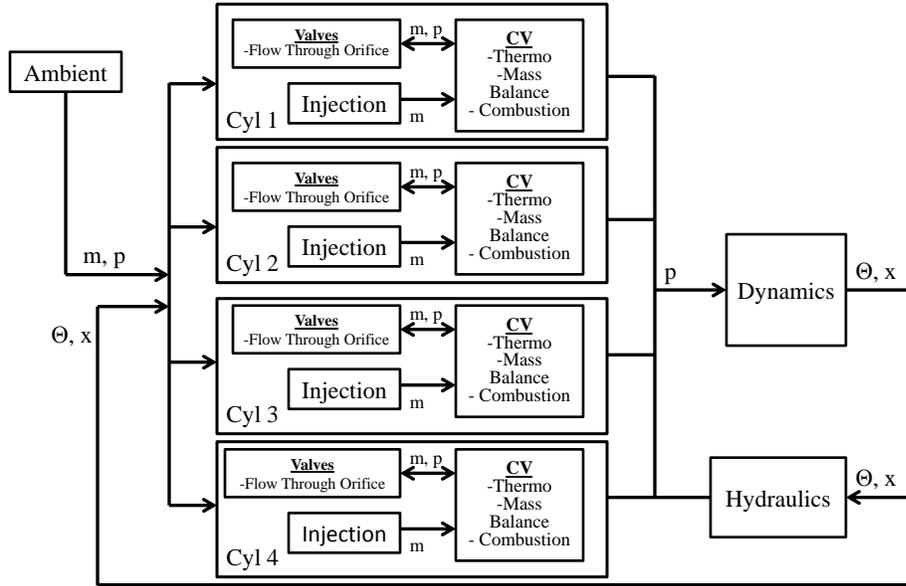
Figure 2.1: MATLAB / Simulink model structure.

2.1 Dynamics

Similar to a single-cylinder engine, the HLE has low rotational inertia and is subject to large speed fluctuations over the duration of a stroke. Filipi and Assanis [19] and Zweiri et al. [119, 120] constructed models to capture the instantaneous dynamics of a single-cylinder engine. The model presented here uses the same principles.

2.1.1 Slider-Crank

A torque balance depicted in Figure 2.2 describes the rotation of the rigid crank,

$$J\ddot{\Theta} = \tau - \tau_f, \tag{2.1}$$

where J is the total rotating inertia, $\ddot{\Theta}$ is the angular acceleration, and τ_f is the frictional torque. Torque, τ, is a geometric projection of the forces acting on the
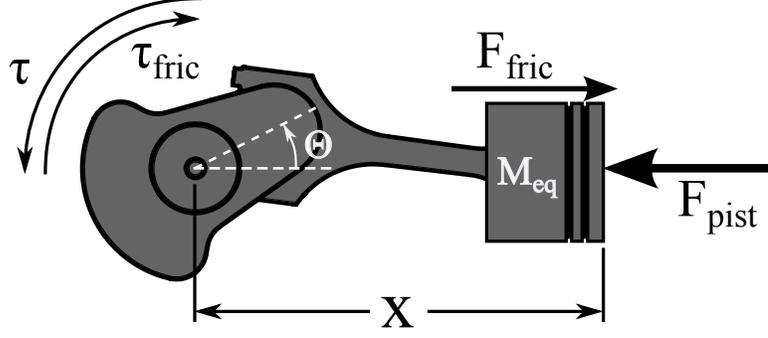
Figure 2.2: Force and torque diagram of slider-crank mechanism for HLE dynamics simulation.

piston, F, and is a function of crank angle, Θ, such that

$$\tau = FrG(\Theta), \tag{2.2}$$

where r is the crank radius and $G(\Theta)$ is the function

$$G(\Theta) = \frac{\sin(\Theta + \beta)}{\cos \beta}. \tag{2.3}$$

The angle between the connecting rod and axis of piston motion is defined as β while F is the sum pressure forces, F_p, and inertial forces, F_{in}. Because the movement of the slider, the pistons, and the pinions are linearly coupled, they are lumped together in a single inertial force balance as follows:

$$F_{in} = m_{eq}a, \tag{2.4}$$

where

$$m_{eq} = m_{12} + m_{34} + \frac{J_{pin}}{r_{pin}^2}. \tag{2.5}$$

Mass and inertia are m and J, respectively, with subscripts denoting the specific assembly. Acceleration, a, is obtained geometrically based on angular acceleration,

velocity, and position,

$$a = r\omega^2 \left[\cos\theta + \frac{r\left(\cos 2\theta + r^2 \sin^4\theta\right)}{\left(L^2 - r^2 sin^2\theta\right)^{\frac{3}{2}}}\right] + r\dot{\omega}\sin\theta \left[1 + \frac{r^2 \cos\theta}{2\sqrt{L^2 - r^2 \sin^2\theta}}\right]. \qquad (2.6)$$

Connection rod length is denoted as L. The pressure force resulting from hydraulic fluid and cylinder gases is a summation of the pressures, p, multiplied by the respective piston area, A, or

$$F_p = \sum A_i p_i = A_{12}(p_1 - p_2) + A_{34}(p_4 - p_3) + A_{hc}(p_{hc2} - p_{hc1}). \qquad (2.7)$$

2.1.2 Friction

The friction model is divided into individual friction contributions from the piston rings, piston skirt, slider, bearings, and air valves. Piston ring friction, piston skirt friction, slider friction, and air valve friction are adapted from correlations reported by [120]. Bearing friction follows from the work of Rezeka and Henein [84] and Cameron [13].

2.1.2.1 Piston Ring Friction

In conventional engines, friction generated from the piston ring acting against the cylinder wall has three main contributions: inertial forces, static tension forces, and gas pressure forces. Because the HLE piston assemblies interact through a rack and pinion mechanism, the crank does not impart side loads on the pistons. The inertial component of Zweiri's friction model [120] is therefore eliminated. It is also assumed that rack and pinion interaction, side loads introduced by the rack and pinion, and gravity are negligible. While decreased side loading enables the use of low tension piston rings that reduce friction, this chapter assumes standard piston ring properties.

The elastic tension of a compressed piston ring exerts a normal force against the

cylinder wall. The frictional torque on the crank shaft resulting from static ring tension, τ_{fr1}, is

$$\tau_{fr1} = \eta r |G(\Theta)| \sum_{n_r}^{k=1} \left[\frac{E_{Y,k} L_g}{7.07 d_r \left(\frac{d_r}{L_{r,i}} - 1 \right)^3} \right] \pi d_r L_{r,i}, \tag{2.8}$$

where E_Y is the modulus of elasticity of the piston ring, L_g is the gap closure of the piston ring, d_r is the piston ring diameter, L_r is the piston ring thickness, n_r is the number of piston rings, and η is the friction coefficient [120].

The torque contribution of gas pressure to ring friction, τ_{fr2}, is described by

$$\tau_{fr2} = \eta r |G(\Theta)| \sum_{n_r}^{k=1} z_i \, |p - p_{atm}| \, \pi d_r L_{r,i}, \tag{2.9}$$

where z_i is a pressure reduction coefficient that captures the decrease of pressure across each ring [120].

Hydraulic piston friction is modeled in a similar fashion, but ignoring the pressure effects.

2.1.2.2 Skirt Friction

The HLE piston skirts produce a frictional torque, τ_{fsk}, such that

$$\tau_{fsk} = \left[\frac{\mu \dot{\Theta} G(\Theta)}{L_0} \right] d_{CV} L_s r G(\Theta), \tag{2.10}$$

where L_0 is the oil clearance, d_{CV} is the cylinder diameter, and L_s is the skirt length [120].

2.1.2.3 Slider Friction

Similar to the piston in a conventional engine, the slider experiences side loads induced by the crank. Adapted as the inertial component of piston ring friction from Zweiri et al. [120], the frictional torque exerted by the slider, τ_{fsl}, is

$$\tau_{fsl} = \eta r |G(\Theta)| \frac{F}{\eta + cot\beta}. \tag{2.11}$$

2.1.2.4 Bearing Friction

Due to the unique configuration, the HLE crank bearings experience combustion pressure loading every 180 crank angle degrees (CAD). Additionally, the large mass of the piston assembly exerts a considerable inertial force on the crank. Because of the high loading and for simplicity, crank bearing friction is assumed to operate in the mixed lubrication regime. According to Razeka and Henein [84] mixed frictional torque is proportional to the bearing load by the inverse of the square root of rotational velocity and can be estimated as

$$\tau_{fb} = \frac{k_{fb}F_{fb}}{cos\beta\sqrt{\dot{\Theta}}}, \tag{2.12}$$

where k_{fb} is a constant coefficient.

The pinion bearings are assumed to operate in the hydrodynamic region. Assuming the bearing eccentricity approaches zero, the hydrodynamic friction force is expressed by Petroff's equation [13],

$$F_{fb} = \frac{2\pi\mu v_s r_b L_b}{L_c}, \tag{2.13}$$

where F_{fb} is the friction force, μ is the oil viscosity, v_s is the surface speed, L_b is the bearing length, r_b is the bearing radius, and L_c is the radial clearance. To obtain the

frictional torque acting on the crank from the pinions, the surface speed becomes the velocity of the piston assembly, $\dot{x}$, and acts on the crank as multiplied by the crank radius and geometric function (2.3),

$$\tau_{fp} = r|G(\Theta)|\frac{2\pi\dot{x}r_bL_b}{L_c}. \tag{2.14}$$

2.1.2.5 Valve Friction Friction

The cam and followers create frictional torque, τ_{fv}, such that

$$\tau_{fv} = K_vL_vn_v\left(1 - 0.00127\dot{\Theta}\right)r|G(\Theta)|, \tag{2.15}$$

where K_v is the valve spring rate, L_v is the valve lift, and n_v is the number of valves [120].

2.2 Thermodynamics
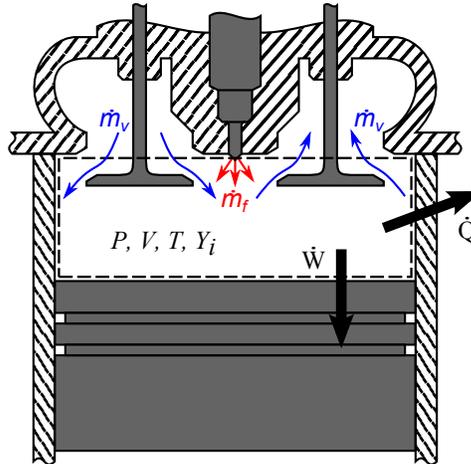
Figure 2.3: In-cylinder control volume considered for thermodynamics simulations.

The in-cylinder control volume highlighted in Figure 2.3 is considered. A mass

balance yields

$$\frac{dm}{dt} = \dot{m} = \sum_j \dot{m}_j. \tag{2.16}$$

The net time rate of change of mass, $\dot{m}$, is the sum of the mass flows from all j streams: intake, exhaust, and injection. We assume the injection rate, $\dot{m}_{inj}$, constant for the duration of the injection pulse, and is calculated based on the fuel command using the prototype HLE's calibrations.

The valve flow, $\dot{m}_v$, is modeled as compressible flow through an orifice[41],

$$\dot{m}_v = \frac{C_{D,a} A_C p_0}{\sqrt{RT_0}} \left(\frac{p_T}{p_0}\right)^{\frac{1}{\gamma}} \sqrt{\frac{2\gamma}{\gamma - 1} \left[1 - \left(\frac{p_T}{p_0}\right)^{\frac{\gamma-1}{\gamma}}\right]}. \tag{2.17}$$

where p_0 and p_T are up and downstream pressures, respectively, R is the ideal gas constant, γ is the ratio of specific heats, $C_{D,a}$ is the discharge coefficient, and A_C is the valve curtain area. If the ratio of downstream to upstream pressure is below the critical ratio,

$$\frac{p_T}{p_0} = \left(\frac{2}{\gamma + 1}\right)^{\frac{\gamma}{\gamma-1}}, \tag{2.18}$$

the valve flow rate is considered choked and is instead governed by

$$\dot{m}_v = \sqrt{\frac{\gamma}{RT_0}} C_{D,a} A_C p_0 \left(\frac{2}{\gamma + 1}\right)^{\frac{\gamma+1}{2(\gamma-1)}}. \tag{2.19}$$

The combustion model tracks individual molecular species as reactants are converted to complete combustion products. The rate of change in mass fraction, Y, of species i is

$$\dot{Y}_i = \sum_j \frac{\dot{m}_j}{m} (Y_{i,j} - Y_i) + \dot{Y}_{i,c}, \tag{2.20}$$

where $\dot{Y}_{i,c}$ is the mass fraction rate of change of species i resulting from combustion, $Y_{i,j}$ is the mass fraction of species i in flow j, and m is the total mass in the control volume.

Applying the first law of thermodynamics to the control volume yields

$$\frac{dE}{dt} = \dot{Q} - \dot{W} + \sum_j \dot{m}_j h_j,$$ (2.21)

where $\frac{dE}{dt}$ is the time rate of change in energy, $\dot{Q}$ is the heat rate into the system, $\dot{W}$ is the work done by the system, and h_j is the enthalpy of flow j. Solving for the rate of change in temperature, $\dot{T}$, while assuming a convective heat loss model and ideal gas behavior, (2.21) becomes

$$\frac{dT}{dt} = \frac{1}{\bar{c}_v} \left[-\frac{RT}{V} \frac{dV}{dt} - \frac{\bar{h} A_h}{m} (T - T_{wall}) - \sum_i u_i \dot{Y}_{i,c} \right.$$
$$\left. + \sum_j \frac{\dot{m}_j}{m} (h_j - u) - \sum_i u_i \sum_j \frac{\dot{m}_j}{m} (Y_{i,j} - Y_i) \right],$$ (2.22)

In (2.22) V is the cylinder volume, A_h is the effective heat transfer area, u is the internal energy, and $\bar{c}_v$ is the mixture's constant volume specific heat. Gas properties $\bar{c}_v$, u, and h depend on the instantaneous temperature and mixture composition.

The convective heat transfer coefficient, $\bar{h}$, is obtained from Hohenberg's correlation [47],

$$\bar{h} = k_{h1} V^{-0.06} p^{0.8} T^{-0.4} (\bar{x} + k_{h2})^{0.8},$$ (2.23)

where k_{h1} and k_{h2} are constants. Ignition delay, t_{ID}, is modeled using the Arrhenius equation,

$$t_{ID} = k_{a1} p^{-k_{a2}} e^{\frac{E_A}{RT}},$$ (2.24)

where E_A is the fuel activation energy and both k_{a1} and k_{a2} are calibration terms. Because temperature, T, and pressure, p, vary instantaneously, the start of ignition, t_{ign}, is calculated as the moment in time when the integral of the reciprocal of t_{ID}

reaches unity [6], or

$$\int_{t_{inj}}^{t_{ign}} \frac{1}{t_{ID}} dt = 1. \tag{2.25}$$

where t_{inj} is the start of injection.

Watson's heat release model [104] describes combustion in the form

$$S'(\tilde{t}) = \frac{dS}{d\tilde{t}} = \beta_S S'_p(\tilde{t}) + (1 - \beta_S) S'_d(\tilde{t}). \tag{2.26}$$

The Watson function captures both the premixed and diffusion processes of a two staged diesel combustion where $S\prime$ is the fraction of fuel burned to total fuel injected, $S_p\prime$ is the premixed contribution, $S_d\prime$, is the diffusion portion, β_S is the ratio of the two, and $\tilde{t}$ is the time since ignition normalized by the combustion duration, $D(t)$ [104]. Combustion duration is specified on a crank angle basis and subsequently transformed into a time duration using the engine's rotational velocity. The Watson correlation is expressed as follows:

$$\tilde{t} = \frac{t - t_{ign}}{D(t)}, \tag{2.27}$$

$$S'_p = C_{p1} C_{p2} \tilde{t}^{(C_{p1}-1)} \left(1 - \tilde{t}^{C_{p1}}\right)^{(C_{p2}-1)}, \tag{2.28}$$

$$S'_d = C_{d1} C_{d2} \tilde{t}^{(C_{d2}-1)} \exp\left(-C_{d1} \tilde{t}^{C_{d2}}\right), \tag{2.29}$$

$$C_{p1} = 2.0 + 1.25 \times 10^{-8} \left(t_{ID} N\right)^{2.4}, \tag{2.30}$$

$$C_{p2} = 5000, \tag{2.31}$$

$$C_{d1} = k_{w1} \phi^{-k_{w2}}, \tag{2.32}$$

$$C_{d2} = k_{w3} C_{d1}^{k_{w4}}, \tag{2.33}$$

$$\beta_S = 1 - \frac{k_{w5} \phi^{k_{w6}}}{t_{ID}^{k_{w7}}}. \tag{2.34}$$

Four parameters are most critical when fitting the Watson correlation to a prescribed burn rate: k_{w1}, k_{w5}, C_{p2}, and $D(t)$. Variable k_{w1} dictates the length and peak rate of the diffusion burn, k_{w5} affects the trade-off between premixed and diffusion burns, C_{p2} influences the length and peak rate of the premixed burn, and $D(t)$ controls the duration and peak of the entire combined burn.

Species generation and consumption from combustion follow the generalized chemical reaction,

$$H_xC_y + v_{O_2}\left(O_2 + 3.76N_2\right)$$
$$\rightarrow v_{CO_2}CO_2 + v_{H_2O}H_2O + v_{N_2}N_2. \tag{2.35}$$
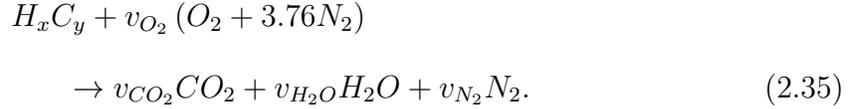
Common diesel fuel consists of a wide variety of species and additives. For simplicity, dodecane, $C_{12}H_{36}$, is used as a diesel surrogate for chemical kinetics [82]. Species generation is described by

$$\dot{Y}_{i,c} = \dot{S}\frac{M_i v_i m_{f,tot}}{M_f m}, \tag{2.36}$$

where

$$\dot{S} = \frac{dS}{dt} = \frac{dS}{d\tilde{t}}\frac{d\tilde{t}}{dt}, \tag{2.37}$$

M is the molar mass, and v_i is the molar consumption or generation of species i per mole of fuel at stoichiometric proportions.

2.3 Hydraulics

Figure 2.4 is an illustration of the hydraulic system. Hydraulic pumping is modeled as turbulent flow through an orifice, similar to Li and Sun [65] or Yuan and Wu [112]. Valve flow, q_v, is governed by the equation

$$q_v = sign(\Delta p_{hc})C_{D,h}A_v\sqrt{\frac{2}{\rho_{hf}}|\Delta p_{hc}|}, \tag{2.38}$$
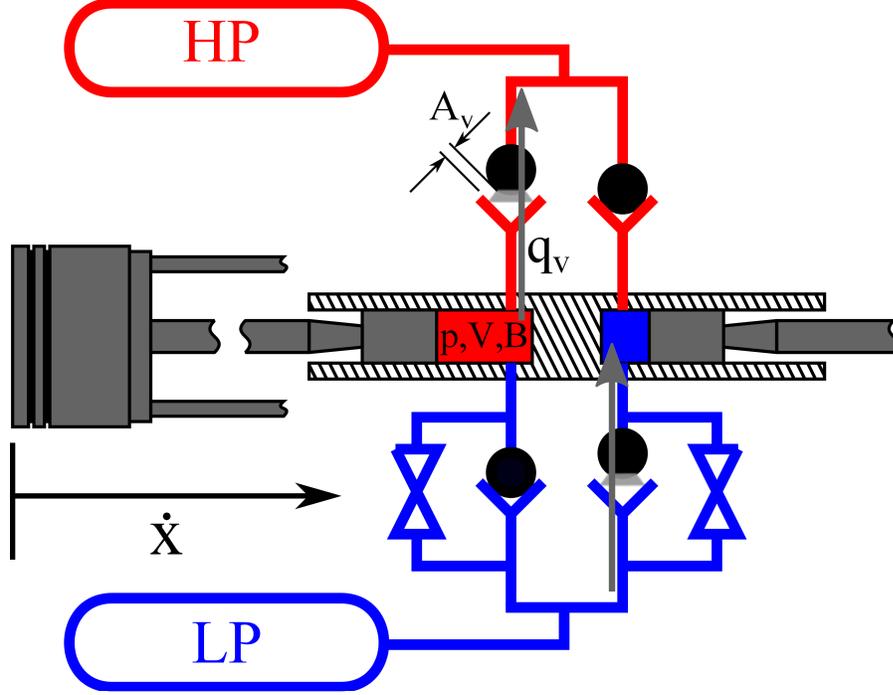
Figure 2.4: Diagram of linear hydraulic pump utilized in the HLE and FPE.

and is driven by the pressure differential between the hydraulic pumping chamber and the accumulator, Δp_{hc}. In (2.38), $C_{D,h}$ is the flow discharge coefficient and ρ_{hf} is the density of the hydraulic fluid. The check valve flow area, A_v, follows the equation

$$A_v = A_{v,max} \frac{\Delta p_{hc} - \Delta p_{cr}}{\Delta p_0 - \Delta p_{cr}}, \tag{2.39}$$

where Δp_{cr} is the minimum valve opening pressure differential and Δp_0 is the pressure differential at which the valves are fully open. Both Δp_{cr} and Δp_0 are constants determined by the check valve spring rate, preload, and compression length.

The accumulators act as constant pressure reservoirs with infinite volume while the change in the hydraulic chamber pressure is modeled as

$$\frac{dp_{hc}}{dt} = \frac{q \times B_{hf}}{V_{hc}}, \tag{2.40}$$

where B_{hf} is the bulk modulus of the hydraulic fluid, V_{hc} is the volume of the hydraulic

chamber, and

$$q = q_v + A_{hc}\dot{x}. \tag{2.41}$$

Here, A_{hc} denotes the cross-sectional area of the hydraulic piston.

2.4 Simulation Study of the HLE

The EPA has conducted preliminary experiments with the HLE at the National Vehicle and Fuel Emissions Laboratory in Ann Arbor, MI. The engine achieved continuous operation at low speed with minimal loading. Further testing is delayed due to hardware issues that impact both engine performance and data quality. The model is therefore used to demonstrate trends in engine behavior to inform future studies with the physical HLE.

Figure 2.5 shows the pressure-volume (P-V) diagram using data obtained from the linear sensor on the prototype HLE. While the P-V data appear to suggest late combustion, the engine's behavior near TDC is a result of unintended mechanical compliance. The linkages are designed to be completely rigid, but instead allowed the piston to abruptly slide away from TDC causing pressures to decrease before the crank passed the turn around. Because the model assumes a rigid structure, it cannot reproduce exactly the recorded HLE behavior. However, the experimental compression path remains unaffected by the mechanical compliance and suitably matches the simulated results. Further, the experimental and modeled data exhibit a similar slope and ratio of specific heats during expansion.

The results of a heat release analysis on the experimental data, shown in Figure 2.6, indicate a relatively short combustion event. For the simulations that follow, the fast rate of heat release is assumed valid, understanding that the witnessed combustion behavior may be an artifact of compliance in the system and measurements. However, a sweep of combustion duration is presented further in this section to un-

58
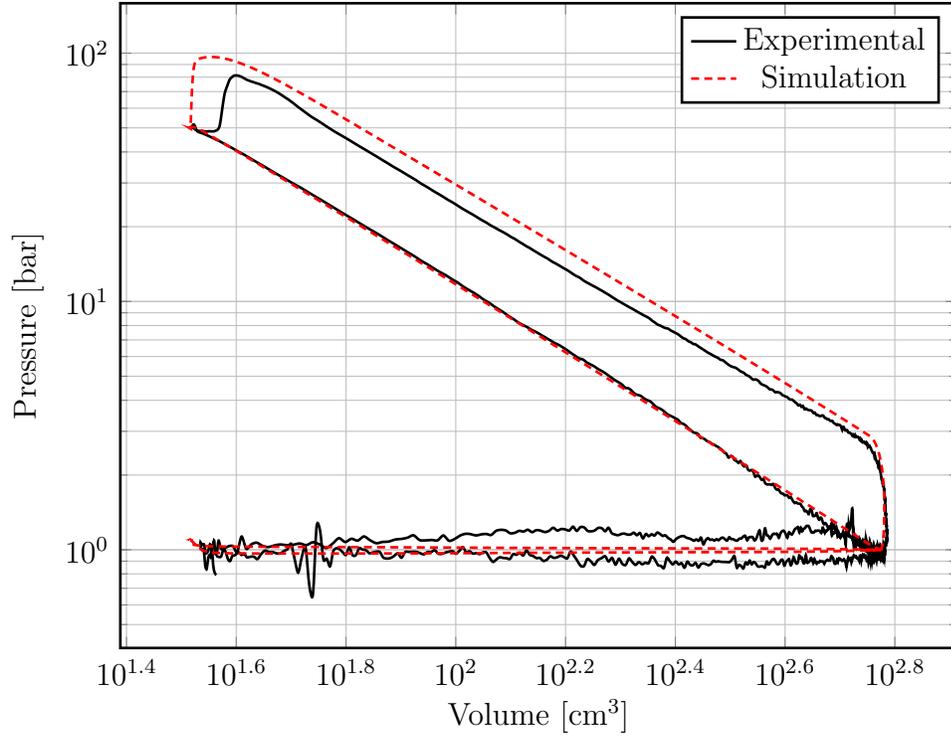
Figure 2.5: Pressure-volume diagram of experimental data and simulation behavior.

derstand sensitivity to this parameter.
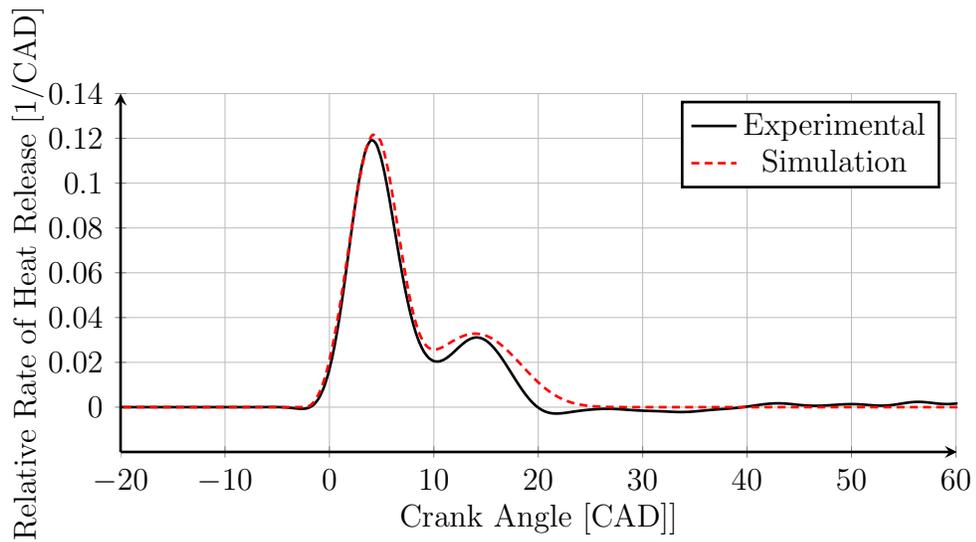
Figure 2.6: Relative rate of heat release during combustion.

As shown by Filipi and Assanis [19] or Zweiri et al. [119, 120], single-cylinder engines are subject to large instantaneous crank speed fluctuations over the duration of

a cycle. The HLE has a similarly low rotational inertia, yet experiences a combustion event every 180 CAD. Figure 2.7 shows the instantaneous HLE rotational velocity as a function of crank angle. While the HLE prototype experiences some mechanical compliance, the simulation assumes rigid coupling, preventing the model from exactly reproducing the experimental data. To compensate, the results obtained from the model and presented in Figure 2.7 are acquired using the same fuel command as applied to the experiment but with additional loading. The simulation captures the general rotational dynamics of the prototype HLE, but cannot replicate the additional oscillations stemming from compliance.
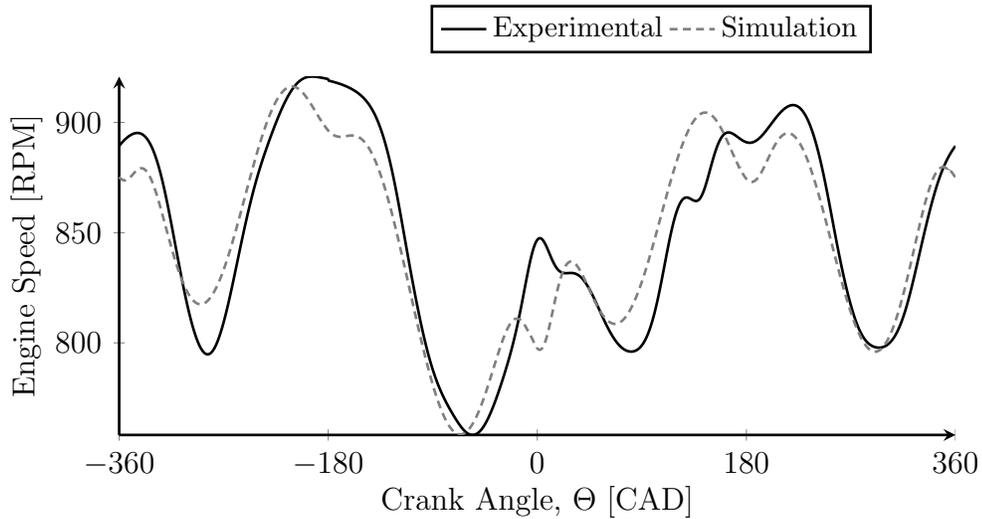
Figure 2.7: Comparison of experimental and modeled engine dynamics at steady state with same fueling.

During operation, the HLE rotational velocity is not fixed by a dynamometer. Instead, the engine controller manages fuel and load to achieve a constant speed. However, variations in cylinder bore make robust control difficult. Traditional integral control fails to balance fueling and results in the large speed fluctuations shown by the experimental dynamics in Figure 2.7. In some circumstances the oscillations become unstable.

Over the course of a stroke, the change in rotational kinetic energy (and rota-

60

tional velocity) of the HLE, is a function of the net work applied to the slider-crank mechanism. If the net work is greater than zero, the kinetic energy increases and vise versa. To achieve a constant speed, the net work should approach zero. A number of processes add or remove energy from the system. Friction and hydraulic loads require work from the slider-crank and decrease the amount of energy. Boundary work resulting from changing in-cylinder volumes interacting with the piston also impact slider-crank energy. Because the HLE is a four-cylinder engine, each cylinder experiences a different process of the four-stroke cycle. Accordingly boundary work from intake, compression, expansion, and exhaust all act on the piston. Fuel energy released into the expansion stroke make it primary source of work addition into the slider-crank. Hence, in order to maintain a constant speed, the amount of energy added through the expansion stroke from fuel must be equivalent to the sum of energy lost, energy removed as work, and boundary work on all the other cylinders. However, the EPA designed cylinders 3 and 4 for the original FPE, with a smaller diameter than cylinders 1 and 2. Accordingly, cylinders 3 and 4 have a different displacement and require a different quantity of boundary work to compress the charge. The cylinder firing order is 1-2-4-3. Given the discrepancies in cylinder bore, combustion in cylinders 2 and 3 require an offset in fuel command to compensate for changes in boundary work during compression. Each cylinder also experiences a unique efficiency due to disparities in heat loss area and compression ratio. For these reasons, the prototype HLE is inherently imbalanced in regards to fueling; even if each cylinder receives the same volume of fuel, they will produce different quantities of work output. Note that the concept of fueling imbalance is somewhat distinct from dynamic imbalance. The HLE is dynamically balanced such that the mass of any oscillating components have been manufactured to minimize vibration.

Given that speed control is necessary for further testing, and because engine imbalances increase vibrations, accelerate wear, and decrease engine life, it is necessary

to adjust the fuel control strategy. Chapter III discusses a discrete, adaptive control structure to balance the estimated rotational kinetic energy of the crank at each turn around point [114].

With a robust control structure in place, it is possible to exercise the model to investigate trends in engine performance. Figure 2.8 shows the effects of speed and load on the indicated efficiency of each cylinder. Load is presented as a percentage of full power extraction (PX), where PX = 0% specifies that the bypass valves are open for the entire stroke (idle) while PX = 100% expresses that the bypass valves are closed for the entire stroke and that the maximum hydraulic work is obtained. The data presented were obtained with an accumulator pressure of 2500 psi. For context, Figure 2.9 shows the power output corresponding to the speed and load. Note that the net indicated efficiency is remarkably high. This efficient behavior is attributed to of a short combustion duration that leads to near constant volume combustion.

As depicted in Figure 2.8, each cylinder behaves somewhat differently. Performance discrepancies are partially accounted for by the unbalanced cylinder displacements, which result in different compression ratios and different heat loss areas. Further, cylinders 3 and 4 have a lower fueling limit as a result of their smaller displacements, i.e. less air is available for combustion. Cylinder 3 has the lowest load limit because the energy from its combustion event is used to compress the charge in cylinder 1, which has a larger displacement. As stated earlier, more work is required to compress the charge in cylinders 1 and 2 than cylinders 3 and 4. In order to maintain a speed set point, energy is taken from the combustion event in cylinder 3.

Additionally, cylinders 1 and 4 experience a different kinematic approach to TDC than cylinders 2 and 3. In a conventional engine, a piston's velocity near BDC is not symmetric to its velocity near TDC, resulting in the 'egg shape' shown in Figure 1.3. Since a combustion event occurs every 180 degrees of HLE crank motion, cylinders 2 and 3 exhibit an inverted phase diagram, shown in Figure 2.10.
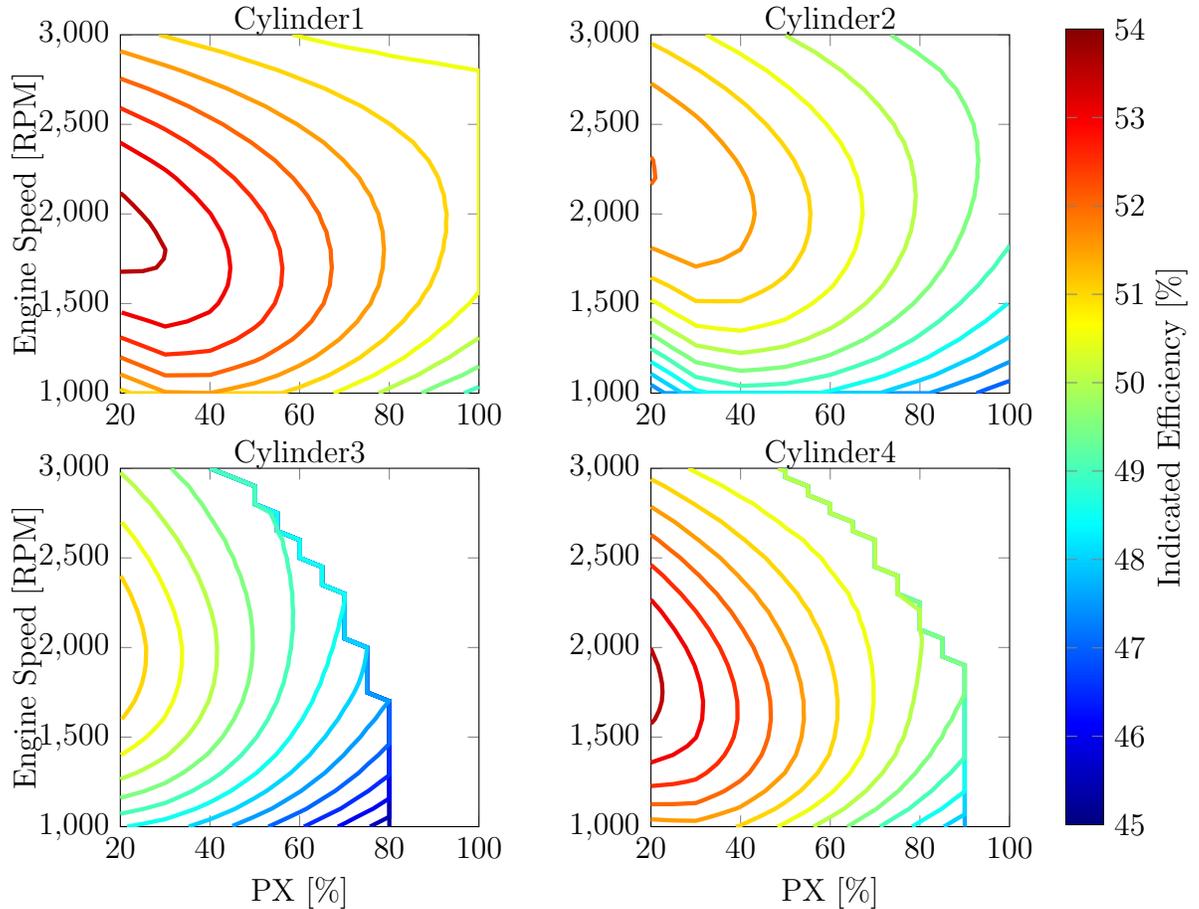
Figure 2.8: Net indicated efficiency of each cylinder as a function of engine speed and load. Load is presented as a percentage of the full power extraction (PX) at 2500 psi accumulator pressure.

Figure 2.11 shows the piston's approach to TDC on a crank angle basis. Cylinders 2 and 3 dwell at TDC for a longer duration of time than cylinders 1 and 4. Additional time at TDC results in higher pressures and temperatures after ignition, more closely approaching constant volume combustion. However, the surface area to volume ratio is large for an increased interval, causing high heat loss, which is compounded by the higher combustion temperatures. As a consequence, the prototype HLE would be imbalanced even if all cylinders had an identical diameter.

The speed and load results presented in Figure 2.8 were obtained using the same crank angle based injection timing for each cylinder and the same combustion duration
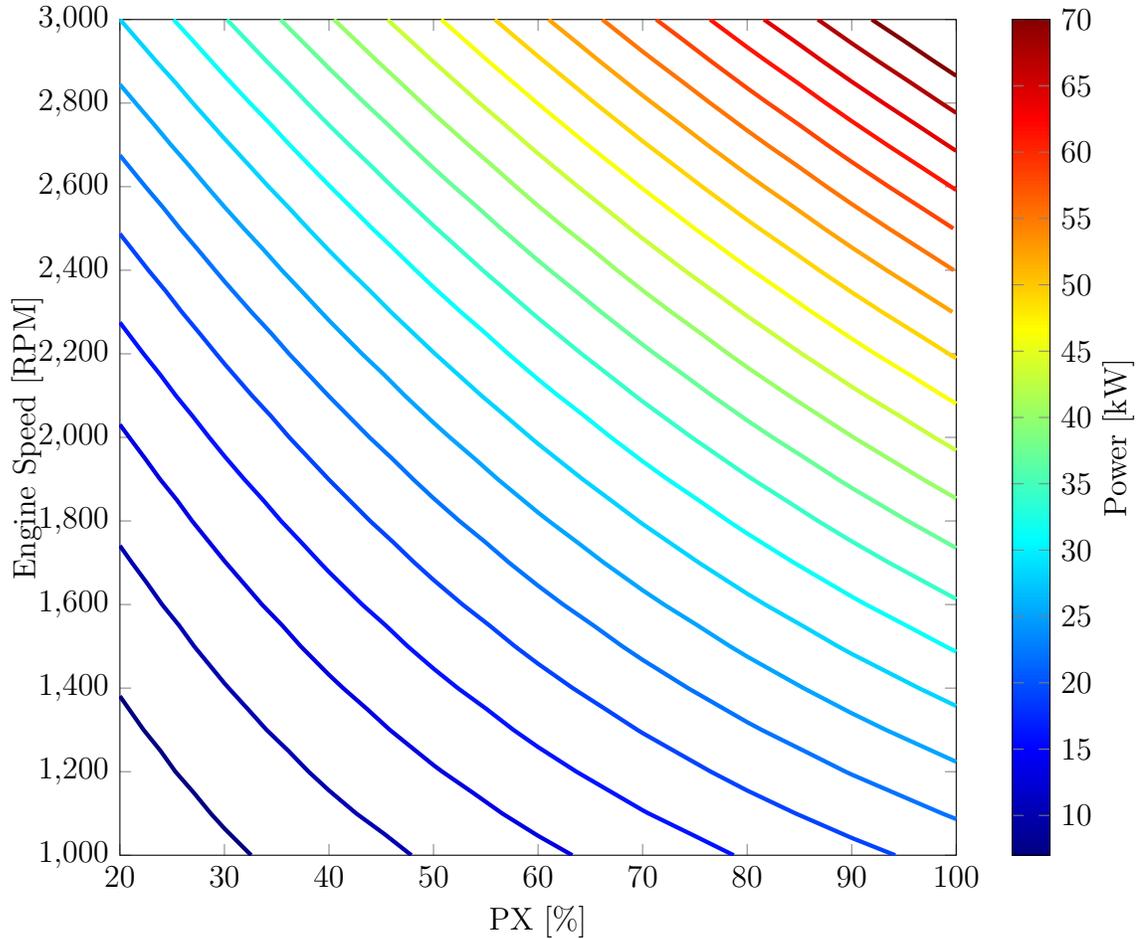
Figure 2.9: Net HLE power output as a function of engine speed and load. Load is presented as a percentage of the full power extraction (PX) at 2500 psi accumulator pressure.

as a parameter in the Watson heat release correlation. Due to the differences in piston dynamics and cylinder bore, each combustion chamber did not necessarily operate at its optimal conditions. Figure 2.12 shows the effects of combustion duration and injection timing on indicated efficiencies for each cylinder. Because cylinders 2 and 3 reside near TDC for a longer duration, they are less sensitive to changes in injection timing and combustion duration. The indicated efficiencies demonstrated by cylinders 1 and 4 have a higher peak value, attributable to lower heat loss, but decrease more quickly as the conditions move away from constant volume combustion. The trends in Figure 2.12 suggest that the HLE would benefit from individual control of injection
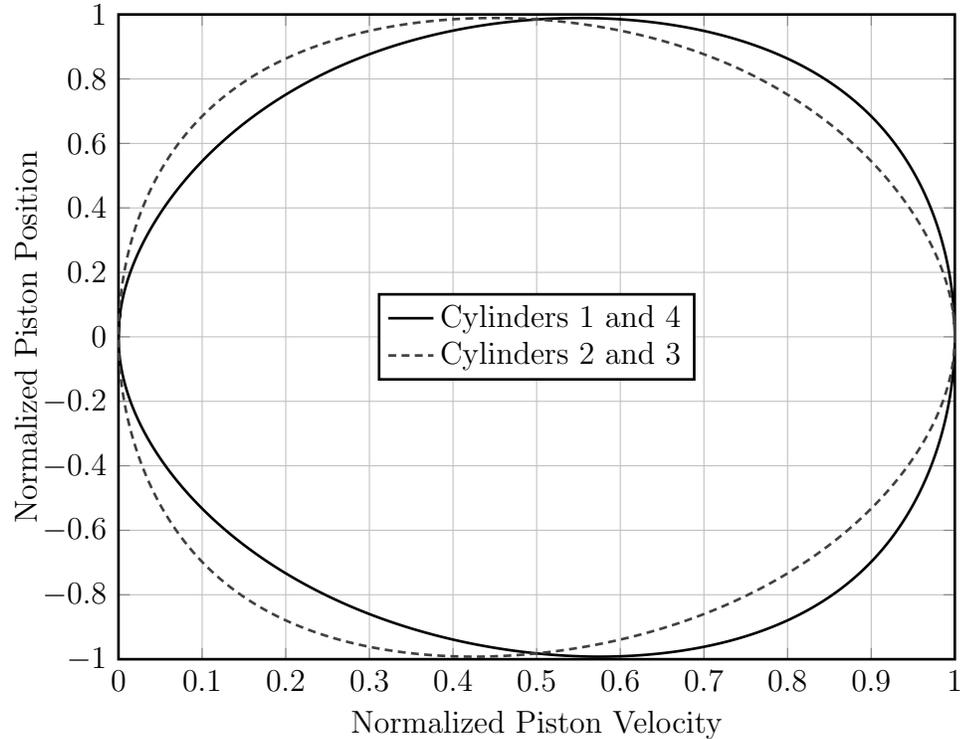
Figure 2.10: Phase diagram depicting the piston dynamics. The piston position is normalized by stroke length such that zero corresponds to BDC and one corresponds to TDC. The piston velocity is normalized by maximum piston speed such that a magnitude of one signifies the peak velocity, positive values denote the piston is traveling toward TDC and negative values denote the piston is traveling toward BDC.

timing and a distinct combustion strategy optimized for each cylinder. For example, being more sensitive to combustion duration, cylinders 1 and 4 could potentially operate in the HCCI-type combustion while cylinders 2 and 3 could operate with conventional combustion strategies to maintain a higher load range. The bypass valve enables the above strategy by allowing the engine to load the power stroke of each cylinder differently. However, by varying the fuel command from stroke-to-stroke, emissions control may become difficult.

Based on the load and speed investigation, shown in Figure 2.13, the peak conversion efficiency of fuel energy into useful hydraulic work is roughly 42%. This is somewhat optimistic, but follows from the high thermal efficiencies and neglects the hydraulic line frictional losses and valve leakage. Peak efficiencies appear at high load
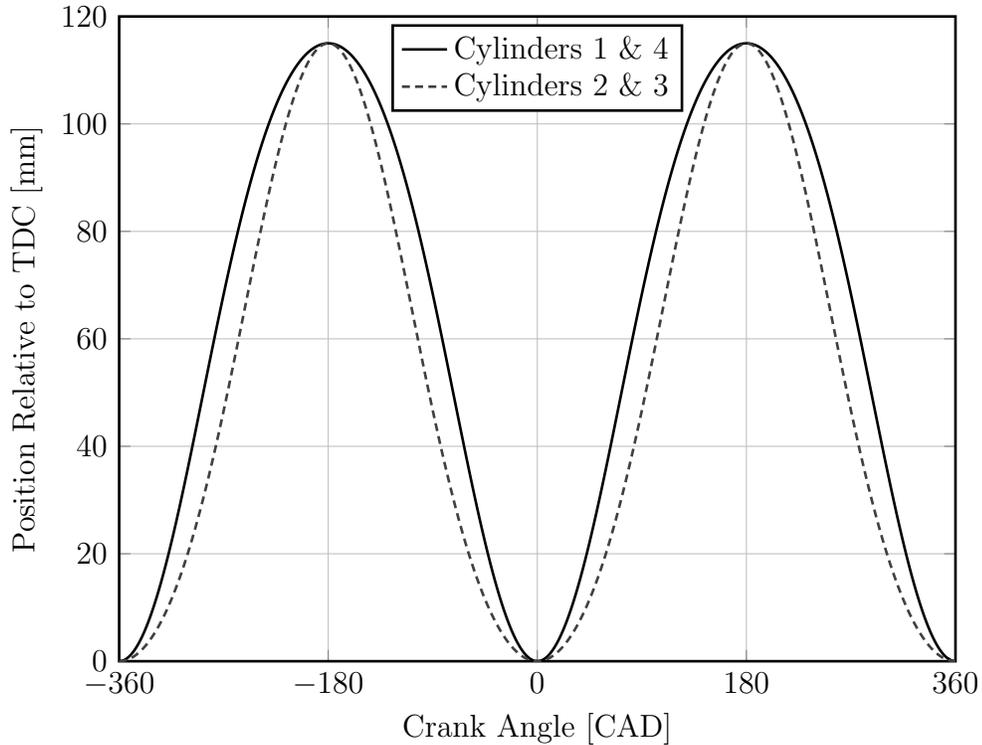
Figure 2.11: Piston position relative to TDC as a function of crank angle, where zero corresponds to TDC associated with combustion.

and low speed, and the load range is limited by the characteristics of cylinder 3.

Figure 2.14 shows the mechanical efficiency behavior of the HLE as a function of speed and load. Mechanical efficiency drops quickly at high speed as friction sharply increases.

The majority of frictional losses stem from the crank bearing due for a singular reason: the mass of the oscillating piston assembly is extraordinarily high. As a result, inertial loads transmitted to the crank bearing increase significantly with engine speed. Figure 2.15 shows the crank bearing load with PX= 50% at 1800 RPM and 2800 RPM. Increasing speed roughly 56% raises the peak bearing load by over 200%. Energy is transmitted to and from the flywheel to change the piston's oscillatory behavior. The large piston assembly mass requires that large amounts of energy be transmitted through the crank, therefore increasing bearing load.

To reduce frictional losses and wear, the engine should operate at low speed to

66
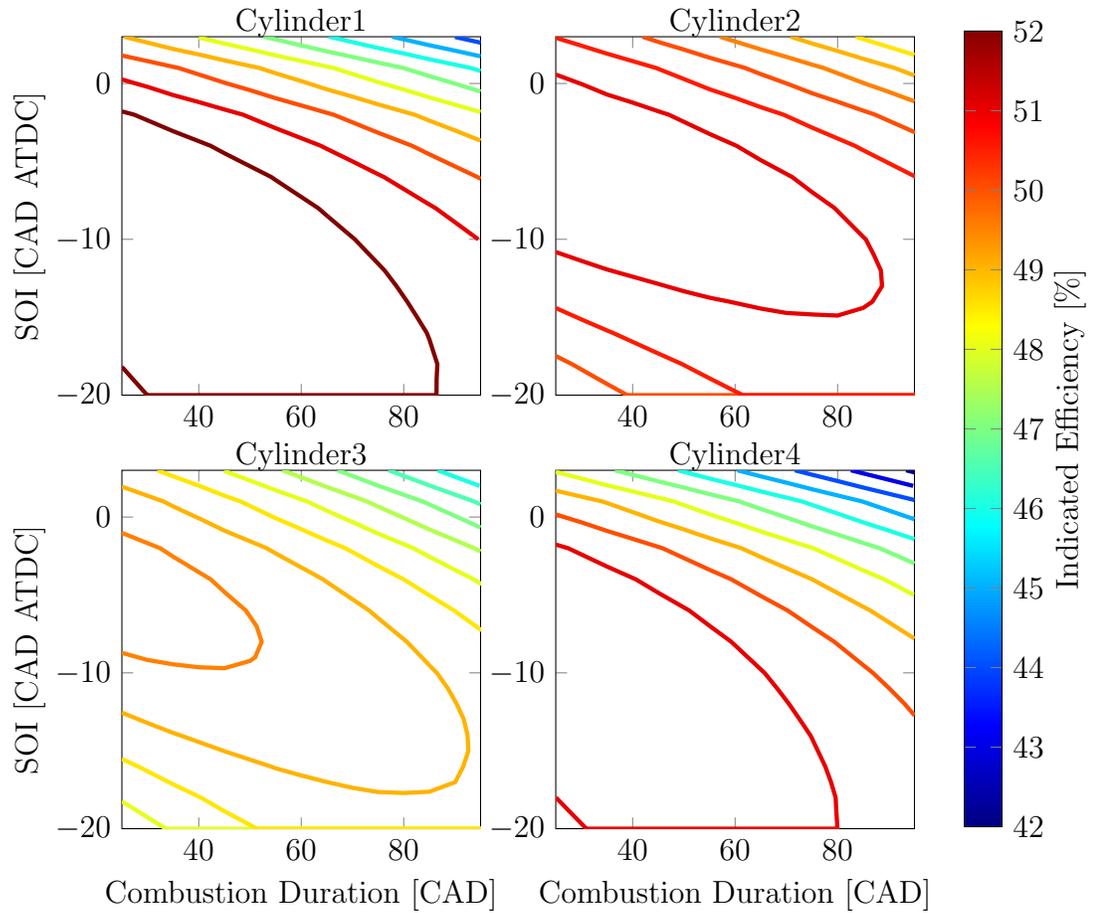
Figure 2.12: Indicated efficiency for each cylinder as a function of injection timing and combustion duration. The Start of Injection is referred to as SOI.

maintain minimal piston inertia and further iterations on the HLE design should strive to decrease the piston assembly mass.
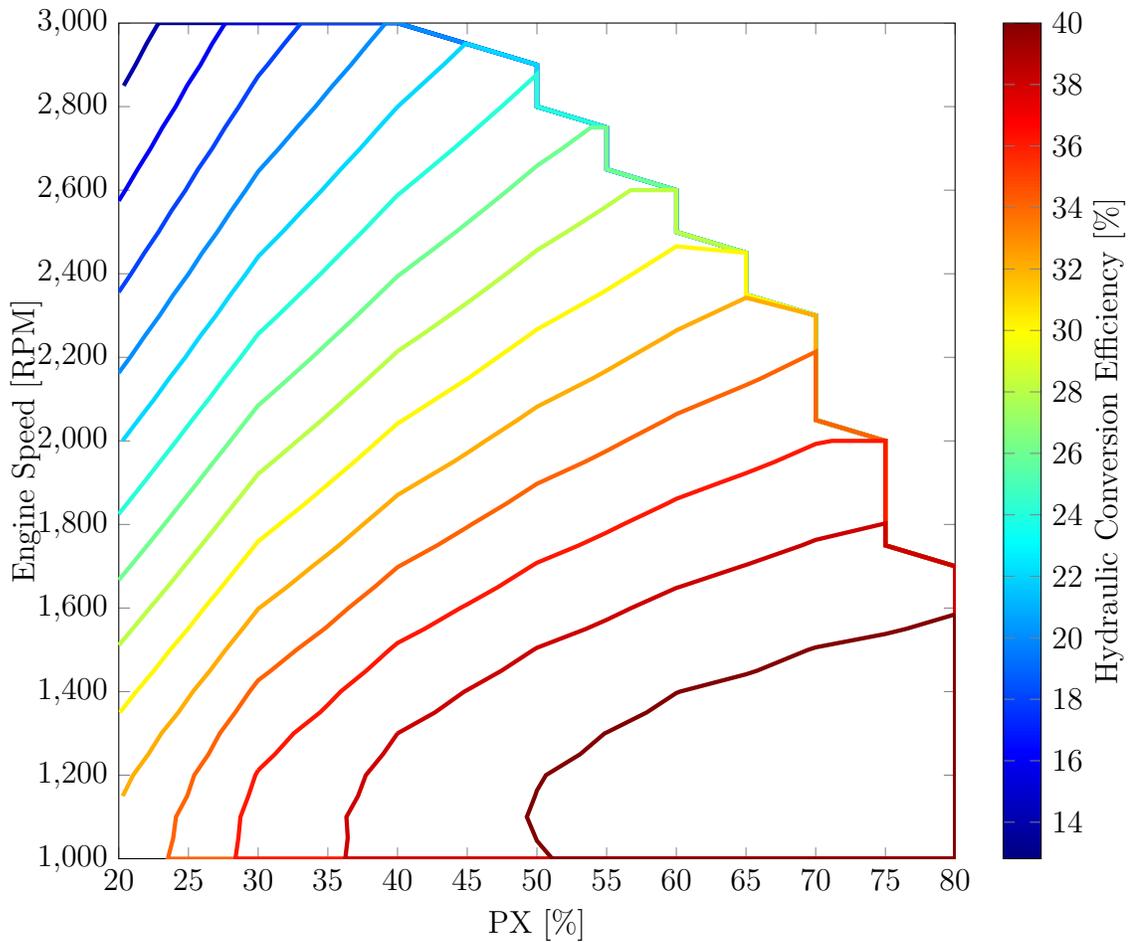
Figure 2.13: Hydraulic conversion efficiency as a function of speed and load. Load is presented as a percentage of the full power extraction (PX) at 2500 psi accumulator pressure.
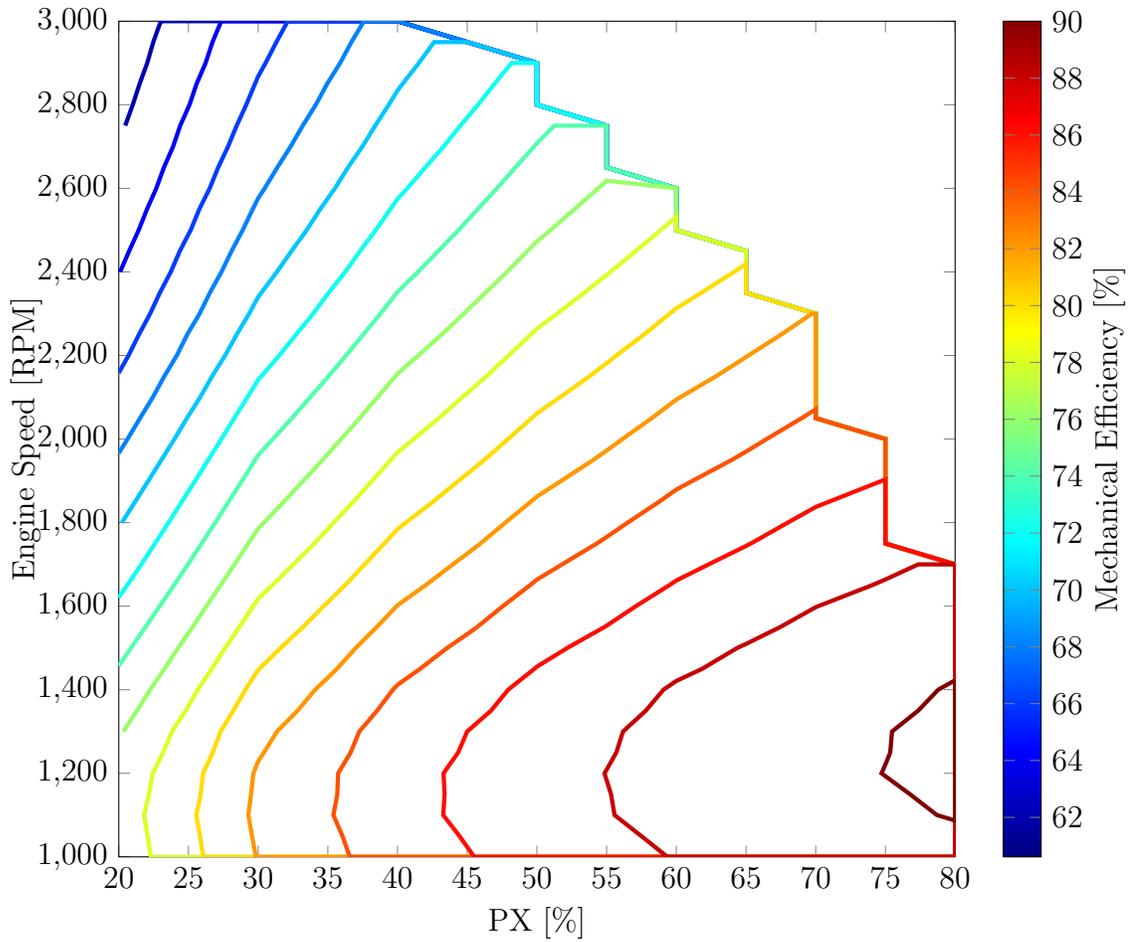
Figure 2.14: Mechanical efficiency as a function of speed and load. Load is presented as a percentage of the full power extraction (PX) at 2500 psi accumulator pressure.
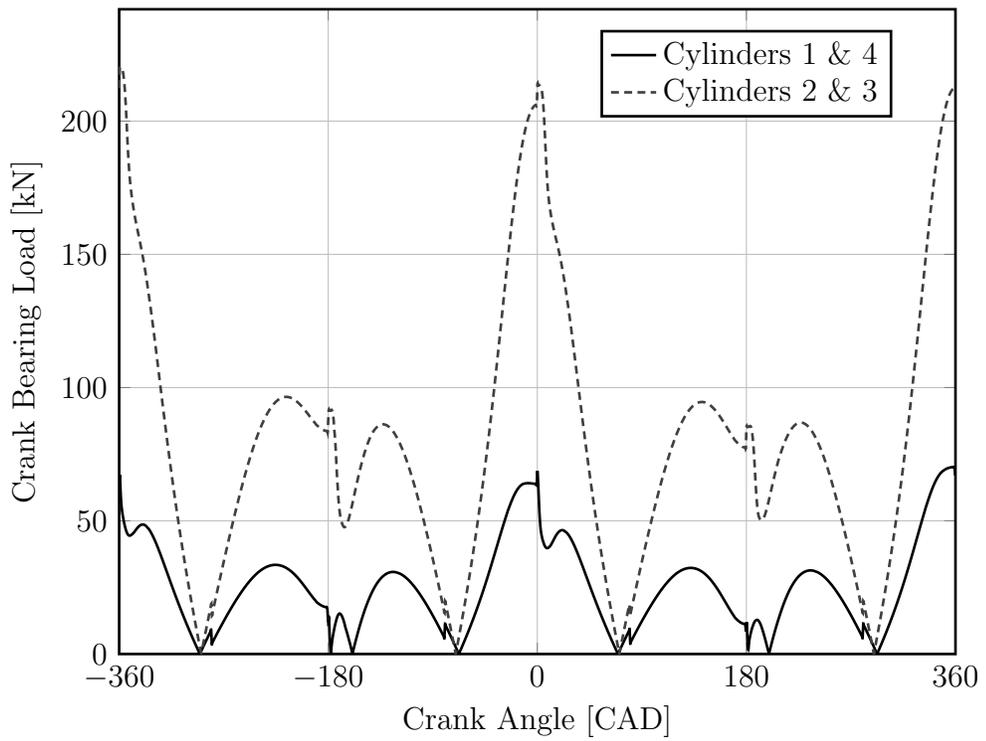
Figure 2.15: Bearing load as a function of crank angle.

2.5 Conclusions

The EPA has developed a novel, hydraulic linear engine prototype based on their prior free-piston engine research. The design extracts hydraulic power from the linear piston motion while using a crank to limit the overall travel and actuate air valves. A physics-based simulation has been developed to supplement engine testing by assisting in the development of control strategies and identifying trends in performance. The model has already proven a useful tool in the development of an adaptive control structure for cylinder balancing, discussed in the subsequent chapter. Model data show that each cylinder behaves differently due to discrepancies in cylinder bore and piston dynamics near TDC, requiring further controls development to optimize injection timing for each cylinder individually.

CHAPTER III

Hydraulic Linear Engine Control

The HLE has low rotational inertia, facilitating brief transients and rapid startups. Consequently, the engine is more susceptible to speed fluctuations and mechanical oscillations associated with cylinder imbalance. Excessive noise, vibration, and harshness (NVH) can cause wear and reduce engine lifespan. As established in Chapter II, the HLE is inherently unbalanced due to discrepancies in cylinder geometry and slider-crank dynamics near TDC; therefore, additional steps are necessary to balance the engine.

Current approaches to cylinder balancing utilize various torque estimation techniques. Once reconstructed, torque imbalances are compared on a cycle-to-cycle basis and attributed to specific combustion events [78, 103]. Alternatively, a periodic engine description can be 'lifted' to create a time-invariant representation of the plant dynamics. Grizzle et al. [36] use this procedure to correct air-to-fuel ratio discrepancies in a spark-ignited engine while relying on a single EGO sensor in the exhaust stream.

In this chapter we apply adaptive control techniques to balance an estimate of engine rotational kinetic energy stroke-to-stroke in the presence of an unknown, periodic disturbance. We design the controller using a simplified representation and validate the strategy with a physics-based simulation.

3.1 Control-Oriented Model

Consider a single cylinder engine near dead center: the piston is momentarily stationary as shown in Figure 3.1. At this location, the rotating components account for all of the mechanical kinetic energy. Performing a simple energy balance between
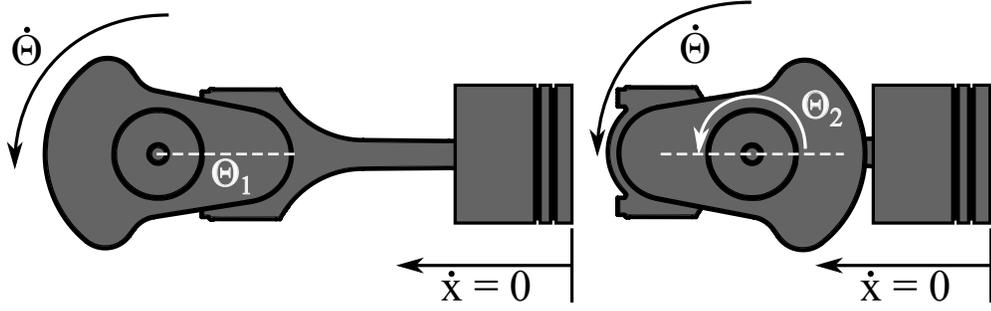
Figure 3.1: Sampling of HLE instantaneous rotational velocity at the turnaround points.

two dead center positions yields,

$$\text{KE}(\Theta_2) - \text{KE}(\Theta_1) = \frac{1}{2}J(\dot{\Theta}^2|_{\Theta=\Theta_2} - \dot{\Theta}^2|_{\Theta=\Theta_1}) = {}_1W_2. \tag{3.1}$$

where KE is the kinetic energy, J is the rotational inertia, Θ is the crank angle, and $_1W_2$ is the work done on the engine. Equation (3.1) is a convenient expression because $_1W_2$ is strictly a function of rotational velocity. Three components contribute to the work: frictional forces, hydraulic pressure forces, and in-cylinder pressure forces. Sampling every 180 CAD, at every dead center position, each of the four cylinders experiences a different process of the four-stroke cycle. Expanding the work term produces

$$_1W_2 = W_{fric} + W_{comp} + W_{exp} + W_{exh} + W_{int} + W_{hyd}, \tag{3.2}$$

where W_{fric} and W_{hyd} are the frictional and hydraulic contributions. Work terms W_{int}, W_{comp}, W_{exp}, and W_{exh} result from the in-cylinder intake, compression, expansion, and exhaust processes. Since each term refers to a different cylinder with varying

geometry, the sum of the work components changes from stroke-to-stroke.

The hydraulic and expansion work terms introduce control inputs into the system. Performing a first law balance on the cylinder undergoing the expansion stroke yields,

$$
\begin{aligned}
\Delta E_{exp} &= Q_{comb} - Q_{ht} - W_{exp} \\
&= V_f \times \rho_f \times \mathbf{LHV} - Q_{ht} - W_{exp}.
\end{aligned}
\tag{3.3}
$$

Heat loss, Q_{ht}, and the work done by the control volume, W_{exp}, both decrease the change in internal energy during expansion, ΔE_{exp}. The heat addition from combustion, Q_{comb}, is the product of injected fuel volume, V_f, fuel density, ρ_f, and the fuel lower heating value, $\mathbf{LHV}$. Fuel volume, V_f, is the controllable parameter. Rearranging (3.3):

$$
W_{exp} = V_f \times \rho_f \times \mathbf{LHV} - Q_{ht} - \Delta E_{exp}.
\tag{3.4}
$$

Assuming the accumulator pressure is constant over the duration of the stroke, the hydraulic work is

$$
W_{hyd} = \int (p_{hp} - p_{lp}) dV = \Delta p_{hc} A_{hyd} D_s \alpha_{px}.
\tag{3.5}
$$

The controllable parameter, α_{px}, is the ratio of the power extraction distance to the stroke length, D_s. We define A_{hyd} as the cross sectional area of the hydraulic pistons and Δp_{hc} as the difference in pressure between the high and low pressure accumulators, p_{hp} and p_{lp}. Substituting (3.4) and (3.5) into (3.1), and sampling every 180 CAD yields,

$$
\mathrm{KE}_{k+1} = \mathrm{KE}_k - V_f \times \rho_f \times \mathbf{LHV} - \Delta p_{hc} A_{hyd} D_s \alpha_{px} + g_k,
\tag{3.6}
$$

where

$$
g_k = W_{comp} + W_{exh} + W_{int} + W_{fric} - Q_{ht} - \Delta E_{exp}.
\tag{3.7}
$$

As defined, g_k is unknown and varies periodically with time step, k. We consider g_k as a disturbance that is a function of cylinder geometry, speed, and load.

Using the aforementioned definitions, the state space representation of (3.6) is

$$x_{k+1} = \begin{bmatrix} 1 & 0 \\ 1 & 0 \end{bmatrix} x_k + \begin{bmatrix} \rho_f \mathbf{LHV} & \Delta p_{hc} A_{hyd} D_s \\ 0 & 0 \end{bmatrix} u_k - \begin{bmatrix} g_k \\ 0 \end{bmatrix},$$

(3.8)

$$y_k = [0 \; 1]x_k,$$

(3.9)

with states and controls defined as

$$x_{1,k} = \mathrm{KE}_k, \; x_{2,k} = \mathrm{KE}_{k-1}, \; u_{1,k} = V_f, \; \text{and} \; u_{2,k} = \alpha_{px}.$$

(3.10)

Because the injection corresponding to u_k occurs just before engine speed is sampled at TDC, the control update must be calculated using the information from KE_{k-1}. The state x_2 accounts for the delay in the output.

3.2   Adaptive Cylinder Balancing

3.2.1   Control Formulation

Figure 3.2 illustrates the adaptive control structure used to adjust for cylinder imbalance.

We break the disturbance, g_k, into four unknown elements, each corresponding to the combustion event of a different cylinder. The individual disturbances, $\theta_1 - \theta_4$, interact with the system through a known regressor, ϕ_k. Let $\phi_k \theta = g_k \frac{1}{\rho_f \mathbf{LHV}}$. As shown in Figure 3.3, the regressor is a collection of four step functions such that
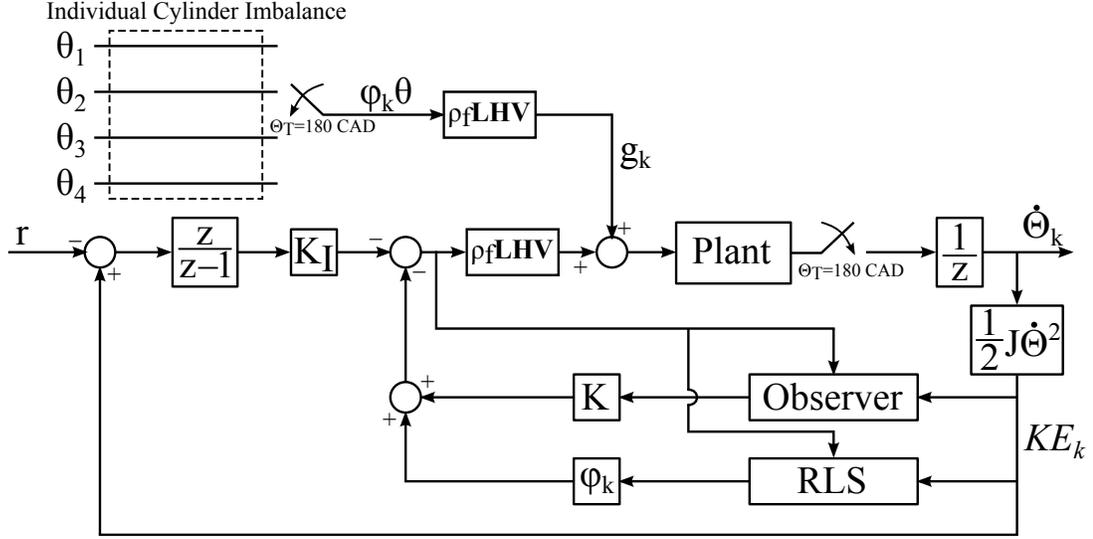
Figure 3.2: Block diagram depicting HLE adaptive control scheme.

$\phi_k = [\phi_{1,k}, \phi_{2,k}, \phi_{3,k}, \phi_{4,k}]$ and

$$\phi_k \theta = \begin{cases} \theta_1 & k = 1, 5, 9, ... \\ \theta_2 & k = 2, 6, 10, ... \\ \theta_3 & k = 3, 7, 11, ... \\ \theta_4 & k = 4, 8, 12, ... \end{cases} . \qquad (3.11)$$

Assuming zero power extraction ($u_{2,k} = 0$, and engine is at idle), (3.8) is written as

$$x_{k+1} = Ax_k + B(u_k + \phi_k \theta), \qquad (3.12)$$

where

$$A = \begin{bmatrix} 1 & 0 \\ 1 & 0 \end{bmatrix}, \ B = \begin{bmatrix} \rho_f \mathbf{LHV} \\ 0 \end{bmatrix}, \ \text{and } C = \begin{bmatrix} 0 & 1 \end{bmatrix}, \qquad (3.13)$$

corresponds to KE_{k-1} taken as output. With the slight abuse of notation, $u_k = u_{1,k}$ in (3.12). Because the observability and controllability matrices are full rank, the system is observable and controllable and we can use state feedback principles to design a stabilizing controller. We define a state observer with the observer gain, L,
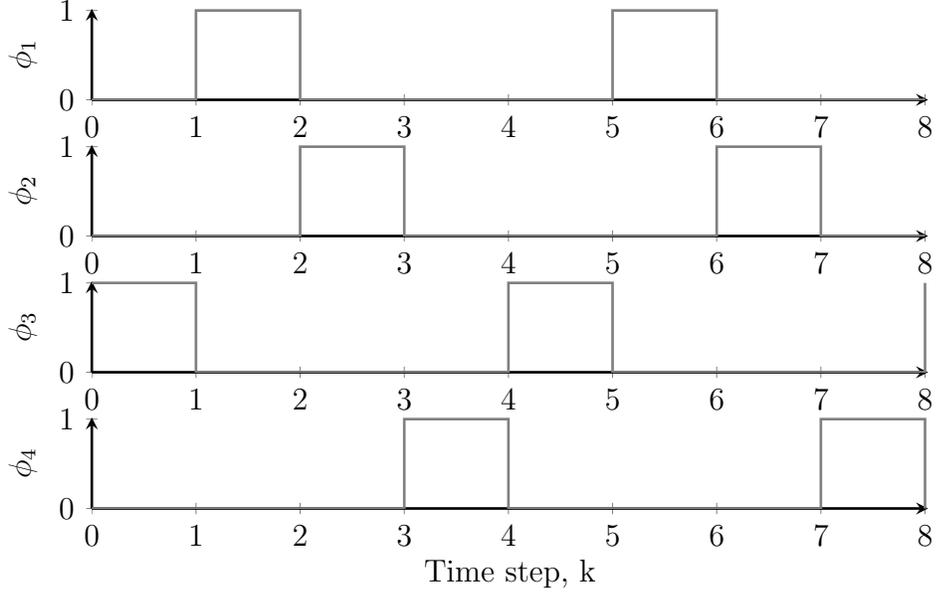
Figure 3.3: Periodic regressor behavior.

so that the state estimate, $\hat{x}$, satisfies

$$\hat{x}_{k+1} = -LCx_k + (A - LC)\,\hat{x}_k + B(u_k + \phi_k\hat{\theta}_k). \qquad (3.14)$$

where $\hat{\theta}_k$ is an estimate of θ. In order to track a reference, r, the system is augmented with an integrator,

$$w_{k+1} = Cx_k + w_k - r. \qquad (3.15)$$

where w_k is the integrator state and the reference is the kinetic energy at the desired speed, $\dot{\Theta}_r$, such that $r = {}^1\!/_2 J\dot{\Theta}_r^2$. An estimate, $\hat{\theta}$ of θ, cancels the periodic disturbance using a recursive least squares algorithm. The control law has the following form:

$$u_k = -[K, K_I]\begin{bmatrix} \hat{x}_k \\ w_k \end{bmatrix} - \phi_k\hat{\theta}_k, \qquad (3.16)$$

where K is a stabilizing state feedback gain and K_I is an integrator gain. Gains K and K_I are chosen such that the eigenvalues of the closed-loop state matrix lie within

77

the unit disc.

At the time step k, we construct a variable z_k using known inputs and measurements,

$$z_k = \frac{1}{\rho_f \mathbf{LHV}}[y_k - y_{k-1}] - u_{k-2} = \psi_k \theta, \tag{3.17}$$

where $\psi_k = \phi_{k-2}$. Equation (3.17) allows for the construction of *a priori* error, ϵ_k, or

$$\epsilon_k = z_k - \psi_k \hat{\theta}_{k-1}, \tag{3.18}$$

where $\hat{\theta}_{k-1}$ is the estimate of θ at discrete-time instant $(k-1)$. A Recursive Least Squares (RLS) algorithm with exponential forgetting yields the following update law for $\hat{\theta}_k$ [31],

$$\hat{\theta}_k = \hat{\theta}_{k-1} + \Gamma_k \epsilon_k, \tag{3.19}$$

$$\Gamma_k = \frac{\lambda^{-1} P_{k-1} \psi_k^\top}{1 + \lambda^{-1} \psi_k P_{k-1} \psi_k^\top}, \tag{3.20}$$

$$P_k = \lambda^{-1} P_{k-1} - \lambda^{-1} \Gamma_k \psi_k P_{k-1}. \tag{3.21}$$

Here, $0 < \lambda < 1$ is an exponential forgetting factor. The persistence of excitation is a sufficient condition for parameter convergence [10, 31], requiring that

$$0 < c_1 I < \sum_{n=k}^{k+T_p} \psi_k^\top \psi_k < c_2 I < \infty \tag{3.22}$$

where c_1 and c_2 are constants such that $0 < c_1 < c_2 < \infty$. Because ψ_k (and by extension $\psi_k^\top \psi_k$) periodically repeats every four iterations, consider $T_p = 3$. Clearly, $\sum_{n=k}^{k+3} \psi_k^\top \psi_k = I$. It follows that for any $T_p \geq 3$, condition (3.22) is satisfied and parameter convergence is guaranteed. Further, because the plant is considered linear and closed-loop stable, the 'key technical lemma' in Goodwin and Sin [31] can be applied to show that the system, including the RLS algorithm, is closed-loop stable and that the output tracking error approaches zero.

Figure 3.4 shows the system response to an arbitrary disturbance of $\theta = [-3, -2, -5, -1]^\top$, commanded to a reference of $r = 6$. Before time step zero, the closed-loop system is allowed to converge without the RLS algorithm. A periodic disturbance creates the periodic error. At time step 10, the adaptive controller is activated with an initial estimate of $\hat{\theta}_0 = [0, 0, 0, 0]^\top$. There is a perturbation while the updated disturbance estimate is abruptly added to the control input. As the disturbance estimation begins to converge to the correct values, the oscillations approach zero and the integrator brings the system to the desired reference. The perturbation can be decreased by using a better initial guess for the disturbance estimate, $\hat{\theta}_0$.

Figure 3.5 demonstrates that the perturbation is significantly decreased by using a better initial guess for the disturbance estimate, $\hat{\theta}_0 = [-3, -3, -3, -3]^\top$.

3.2.2 Results and Validation

The adaptive controller described in Sections 3.1 and 3.2.1 has been applied to the physics-based model in Chapter II.

Figure 3.6 shows the response of the HLE model with the adaptive RLS control scheme. The engine is at idle with zero power take-off, commanded to a speed of 1000 RPM, which corresponds to a rotational kinetic energy of approximately 1.6 kJ. Prior to iteration zero an integral controller has converged but is unable to reject the periodic disturbance resulting from the imbalanced cylinder geometry. At iteration 50 the adaptive controller is activated with an initial guess of $\hat{\theta} = [0, 0, 0, 0]^\top$. Similar to the low-fidelity response in Figure 3.4, the engine speed flares as the disturbance estimate is abruptly added. Subsequently, the disturbance estimate converges and engine speed settles to the set-point. The adaptive controller successfully decreases the amplitude of oscillations around the target by 99%.

The fuel command, u_k, is measured as volume in cubic millimeters. It follows from the definition in (3.12), that the disturbance, θ, has the same units as the fuel
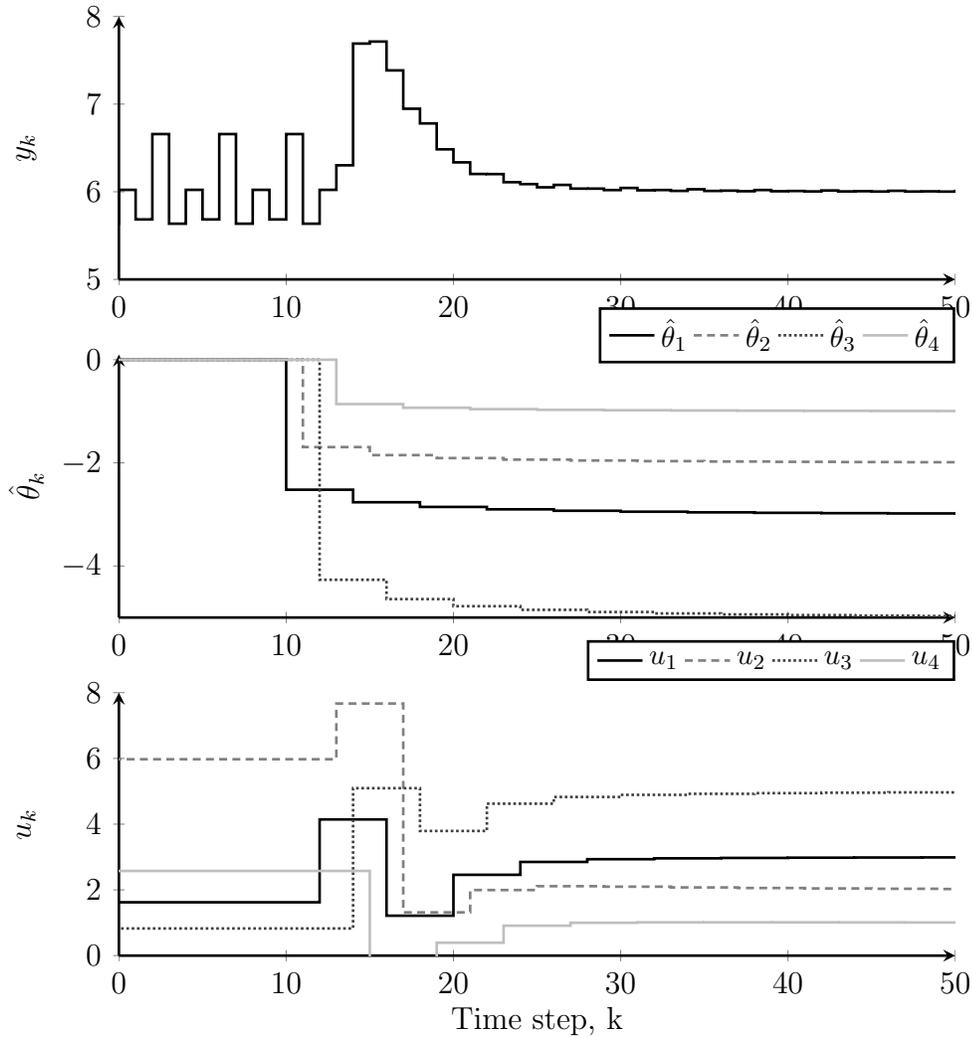
Figure 3.4: Closed-loop response of the control-oriented model and the proposed adaptive control scheme to a periodic disturbance.

command. Also note that θ is a scalar multiple of g_k, which is roughly a measurement of losses over a single stroke. Thus the disturbance estimate can be interpreted as the amount of fuel, in cubic millimeters, that does not contribute to useful work over the duration of a single stroke. In fact, the data presented in Figure 3.6 are consistent with the idea of engine idle. The disturbance estimate converges to the same value but opposite sign as the fuel command, suggesting that none of the energy in the fuel is extracted as useful work. Instead, it is all used to overcome friction and heat transfer losses.
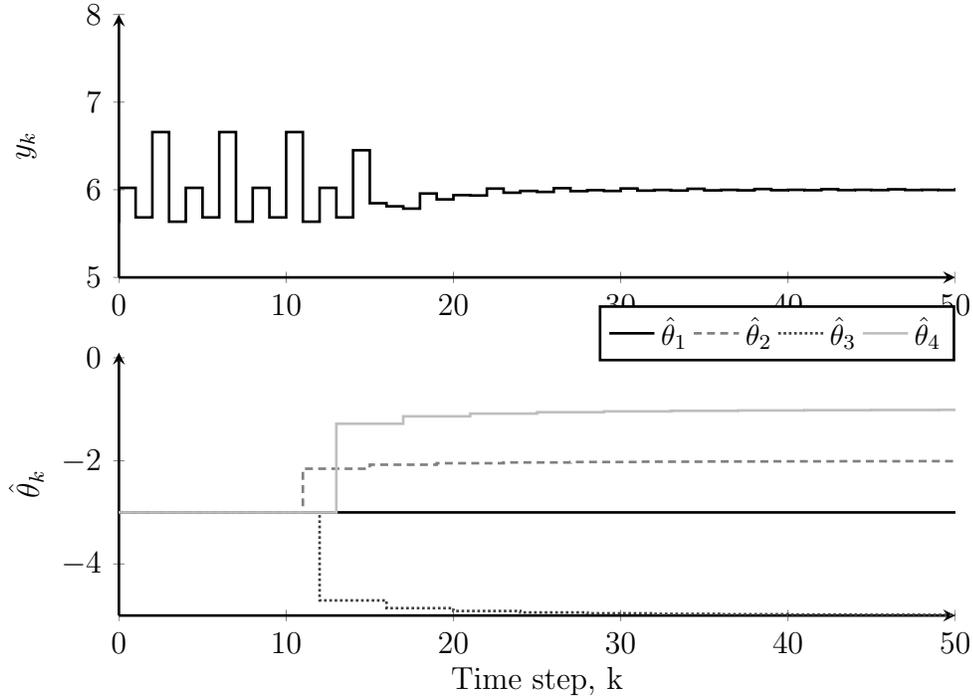
Figure 3.5: Closed-loop response of the control-oriented model and the proposed adaptive control scheme to a periodic disturbance with an improved initial disturbance estimate.

Injector calibrations convert a fuel quantity command into a pulse width. An error in calibration would result in the injection of an incorrect fuel quantity for a given command. The adaptive control scheme described in Section 3.2.1 automatically adjusts for this type of calibration errors. However, a particular fuel command would no longer directly correspond to the actual volume of fuel injected into the cylinder. As a result, the physical interpretation of the disturbance estimate loses its meaning.

Figure 3.6 displays the rotational velocity as sampled by the controller every 180 CAD. The adaptive scheme proposed focuses specifically on reducing the differences in speed between each sample. This snapshot is sufficient to balance the cylinders but is not representative of instantaneous engine dynamics shown in Figure 2.7. Large engine speed fluctuations are the result of low rotational inertia compounded by cylinder imbalance. All instantaneous variations cannot be completely eliminated because of the discrete nature of the input, yet they can be reduced through cylinder

81
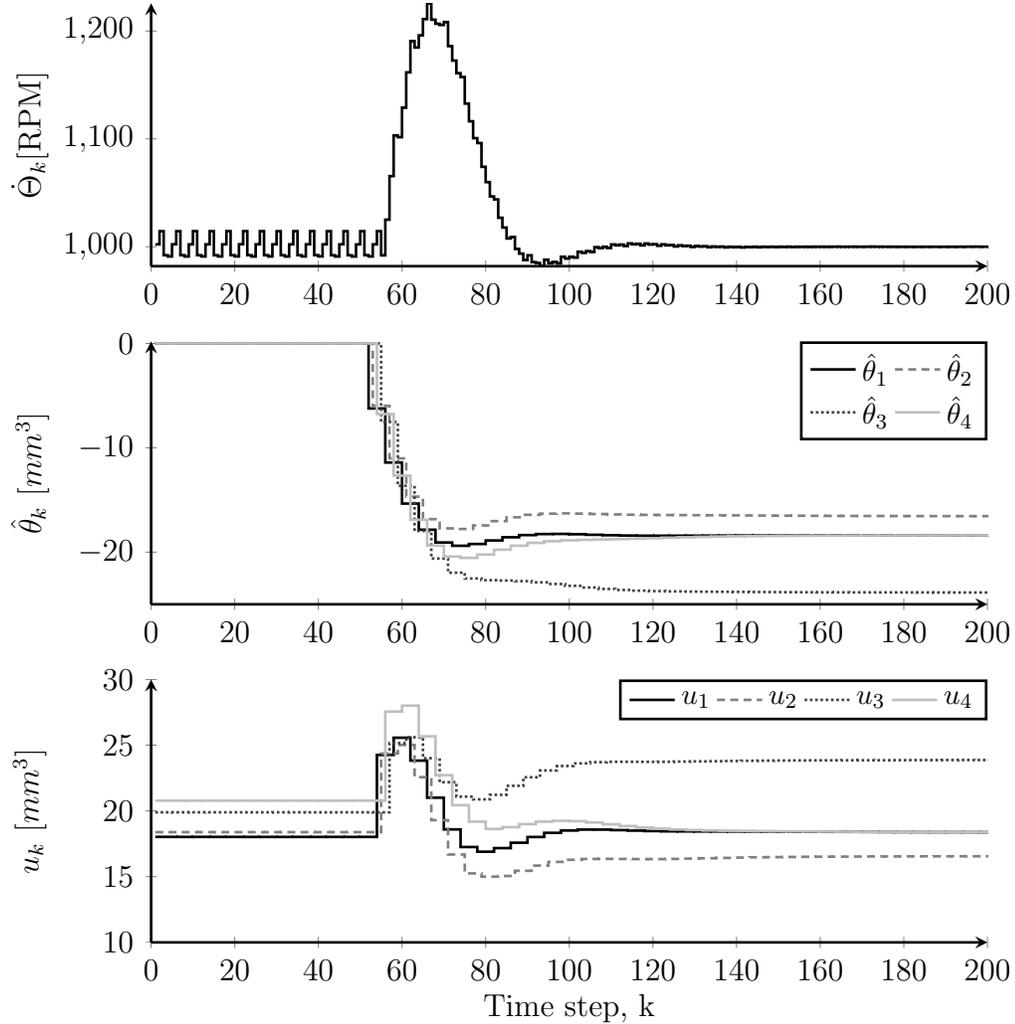
Figure 3.6: Closed-loop response of the high-fidelity model and the proposed adaptive control scheme to a periodic disturbance.

balancing. Figure 3.7 superimposes the results of applying the adaptive controller at a reference speed of 900 rpm to the high fidelity model onto the fixed fueling data illustrated in Figure 2.7. The unbalanced conditions in Figure 2.7 demonstrate the large speed fluctuations resulting from discrepancies in cylinder behavior. Balancing the engine reduces overall variation in engine speed at a given operating point.

Based on results from a physics-based simulation, Figure 3.8 illustrates the controller's capability to adjust for variations in loading of each cylinder independently. A different load, α_{px}, is applied to each cylinder at various iterations. After four
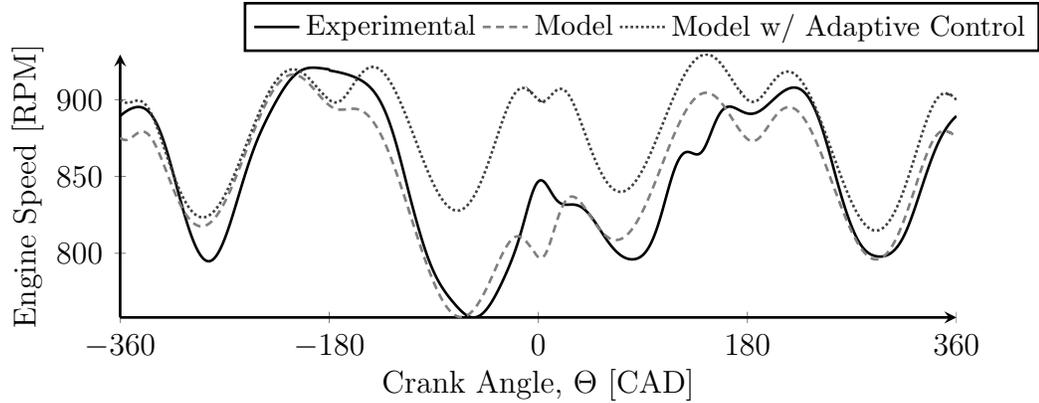
Figure 3.7: Comparison of balanced and unbalanced engine dynamics. The adaptive control scheme balances each cylinder and reduces cyclic engine speed fluctuations.

load perturbations, the speed settles to the targeted 1000 RPM and each cylinder is producing a different quantity of hydraulic work output. Speed deviations can be minimized by including an open loop estimate of the load. Individual cylinder fuel control enables the engine to run in a number of attractive configurations. For instance, it may be more efficient at lower loads to run a number of cylinders near full load while deactivating others. Alternatively, different cylinders could operate with different combustion modes, some with normal compression ignition and others with homogeneous charge compression ignition (HCCI) type combustion.
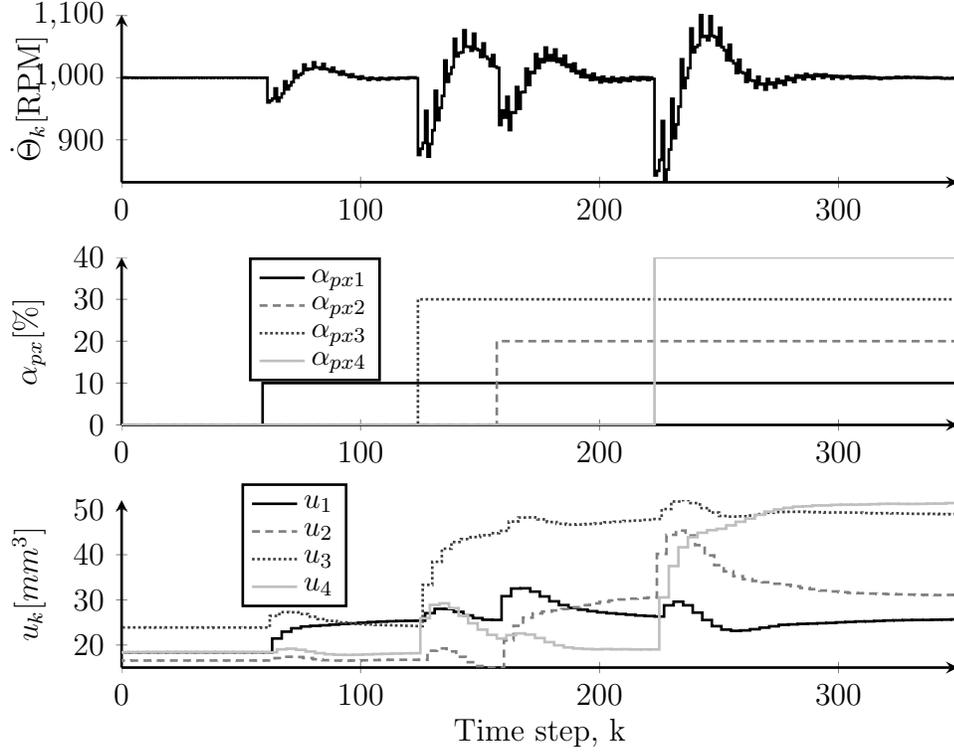
Figure 3.8: Closed-loop response of the high-fidelity model and the proposed adaptive control scheme to cylinder-dependent load variations. Each cylinder is subject to a different load applied at different time steps.

3.3 Gradient-Based Optimal Injection Timing Control

3.3.1 Extremum Seeking Algorithm

Simulation-based study of the HLE presented by Zaseck et al. in [113] and in Chapter II suggest that each cylinder behaves differently, implying that individual injector control is necessary to optimally manage fuel volume and injection timing. A comprehensive engine map would include seven dimensions: each injector (4 dimensions), engine speed, hydraulic load (PX), and accumulator pressure. The engine testing time necessary to complete and optimize a seven dimensional map is very substantial. Hence we employ an extremum seeking (ES) algorithm to adjust the injection timing of each cylinder.

There is extensive literature concerning extremum seeking methods in automo-

tive applications. For example, Popovic et al. [81] demonstrate a gradient search technique to minimize fuel consumption by applying ES to spark and valve timing. Alternatively, Killingsworth et al. [58] apply a sinusoidal perturbation to optimize HCCI combustion timing. While ES can be used to minimize offline calibration, we also envision taking advantage of the series hybrid architecture by employing ES as an on-board optimization algorithm similar to the work reported by Gupta et al. [40].

The preliminary optimization objective for the HLE is to adjust the injection timing vector, δ, as to minimize fuel consumption over the duration of one cycle while simultaneously maintaining the desired speed i.e.,

$$\min_{V_{f,k},\delta_k} \sum_{k}^{k+3} V_{f,k} \to \min, \tag{3.23}$$

subject to the constraint

$$E_k(\dot{\Theta}_k) = r; (\text{same as } \dot{\Theta}_k = \dot{\Theta}_r). \tag{3.24}$$

Future ES-based optimization will explore impacts of valve-timing.

As described in Section 3.2, the cylinder-balancing controller has already been designed to maintain speed by managing fuel quantity. To optimize the injection timing, we augment the established adaptive controller with a slower gradient search, ES algorithm as shown in Figure 3.9.

The quantity minimized is the sum of the fuel over a complete cycle, or

$$s_l = \sum_{k}^{k+3} V_{f,k} = f(\delta_l, \Delta p_{hc}, \dot{\Theta}, \alpha_{px}), \tag{3.25}$$

where δ_l denotes the injection timing vector applied in the lth iteration, $\dot{\Theta}$ is engine speed, α_{px} is the power extraction ratio, and Δp_{hc} is the pressure differential in pressure between the high and low pressure accumulators. Because we assume α_{px}
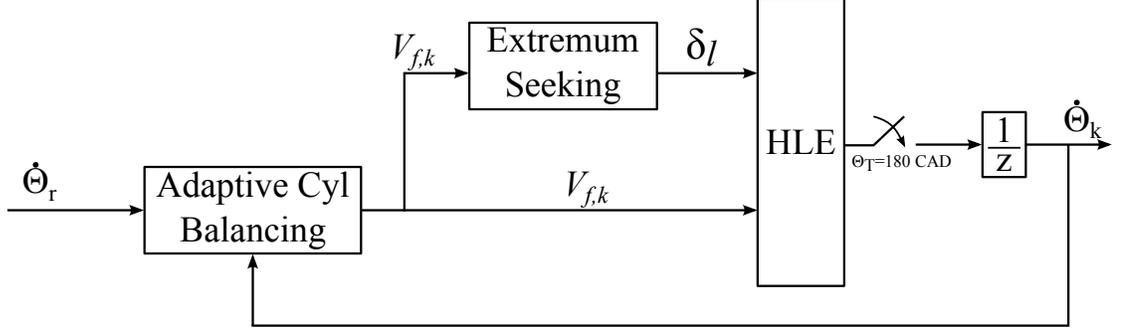
Figure 3.9: An adaptive control structure adjusts for cylinder imbalances and maintains a constant speed while an extremum seeking algorithm searches for the optimal injection timing to minimize fuel delivered to the engine.

and p_{HP} are constant and because the adaptive scheme manages speed, measurement (3.25) can be viewed as $s_l = f(\delta_l)$.

In order to estimate the gradient, we perturb the vector δ_l, in direction v_l, by a magnitude ζ. The possible perturbation directions are

$$
\begin{aligned}
v_1 &= [1, 1, 1, 1]^\top, v_2 = [-1, 1, 1, 1]^\top, v_3 = [1, -1, 1, 1]^\top, \\
v_4 &= [1, 1, -1, 1]^\top, v_5 = [1, 1, 1, -1]^\top, v_6 = [-1, -1, 1, 1]^\top, \\
v_7 &= [-1, 1, -1, 1]^\top, v_8 = [-1, 1, 1, -1]^\top.
\end{aligned}
\tag{3.26}
$$

In what follows, we apply a persistently exciting finite difference (PEFD) ES algorithm, [93], wherein the direction is chosen from a predetermined list of all possible directions recursively and in a set order. Alternatively, we also use the simultaneous perturbation stochastic approximation (SPSA) method, [91], where the direction is chosen at random.

When the HLE is perturbed, the adaptive controller returns the engine to the speed set point by adjusting the fuel command. After the system has settled, the ES scheme measures the new $f(\delta_l + \zeta v_l)$, allowing some extra time to filter the signal. Subsequently, the ES algorithm perturbs the injection timing command by the same magnitude in the opposite direction, $-v_l$, and evaluates $f(\delta_l - \zeta v_l)$. When both

measurements are available, the algorithm updates the vector of injection timings so that

$$\delta_{l+1} = \delta_l - \gamma_l v_l \frac{f(\delta_l + \zeta v_l) - f(\delta_l - \zeta v_l)}{2\zeta}, \qquad (3.27)$$

where γ_l is the update step size.

3.3.2 Results and Validations

To validate the convergence, we first apply the ES methods to the simplified system described by equations (3.8) and (3.9) where θ is modeled as a function of injection timing, δ_k, so that

$$
\begin{aligned}
\theta_1 &= -5(\delta_1 - 6)^2 - (\delta_2 - 2)^2 - (\delta_3 - 5)^2 - (\delta_4 - 3)^2 - 3, \\
\theta_2 &= -(\delta_1 - 6)^2 - 5(\delta_2 - 2)^2 - (\delta_3 - 5)^2 - (\delta_4 - 3)^2 - 2, \\
\theta_3 &= -(\delta_1 - 6)^2 - (\delta_2 - 2)^2 - 5(\delta_3 - 5)^2 - (\delta_4 - 3)^2 - 5, \\
\theta_4 &= -(\delta_1 - 6)^2 - (\delta_2 - 2)^2 - (\delta_3 - 5)^2 - 5(\delta_4 - 3)^2 - 1.
\end{aligned}
\qquad (3.28)
$$

In the simplified model δ_1, δ_2, δ_3, and δ_4 are values measured relative to certain nominal values. Figure 3.10 shows the response of a PEFD-based ES algorithm. As expected, the injection timing vector converges to the vicinity of $\delta = [6, 2, 5, 3]^\top$ and the minimum s_l is roughly 11.

Figure 3.11 shows the response s_l from the simplified model when a SPSA-based algorithm is applied. Like the PEFD case, the SPSA method successfully minimizes the function. However, because of the random direction choice, performance is not consistent. Similar behavior was shown by Popovic et al. [81]. Theoretically, with more samples and steps, the effects are minimized. Regardless, for now we choose to only apply the PEFD approach to the physics-based model.

Figure 3.12 shows the response of the physics-based model and PEFD extremum seeking algorithm at a constant speed and load. The ES algorithm successfully de-
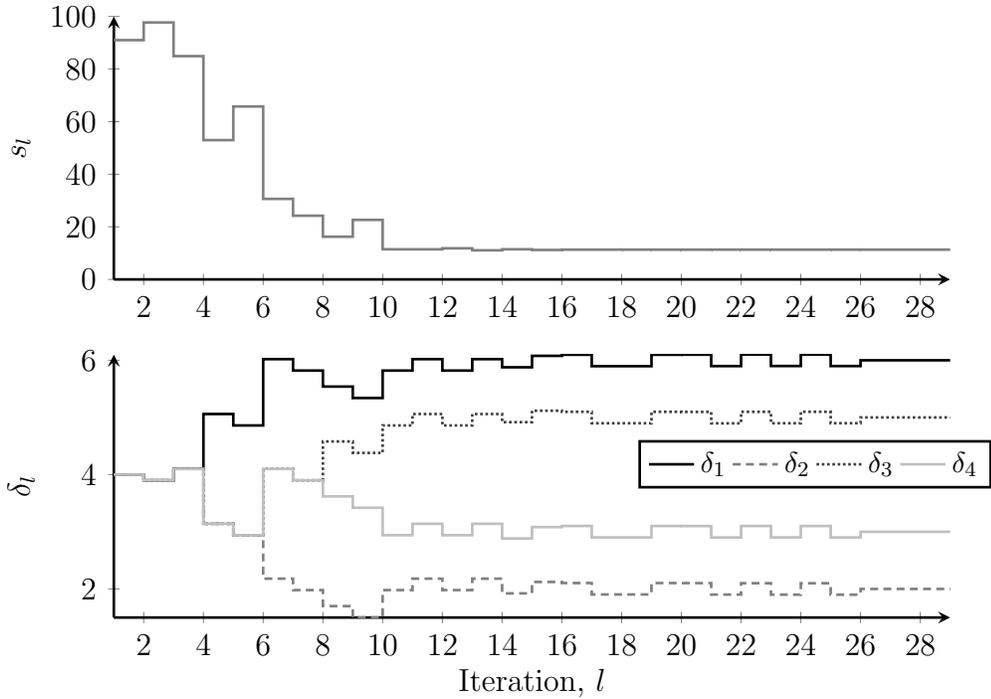
Figure 3.10: Response with the PEFD-based ES approach to on the simplified model.
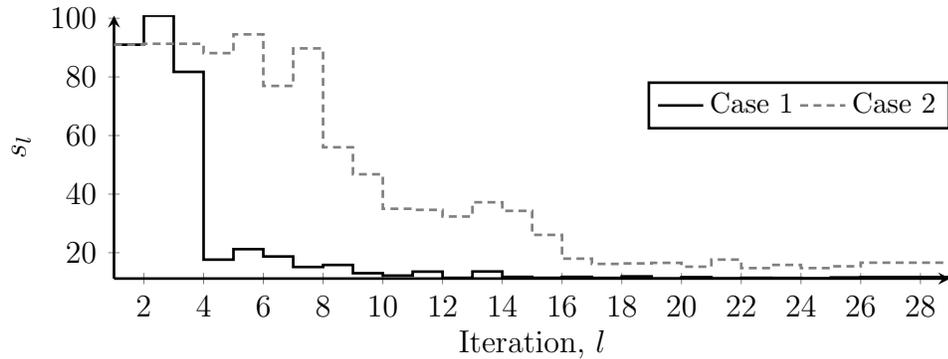
Figure 3.11: Response with the SPSA-based ES approach to on the simplified model.

creases fuel consumption. As expected, based on the results in Zaseck et al. [113] and Chapter II, the optimal injection timing response of cylinders 1 and 4 is similar. Likewise, the response of injectors for cylinders 2 and 3 is similar.
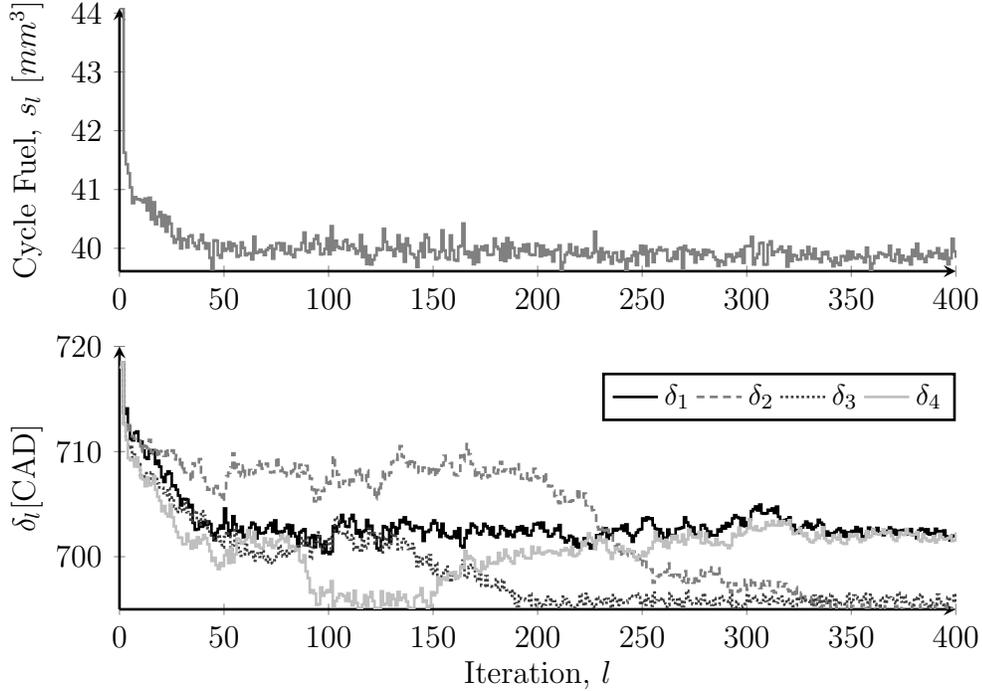
Figure 3.12: Closed-loop response of the high-fidelity model with the proposed PEFD-based ES algorithm at idle and 2000 RPM.

3.4 Conclusions

An adaptive control scheme has been developed to correct cylinder imbalance for a novel hydraulic linear engine prototype developed by the EPA. The balancing relies on estimating engine speed near dead center every 180 CAD, computing the kinetic energy, and balancing the energy using RLS algorithm with exponential forgetting. A high fidelity physics-based model was developed and used for controller development and validation. We demonstrated that the controller minimizes speed variations stroke-to-stroke by adjusting the fuel command to each cylinder individually. This also enables the engine to operate with different loads for different cylinders.

The increased number of parameters associated with optimizing injection timing make conventional approaches to engine mapping difficult and time consuming. Extremum seeking techniques intelligently search for the optimal conditions, often by estimating the local gradient by perturbing the system. In this chapter, we applied

and showed that a PEFD approach to ES improves the fuel consumption of the HLE by adjusting individual injector timing commands.

CHAPTER IV

Free-Piston Engine Control

Free-piston engines do not possess a crank to constrain piston motion. Consequently, FPE compression ratio can be rapidly tailored to a variety of combustion strategies and fuel types. As an additional benefit, FPE friction is relatively low compared to conventional internal combustion engines. The EPA has developed an FPE for application in a series hybrid vehicle, shown in Figure 1.8 [12]. However, one of the biggest hurdles preventing the proliferation of free-piston engine technology is repeatable, reliable, and robust stroke length control. Adding too much fuel can result in piston collision with the cylinder head. Insufficient fuel will produce lower than ideal compression ratios, combustion instabilities, or may even stall the engine completely. In this chapter, we consider the control of the diesel, hydraulic FPE.

Few approaches to FPE piston position control exist. Most methods to-date utilize simple PID structures and tune control gains to achieve stability. Few studies analyze or guarantee stability over a range of operating conditions.

4.1 FPE Control Literature Review

A two-part study by Mikalsen and Roskilly investigates the control of a single-cylinder, diesel FPE with a linear alternator that utilizes a bounce chamber for rebounding [72, 73]. Part one uses a model to highlight control objectives and comment

on actuator influence on the piston travel, specifically exploring injection timing, injected fuel mass, air mass in the bounce chamber, and load. The study concludes that injection timing is more appropriate for system optimization than control of a dead center position. While fuel mass, bounce chamber air, and load all affect both TDC and BDC position, the bounce chamber has a stronger correlation with BDC position rather than TDC. Further, the results stress the importance of TDC position accuracy to FPE operation and compression ratio control [72].

In part two of Mikalsen and Roskillys investigation [73], the authors considerengine dynamics and piston motion control. Their goal is to maintain a TDC piston position within ± 1 mm while keeping the compression ratio between 13 and 18. The performance outputs Mikalsen and Roskilly consider are operating frequency, TDC position, and BDC position while the control inputs are fuel mass, air mass in bounce chamber, and electric load force. Similar to previous work by Johansen [52], Mikalsen and Roskilly use intuition to reduce the complex structure into three, separate single-input single-output systems. Specifically, the authors use a continuous domain PID controller, choosing fuel mass to control TDC position and bounce chamber air mass to control BDC position. The authors ignore engine speed because it is a function of load and compression ratio. The results show that a step change in load can cause significant errors in TDC position. The paper concludes that a standard proportional plus integral control structure is not sufficient to reduce error peaks resulting from load fluctuations. As an alternative, Mikalsen and Roskilly propose combining a pseudo-derivative feedback controller with feed-forward disturbance corrections, tuned specifically to improve TDC response to a load step change. Pseudo-derivative feedback control marginally decreases TDC position error during a load change, but does not appear to satisfy the authors' requirements. The paper also comments that cycle-to-cycle variation can have a considerable effect on the response [73].

The single-cylinder, hydraulic Chiron FPE utilizes pulse-pause modulation (PPM)

as a method for compression ratio and frequency control. Since the Chiron does not have a bounce chamber, the piston assembly comes to rest after each stroke. To initiate a subsequent stroke, the Chiron FPE uses hydraulics to accelerate the piston toward the opposing cylinder head. Pulse-pause modulation alters the resting duration between strokes to modify the power output and engine speed [2]. Each stroke is an isolated event without significant impact on other strokes. The method appears to be calibration-based, without active feedback to adjust discrepancies in TDC position. Pulse-pause modulation is a popular method of control for single-cylinder free-piston engines. For instance, Hibi and Ito use PPM to control the frequency of an opposed-piston, hydraulic FPE [43].

Researchers at the Beijing Institute of Technology propose and demonstrate an augmentation to PPM techniques [37, 38, 48, 116, 117]. position feedback modulation (PFM) exploits the same resting duration control strategy outlined by Achten [2] as PPM, but uses feedback measurements and predictions of piston position to better operate the control valves and fuel injection [37]. Further studies refine the technique by adding PID control of injection timing to minimize variations in BDC position [38]. Note that injection timing-based BDC control is in conflict with the findings of Mikalsen and Roskilly who suggest using injection timing as an optimization parameter [72]. Later studies by the same institution appear to abandon injection-timing as an actuator in favor of fuel quantity-based BDC control while also implementing misfire detection via a comparison of predicted piston velocities [117]. Cyclic variation also has a small impact of up to 1% on TDC position and 3% on BDC position [116], although PFM is reported as immune [48].

Tikkanen and Vilenius propose energy balance control of a dual-piston, hydraulic FPE [97]. Specifically they use PID control with feed-forward load compensation. However, the definition of the energy control parameter is vague. The method also does not adjust for or capture discrepancies in energy compounded from previous time

steps; it only considers the error associated with measurements at the current time step. Since BDC error from the previous strokes can change the amount of air in the combustion chamber, it is important to consider preceding errors. The authors choose an estimate of indicated work as the primary controller state. Tikkanen and Vilenius control stroke length by comparing compression work to a reference compression ratio and applying an integrator state. The researchers demonstrate controller performance through simulation.

Johansen et al. [51, 52, 53] investigate the control of a two-stroke, single-cylinder FPE air compressor and power turbine. The authors separate stroke length management into two single-input single-output systems using air cushion mass to control BDC position and fuel mass to control TDC position. The control scheme is built upon energy balance principles and uses simple PID structures to stabilize and track a reference. Although the researchers present experimental results to demonstrate adequate controller behavior, the system does not appear to converge to a stable, steady-state operation [51, 53]. Johansen et al. [52] further refine their control design to include a series of state estimators that are dependent on operating frequency. The estimations are empirical in nature and lack physical interpretation or correlation. Rather, a sinusoidal function predicts certain engine behavior using a piston position measurement sampled at a fixed frequency. Once again, PI and PID control stabilize and ensure reference tracking for two single-input single-output systems. While the state estimations offer more encouraging experimental results, including stable TDC and BDC control, fluctuations are larger than the ± 1mm constraint suggested by other authors [73].

Researchers at the University of Minnesota are responsible for some of the most recent advances in FPE control through both simulation and experimental efforts on a dual-piston, hydraulic design donated by Ford Motor Company. Early efforts mirror previous FPE control publications. In 2011, Li and Sun presented a model-based

study of FPE control using PID principles to manage compression ratio by altering injected fuel mass [65]. Somewhat uniquely, however, the authors of [65] assume HCCI-type combustion. A subsequent study investigates the stability of the same hydraulic FPE with HCCI combustion. Li and Sun construct a six-state system and linearize it about a single operating point. The linearized model suggests that the system is unstable at the chosen condition. The authors only consider one equilibrium point and do not attempt to interpret the physical meaning of their results [66]. More recently, Li et al. [63] leverage repetitive control techniques with a hydraulic servo valve to control hydraulic pumping chamber pressure and piston motion. Preliminary results present effective piston motion control in three stages: without in-cylinder gas dynamics, with modeled motoring gas dynamics, and full experimental motoring. The study does not consider any firing conditions [63].

The control structure proposed in this thesis uses principles similar to Tikkanen and Vilenius [97] and Johansen et al. [52], but expands the concepts in several ways. We begin with the derivation of a control-oriented model based on the first law of thermodynamics. Similar to Li and Sun [66], by linearizing the simplified model about various equilibria, we comment on stability and sensitivity of the FPE across a range of compression ratios and loads. A state feedback control law based on dynamic inversion guarantees local stability of the closed-loop system where a Smith predictor compensates for a single time step output delay. A RLS algorithm estimates and compensates for systemic losses and other uncertainties. Finally, a reference governor manages hydraulic power take-off to ensure the piston remains within prescribed boundaries during a requested load change.

4.2 Control-Oriented Model of FPE

Figure 4.1 presents the proposed discrete FPE control structure. Similar to any conventional engine (or the HLE), the stroke of an FPE represents a discrete event

wherein fuel injection occurs only at the beginning of the stroke and fuel volume is fixed for the duration of the stroke. However, an FPE does not possess a crank to constrain piston travel. Instead, the stroke length of an FPE is determined by the balance of energy entering the system through combustion and energy leaving the system through either losses or useful work.
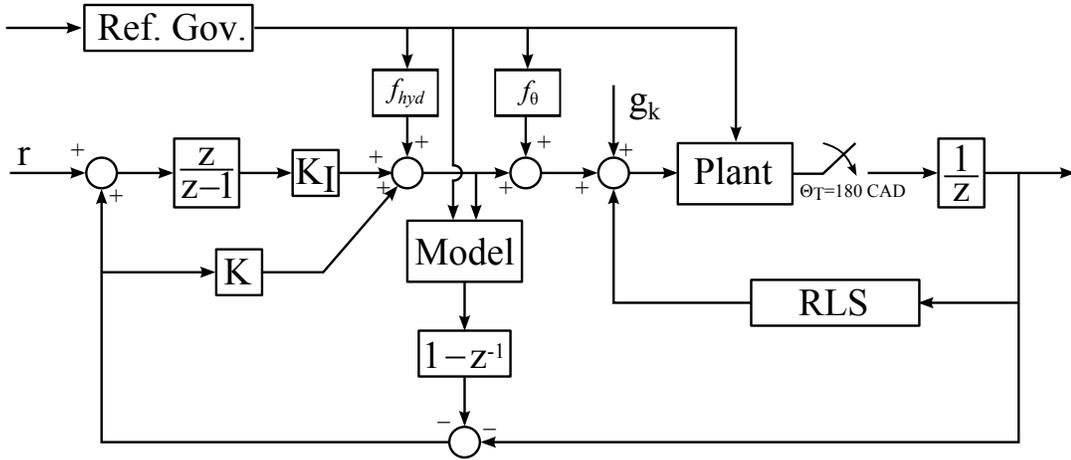
Figure 4.1: Block diagram depicting feedback control of FPE.

In order to prevent hardware damage and ensure adequate combustion conditions, the primary control objective is to maintain a reference TDC position, x_r, with minimal error. The same control objective is advocated by Mikalsen and Roskilly [72, 73]. Some researchers create an estimate of energy based on position [52], manage compression ratio [97], or constrain piston trajectory [63] as a roundabout way of TDC position control. Alternatively, we directly choose clearance height at the turnaround point as the performance variable and model state x_k because it is the critical parameter. Figure 4.2 depicts the measurement of FPE states at time step k as represented by a single dual-piston assembly.

Analogous to (3.1) in Chapter III, for any FPE there exists a function, f, describing the change in kinetic energy (or net work done on the piston assembly) between
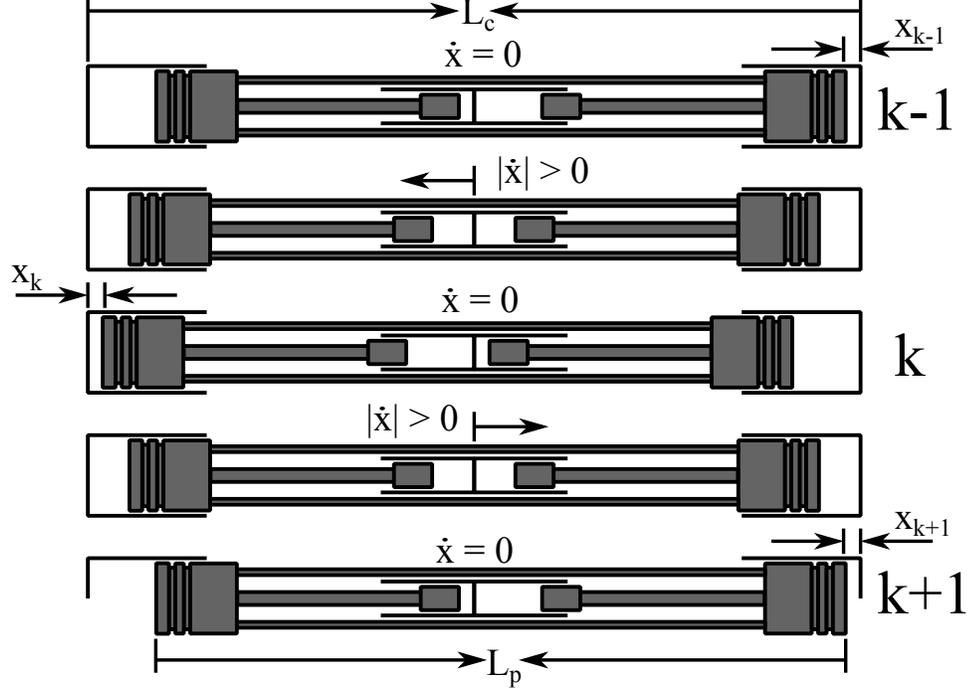
Figure 4.2: Sampling of state x at time steps $k-1$, k, and $k+1$ including depictions of piston velocity and FPE measurements.

two subsequent turn around points that satisfies the conservation of energy, or

$$f(x_{k+1}, x_k, x_{k-1}, u_k, \theta) = W_{comp} + W_{exp} + W_{exh} + W_{int} + W_{hyd} + W_{fric} = 0. \quad (4.1)$$

Here θ is a loss parameter and u_k is control input consisting of a fuel quantity command, $u_{1,k}$, and a hydraulic power extraction command, $u_{2,k}$. The function F corresponds to (4.1) and describes the evolution of x_k such that

$$x_{k+1} = F(x_k, x_{k-1}, u_k, \theta). \quad (4.2)$$

Like (3.2), W_{int}, W_{comp}, W_{exp}, and W_{exh} denote the boundary work from each process of the four-stroke cycle, W_{fric} is the work lost to friction, and W_{hyd} is the hydraulic work output. Elaborating on (4.1), the piston assembly is by definition stationary at the dead center positions and kinetic energy is zero regardless of the clearance height.

Therefore, the change in kinetic energy between two sampled points is necessarily zero. It follows that the net work done on and by the system is also zero. The objective is to control the energy balance using fuel quantity and hydraulic power extraction such that the TDC clearance approaches a set-point, x_r. Otherwise put, the control law, u_k, must lead to $x_k \to x_r$ as $k \to \infty$.

In order to construct a simplified control-oriented model, we approximate f as $\hat{f}$ such that

$$\hat{f}(x_{k+1}, x_k, x_{k-1}, u_k, \theta) = \hat{W}_{comp} + \hat{W}_{exp} + \hat{W}_{exh} + \hat{W}_{int} + \hat{W}_{hyd} + \hat{W}_{fric} = 0. \quad (4.3)$$

As expressed by a four-stroke Otto cycle, the boundary work terms are

$$\hat{W}_{exp} = - \left(u_{1,k} \rho_f \mathbf{LHV} + \frac{p_i A}{\gamma - 1} \frac{(L - x_{k-1})^\gamma}{x_k^{\gamma-1}} \right) \eta_k, \quad (4.4)$$

$$\hat{W}_{comp} = \frac{p_i A (L - x_k)}{\gamma - 1} \left(\left[\frac{L - x_k}{x_{k+1}} \right]^{\gamma-1} - 1 \right), \quad (4.5)$$

$$\hat{W}_{int} = p_i A \left(L - x_{k+1} - x_k \right), \quad (4.6)$$

$$\hat{W}_{exh} = -p_e A \left(L - x_{k+1} - x_k \right), \quad (4.7)$$

$$\hat{W}_{hyd} = -\Delta p_{hyd} A_{hyd} \left(u_{2,k} - x_{k+1} \right), \quad (4.8)$$

where the control input, $u_{1,k}$, is the volume of fuel injected, $\mathbf{LHV}$ is fuel's lower heating value, ρ_f is the fuel density, p_i is the intake pressure, p_e is the exhaust pressure, A is the cross sectional cylinder area, γ is the ratio of specific heats, Δp_{hyd} is the hydraulic pressure differential, A_{hyd} is the cross sectional area of the hydraulic chamber. The variable η_k is similar to the Otto cycle efficiency,

$$\eta_k = 1 - \left[\frac{x_k}{L - x_{k+1}} \right]^{\gamma-1}. \quad (4.9)$$

The piston's total travelable length, L, is the difference between the distance between the cylinder heads, L_c, and the piston assembly length, L_p, or $L = L_c - L_p$. The model assumes isentropic compression and expansion processes as well as constant volume heat addition and heat rejection. Unlike other hydraulic FPEs, the EPA design possesses some flexibility to modify hydraulic work output by altering the power extraction length as control input $u_{2,k}$. For preliminary feedback control, we assume $u_{2,k}$ and Δp_{hyd} are fixed and consider the associated terms as a disturbance. Section 4.9 discusses hydraulic more in depth. Frictional work is approximately proportional to the stroke length, or

$$\hat{W}_{fric} = (L - x_{k+1} - x_k)\theta, \tag{4.10}$$

where θ is an uncertain loss parameter. Note that the work terms assume a flat piston geometry where cylinder-volume is zero at $x_k = 0$. Alterations to (4.1) and (4.9) are necessary to capture the impacts of piston bowl on cylinder geometry.

For this study we assume intake and exhaust both occur at the same pressure ($p_i = p_e$) implying that W_{int} and W_{exh} have the same magnitude but opposite sign. Consequently, intake and exhaust work cancel.

Note that expansion work in (4.4) can be interpreted as the fuel energy multiplied by some efficiency plus the amount of energy recovered from the compression work. Because the intake event concluding at time step $k-1$ corresponds to the combustion chamber undergoing expansion starting at time step k, (4.4) is dependent on x_{k-1}. By contrast, if $x_{k+1} = x_k = x_{k-1} = x_r$, all compression work is recovered in the expansion stroke and $W_{exp} + W_{comp} = u_{1,k}\rho_f\mathbf{LHV}\eta_r$.

4.3 Linear FPE Control

Equations (4.3)-(4.10) implicitly approximate the behavior of x_{k+1} as $\hat{F}$, or

$$x_{k+1} = F(x_k, x_{k-1}, u_k, \theta) \simeq \hat{F}(x_k, x_{k-1}, u_k, \theta). \tag{4.11}$$

Using the first-order Taylor series expansion and assuming losses enter the system as the unknown parameter g_k, a linear approximation has the form,

$$
\begin{bmatrix} x_{k+1} \\ x_k \end{bmatrix} = \begin{bmatrix} \frac{\partial \hat{F}}{\partial x_k} & \frac{\partial \hat{F}}{\partial x_{k-1}} \\ 1 & 0 \end{bmatrix} \begin{bmatrix} x_k \\ x_{k-1} \end{bmatrix} + \begin{bmatrix} \frac{\partial \hat{F}}{\partial u_{1,k}} \\ 0 \end{bmatrix} \begin{bmatrix} u_{1,k} - \begin{bmatrix} g_k \\ 0 \end{bmatrix} \end{bmatrix}.
$$

$$\tag{4.12}$$

Exploiting (4.3), the sensitivity functions are

$$\frac{\partial x_{k+1}}{\partial x_k} \simeq \frac{\partial \hat{F}}{\partial x_k} = \frac{\partial \hat{f}}{\partial x_k} \left(\frac{\partial \hat{f}}{\partial x_{k+1}} \right)^{-1} \Bigg|_{(x=x_r, u=u_{hyd}, \theta=\hat{\theta}_{ol})}, \tag{4.13}$$

$$\frac{\partial x_{k+1}}{\partial x_{k-1}} \simeq \frac{\partial \hat{F}}{\partial x_{k-1}} = \frac{\partial \hat{f}}{\partial x_{k-1}} \left(\frac{\partial \hat{f}}{\partial x_{k+1}} \right)^{-1} \Bigg|_{(x=x_r, u=u_{hyd}, \theta=\hat{\theta}_{ol})}, \tag{4.14}$$

$$\frac{\partial x_{k+1}}{\partial u_{1,k}} \simeq \frac{\partial \hat{F}}{\partial u_{1,k}} = \frac{\partial \hat{f}}{\partial u_{1,k}} \left(\frac{\partial \hat{f}}{\partial x_{k+1}} \right)^{-1} \Bigg|_{(x=x_r, u=u_{hyd}, \theta=\hat{\theta}_{ol})}, \tag{4.15}$$

where $\hat{\theta}_{ol}$ is an open-loop disturbance estimate. The equilibrium fuel volume, $u_{1,k} = u_{hyd}$, ignores friction and assumes fuel is only necessary to balance the hydraulic work, or

$$u_{hyd} = \frac{\Delta p_{hyd} A_{hyd}}{\rho_f \mathbf{LHV} \eta_r} (u_{2,k} - x_r). \tag{4.16}$$

At equilibrium, η_k is the Otto cycle efficiency η_r. Because the injectors deliver fuel volume $u_{1,k}$ before the corresponding measurement of TDC clearance state x_k is avail-

able, the output y experiences a single time step pure delay such that

$$y_k = \begin{bmatrix} 0 & 1 \end{bmatrix} \begin{bmatrix} x_k \\ x_{k-1} \end{bmatrix}. \tag{4.17}$$

By evaluating the partial derivatives in (4.12)-(4.15) at the desired set-point, a time-invariant system model is obtained.

Figure 4.3 presents partial derivates $\frac{\partial \hat{F}}{\partial x_k}$, $\frac{\partial \hat{F}}{\partial x_{k-1}}$, and $\frac{\partial \hat{F}}{\partial u_{1,k}}$ as a function of equilibrium clearance height for various loading conditions. The partial derivatives represent the model sensitivity to x_k, x_{k-1}, and u_k. Because the sensitivities are not constant, the model demonstrates nonlinear behavior.

In Figure 4.3, $\frac{\partial \hat{F}}{\partial x_k}$ has higher magnitudes than $\frac{\partial \hat{F}}{\partial x_{k-1}}$ suggesting that x_{k+1} is more sensitive to x_k than x_{k-1}. Physically, a higher sensitivity to x_k implies that the future clearance height is more dependent on accuracy of the TDC than BDC. At equilibrium of $x_r = 0$, the piston is in contact with the cylinder head and (4.3) experiences a singularity. As the equilibrium approaches zero, η_r approaches unity. Consequently, $\frac{\partial \hat{F}}{\partial x_{k-1}}$ decreases towards zero and sensitivity to x_k moves towards one. More importantly, Figure 4.3 shows that control authority ($\frac{\partial x_{k+1}}{\partial u_{1,k}}$) approaches zero as $x_r \to 0$. Reduced control authority indicates that as the equilibrium advances closer to the cylinder head, the system experiences a less significant change in clearance due to alterations or variations in fuel quantity. Higher compression ratios are therefore more robust to combustion-related disturbances but require greater actuator effort to change position. These results insinuate that it is desirable for an FPE to possess the greatest possible compression ratio at $x_r = 0$ to prevent collision with the cylinder head. As modeled, the compression ratio, and by extension compression work, become infinite at the cylinder head. The addition of a piston bowl increases volume at $x_r = 0$ and thus is potentially detrimental. Further investigation is necessary to determine the exact impact and validate these considerations.
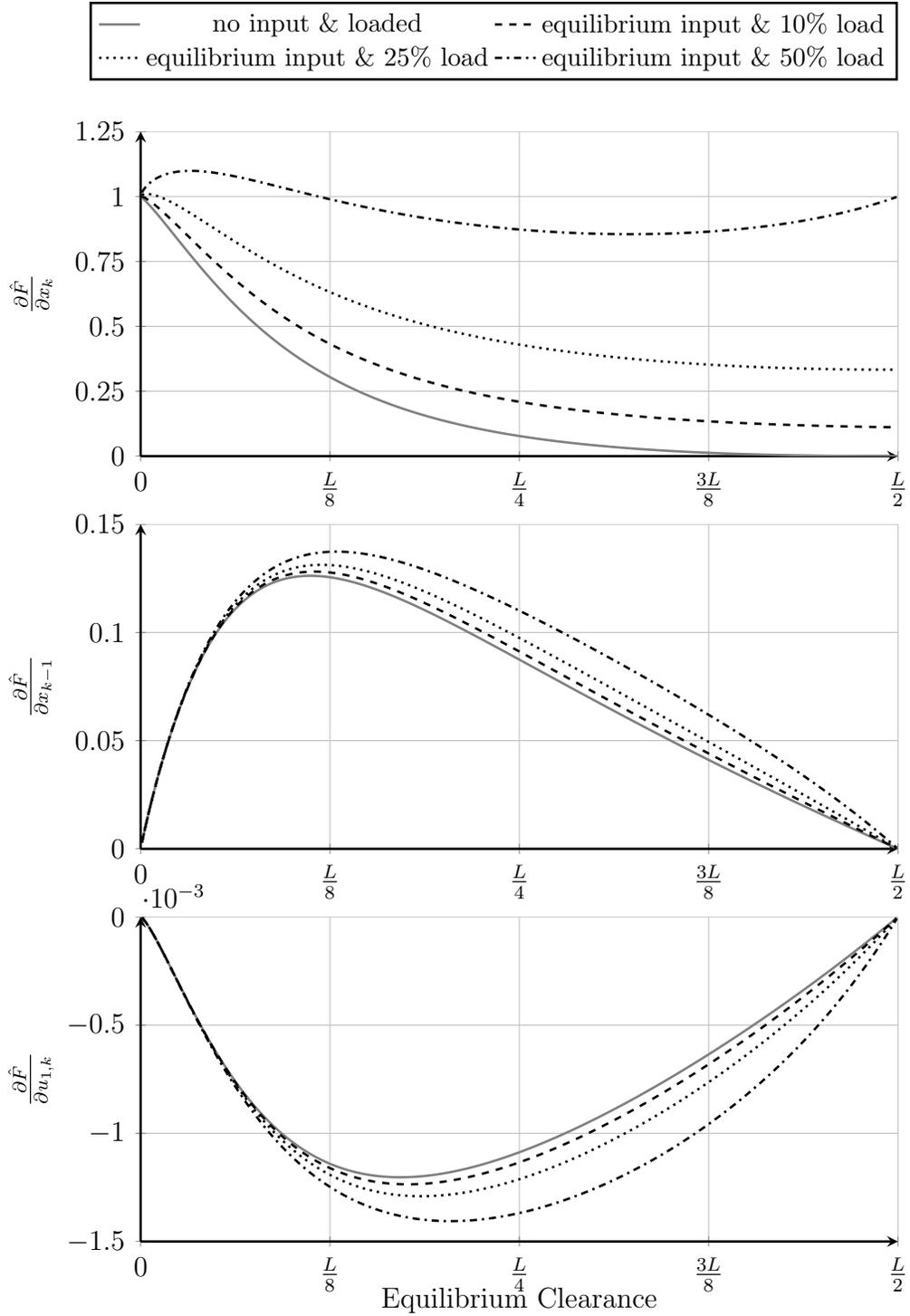
Figure 4.3: Sensitivity of control-oriented model parameter x_{k+1} to x_k, x_{k-1}, and u_k linearized over a range of equilibria for a variety of loading conditions.

The idealized analysis portrayed in Figure 4.3 extends to a range of equilibria and compression ratios where combustion is not necessarily realistic due to either

insufficient activation energy or excessive pressure rise. At equilibrium $x_r = \frac{L}{2}$ the piston is stationary halfway between the cylinder heads, the compression ratio is 1:1, and η_r becomes zero.

Figure 4.4 shows the maximum eigenvalue magnitude corresponding to open-loop system (4.12). Since the description is discrete, the approximation is stable if all eigenvalues fall within the unit disc [57]. The plot considers the system with and without fuel, both loaded and unloaded. The unloaded condition does not consider friction while the loaded conditions include lump friction with hydraulics. Note that event-to-event sampling effectively aliases the system, removing the oscillatory behavior. As a result, the eigenvalues in Figure 4.4 lie on the real axis. Without load and fuel input, the simplified FPE model presents a maximum eigenvalue magnitude of 1.0 at every equilibrium in Figure 4.4 indicating the system is marginally stable. At these conditions, the FPE is essentially a mass oscillating between two lossless air-springs, repeating the same clearance measurement at every sample. Figure 4.4 reveals that when loaded but without fuel, all model eigenvalues are within the unit disc and the system is open-loop stable for the entire considered range. Intuitively, with an excess of energy leaving, the FPE may start at some initial displacement and decay until it reaches an equilibrium of $\frac{L}{2}$.

For the equilibrium input in Figure 4.4, $u_{1,k} = u_r = u_{hyd}$. As fuel and load increase, Figure 4.4 indicates that the open-loop system becomes progressively more unstable for an equilibrium close to the cylinder head. At any loaded and fueled condition, additional displacement increases the magnitude of both energy entering the system as boundary work and the energy leaving the system as frictional or hydraulic work. However, instability at high fuel equilibria occurs because the change in work entering is greater than the change in work out. As an illustrative example, suppose the FPE is operating at an unstable equilibrium with constant fuel. If any disturbance causes an increase in displacement, the increased expansion stroke boosts
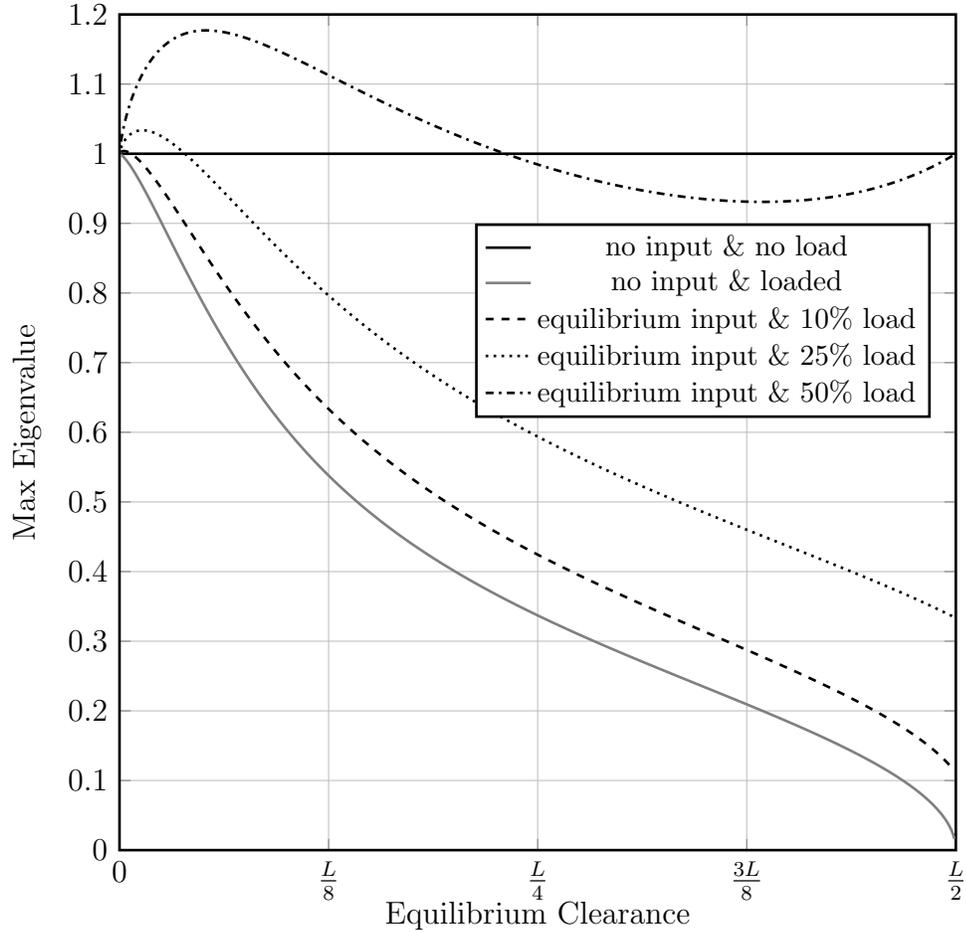
Figure 4.4: Max eigenvalue of the control-oriented model linearized over a range of equilibria for a variety of loading conditions.

efficiency and increases the quantity of usable fuel energy entering the system. The additional stroke length also increases compression work in the opposing cylinder. Hydraulic and frictional work are both proportional to stroke length and increase as well. At the unstable conditions, the increase of usable fuel energy is greater than sum of compression, hydraulic, and frictional work leaving the system. As a result, with constant fuel the subsequent clearance height decreases, further compounding the efficiency improvement. Compression ratio and efficiency continue to increase with decreasing clearance, with the piston asymptotically approaching the cylinder head. The converse is also true: if the disturbance causes a decrease in displacement, reduced efficiencies cascade and clearance heights decline. The results in Figure 4.4

agree with Li et al. [66] who predicted an unstable equilibrium for a single operating point.

As stated previously, the control objective is to track and maintain a reference clearance height, x_r. Working from the linearized representation (4.12), we augment the system with an integrator state, w_k, to ensure reference tracking analogous to the method illustrated in Chapter III where

$$w_{k+1} = y_k + w_k - x_r. \tag{4.18}$$

Because the system is potentially open-loop unstable, an integrator is not sufficient to stabilize the FPE at a desired equilibrium clearance height. Rather, we use state feedback techniques to ensure a stable closed-loop system. The feedback control law for $u_{1,k}$ based on dynamic inversion [88] is

$$u_{s,k} = -\left(\frac{\partial \hat{F}}{\partial u_k}\right)^{-1} \left[\frac{\partial \hat{F}}{\partial x_k} + K_1, \quad \frac{\partial \hat{F}}{\partial x_{k-1}} + K_2, \quad K_I\right] \begin{bmatrix} x_k \\ x_{k-1} \\ w_k \end{bmatrix}. \tag{4.19}$$

We choose gains K_1, K_2, and K_I such that the closed-loop poles of the linearized system based on (4.12), i.e., of

$$\begin{bmatrix} x_{k+1} \\ x_k \\ w_{k+1} \end{bmatrix} = \begin{bmatrix} -K_1 & -K_2 & -K_I \\ 1 & 0 & 0 \\ 0 & 1 & 1 \end{bmatrix} \begin{bmatrix} x_k \\ x_{k-1} \\ w_k \end{bmatrix} + \begin{bmatrix} 0 \\ 0 \\ 1 \end{bmatrix} x_r - \begin{bmatrix} g_k \\ 0 \\ 0 \end{bmatrix},$$

$$\tag{4.20}$$

lie within the unit disc, guaranteeing local stability [57]. To place the poles of (4.3), we utilize linear quadratic regulator techniques.

4.4 Smith Predictor

The FPE output measurement of state x_k suffers from a single time step delay because fuel is injected shortly prior to the associated TDC position. Accordingly, not all states are accessible for full state feedback techniques such as the control law proposed in (4.19). We therefore add a Smith predictor to compensate for the delay [76, 89]. For example, consider a discrete-time system with closed-loop transfer function

$$T(z) = \frac{C(z)G(z)}{1 + C(z)G(z)}. \tag{4.21}$$

Feedback controller $C(z)$ is designed for plant $G(z)$ in the absence of any delay to produce the desired closed-loop transfer function $T(z)$. If $C_d(z)$ is another controller designed on the basis of $C(z)$ that compensates for the plant with a delay, the closed-loop transfer function with a delay of d steps becomes

$$T_d(z) = \frac{C_d(z)G(z)z^{-d}}{1 + C_d(z)G(z)z^{-d}}. \tag{4.22}$$

A Smith predictor functions by matching $T_d(z)$ to $T(z)z^{-d}$. In order to ensure that

$$T_d(z) = \frac{C(z)G(z)}{1 + C(z)G(z)}z^{-d}, \tag{4.23}$$

the new controller, $C_d(z)$, must necessarily have the form

$$C_d(z) = \frac{C(z)}{1 + C(z)G(z)[1 - z^{-d}]}. \tag{4.24}$$

Because the delay makes the output of $G(z)$ inaccessible at time step k, a Smith predictor estimates states x_k and x_{k-d} as $\hat{x}_k$ and $\hat{x}_{k-d}$ using the plant model $\hat{G}(z)$. As shown in Figure 4.5, a Smith predictor adjusts the final feedback signal from using the unavailable state x_k to the quantity $x_{k-d} + \hat{x}_k - \hat{x}_{k-d}$.
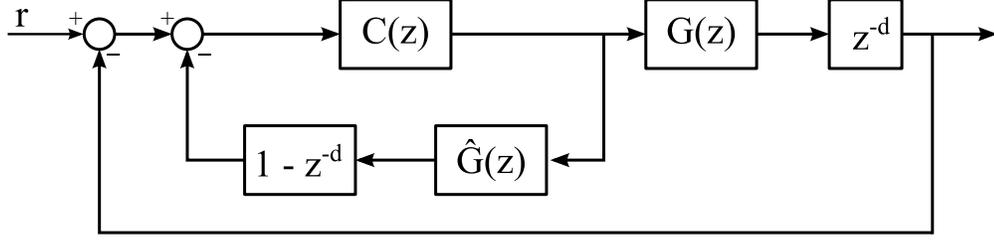
Figure 4.5: Block diagram depicting theoretical Smith predictor.

The FPE experiences a single time step delay, or $d = 1$. The control-oriented model $\hat{F}$ estimates states x_k and x_{k-1} as $\hat{x}_k$ and $\hat{x}_{k-1}$, respectively. Implementing the Smith predictor, the control law (4.19) is modified to

$$
u_{s,k} = -\left(\frac{\partial \hat{F}}{\partial u_k}\right)^{-1} \left[\frac{\partial \hat{F}}{\partial x_k} + K_1, \quad \frac{\partial \hat{F}}{\partial x_{k-1}} + K_2, \quad K_I\right] \begin{bmatrix} \hat{x}_k + x_{k-1} - \hat{x}_{k-1} \\ \hat{x}_{k-1} + x_{k-2} - \hat{x}_{k-2} \\ w_k \end{bmatrix}.
$$
(4.25)

Incorporating a Smith predictor introduces two potential issues: $\hat{F}$ cannot be found explicitly from the model $\hat{f}$ and discrepancies in model and plant behavior may produce a steady state position error. As a remedy, we use Newton's method to estimate the implicit function $\hat{F}$ and we use an adaptive RLS algorithm to adjust for losses and uncertainty.

4.5   Prediction

Because $\hat{f}$ is an implicit function, an explicit solution for $\hat{F}$ does not exist. As an alternative, we implement Newton's method to approximate $\hat{F}$. Newton's method is an iterative root finding technique applicable to differentiable, real-valued functions. It can be verified that for $\hat{f}$ defined in (4.1), there is necessarily some $\hat{x}_k$ for which $\hat{f}(\hat{x}_k, x_{k-1}, x_{k-2}, u_{k-1}, \theta) = 0$. Supposing $\hat{f}$ is continuously differentiable with a nonzero derivative at $\hat{x}_k$, Newton's method guarantees convergence to $\hat{x}$ for a sufficiently close initial guess, $\hat{x}_{k,0}$. We initialize the system at $\hat{x}_{k,0} = y_k = x_{k-1}$. The

search algorithm has the form

$$\hat{x}_{k,i+1} = \hat{x}_{k,i} - \frac{\hat{f}(\hat{x}_{k,i}, y_k, y_{k-1}, u_{k-1}, \theta)}{\frac{\partial \hat{f}}{\partial \hat{x}_k}\Big|_{\hat{x}_{k,i}, y_k, y_{k-1}, u_{k-1}, \theta}}, \tag{4.26}$$

where i denotes the iteration number. In practice, (4.26) iterates until the relative change in subsequent solutions reduces below a specified threshold, or is alternately terminated after a fixed number of iterations. With a threshold of $\frac{|\hat{x}_{k,i} - \hat{x}_{k,i-1}|}{min(|\hat{x}_{k,i}|, |\hat{x}_{k,i-1}|)} < 1 \times 10^{-9}$, we observe Newtons method converging within approximately 15 iterations.

4.6 FPE Model Adaptation

Errors in estimate $\hat{x}_k$ negatively impact controller stability and tracking. We therefore implement a recursive least squares algorithm to adapt for and decrease discrepancies between x_k and $\hat{x}_k$. The basic approach involves estimating the loss parameter, θ, online assuming the a relation

$$\hat{f}(x_k, x_{k-1}, u_{k-1}, \theta) = \hat{f}(\hat{x}_k, \hat{x}_{k-1}, u_{k-1}, \theta) + \hat{f}_E(x_k, x_{k-1}, u_{k-1}, \theta), \tag{4.27}$$

where

$$\hat{f}_E = (L - x_{k-1} - x_k)\theta. \tag{4.28}$$

Because the idealized Otto cycle model $\hat{f}$ does not account for losses, we assume friction is the primary component of error function, f_E. Therefore the deficit between x_k and $\hat{x}_k$ is proportional to stroke length, analogous to (4.10). Recalling $y_k = x_{k-1}$, (4.27) and (4.28) can be evaluated using known measurements and inputs at time step k corresponding to

$$\hat{f}(y_k, y_{k-1}, u_{k-2}, \theta) = \hat{f}(\hat{y}_k, \hat{y}_{k-1}, u_{k-2}, \theta) + (L - y_{k-1} - y_k)\theta. \tag{4.29}$$

Using relationship (4.29), z_k is an *a priori* error parameter defined as

$$z_k = \frac{\hat{f}(y_k, y_{k-1}, u_{k-2}, \theta) - \hat{f}(\hat{y}_k, \hat{y}_{k-1}, u_{k-2}, \theta)}{L - y_{k-1} - y_k}. \tag{4.30}$$

The adaption is based on the RLS algorithm described by (3.18)-(3.21) in Chapter III and estimates θ as $\hat{theta}_k$.

For the majority of control design we have assumed constant hydraulic load, for which θ would remain close to stationary. However, as load and fuel increase, friction and hence θ also increase. While the proposed RLS mechanism effectively adjusts for changes in θ, accuracy becomes more critical when ensuring the piston tracks the desired clearance during a load change. To assist with load following, we include an open-loop disturbance estimate, $\hat{\theta}_{ol}$, where for out model

$$\hat{\theta}_{ol} = -27163 \times u_{2,k} - 504, \tag{4.31}$$

and $u_{2,k}$ is the hydraulic load command. Equation (4.31) describes a linear relationship between $u_{2,k}$ and $\hat{\theta}_{ol}$ based on the model data shown in Figure 4.6. Based on
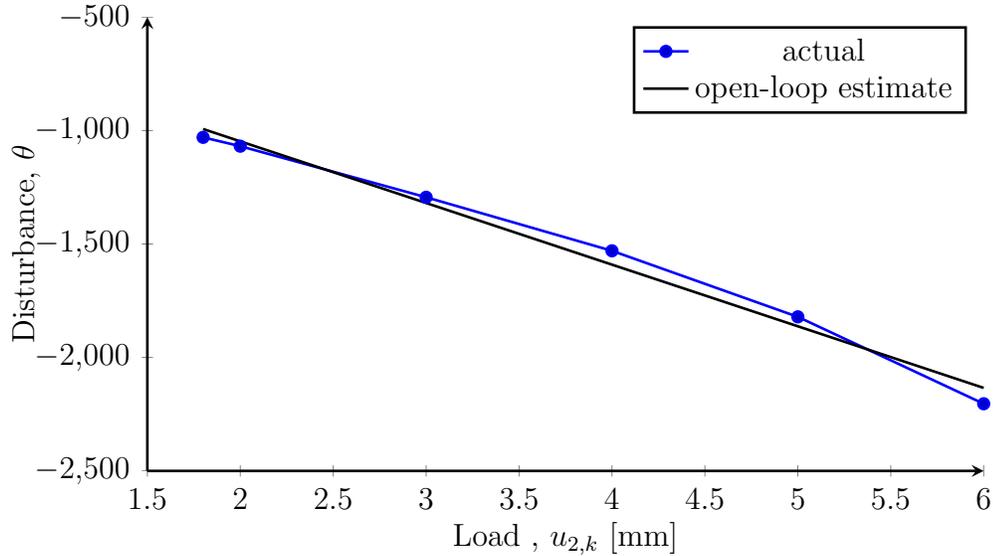
Figure 4.6: Open-loop disturbance estimate as a function load.

109

energy / work interpretations, the control update to adjust for losses is

$$u_\theta = -\frac{(L - 2x_r)\tilde{\theta}}{\rho_f \mathbf{LHV} \eta_r},$$

(4.32)

where

$$\tilde{\theta} = \hat{\theta}_k + \hat{\theta}_{ol}.$$

(4.33)

4.7   Final Control Update

The final control update combines the above constituents,

$$u_{1,k} = u_s + u_\theta + u_{hyd},$$

(4.34)

where (4.16) functions as on open-loop hydraulic work correction term, u_{hyd}, to improve transient response during a load change.

4.8   Feedback Control Results

Figure 4.7 shows the closed-looped response of both the physics-based and control-oriented FPE models to step changes in reference clearance position as governed by the controller described in Sections 4.2 - 4.7. Shifting clearance is a rapid process, taking roughly one second to complete. Overall, there is a strong agreement between the control-oriented and physics-based model response.

Figure 4.8 portrays the simulated, physics-based FPE behavior at an unstable operating condition. Prior to deactivation at time, $t = 4$ seconds, the proposed controller stabilizes the system in Figure 4.8. However, in the absence of a stabilizing feedback, the clearance quickly decays and eventually combustion becomes impossible.

As suggested by Johansen et al. [52] and Achten [2], cycle-to-cycle variations
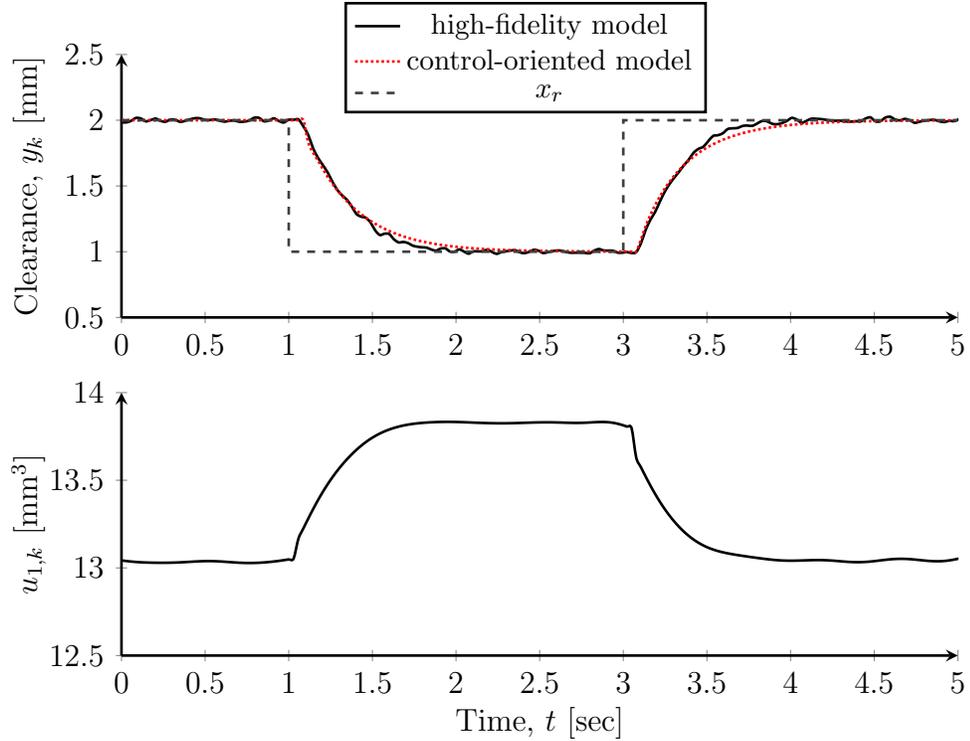
Figure 4.7: Closed-loop response of the high-fidelity and control-oriented FPE models with the proposed feedback control algorithm. At $t = 1$ second a step change to the reference from 2 mm to 1 mm drives the FPE to a new equilibrium. At $t = 3$ seconds, the reference changes from 1 mm to 2 mm.
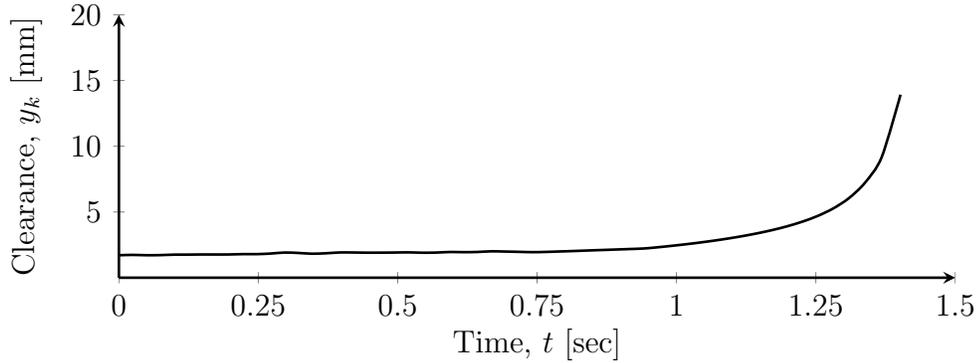
Figure 4.8: Open-loop response of high-fidelity FPE model to constant fueling. Prior to $t = 0$, the system is stabilized at an open-loop unstable equilibrium using the proposed feedback control algorithm. At $t = 0$, the controller is deactivated and fuel is held constant.

in pressure potentially cause fluctuations in the FPE piston behavior. To examine

robustness of the proposed controller to cyclic variations, we introduce some uncer-

tainty into the combustion parameters. Specifically, we add a Guassian distribution to the ignition delay and combustion duration parameters discussed in Chapter II to approximate the peak pressure distribution shown by Kouremenos et al. [61]. The peak pressure distribution of the physics-based model, recorded in Figure 4.9, agrees closely with the distribution of the single-cylinder, DI, diesel engine considered by Kouremenos et al. [61].
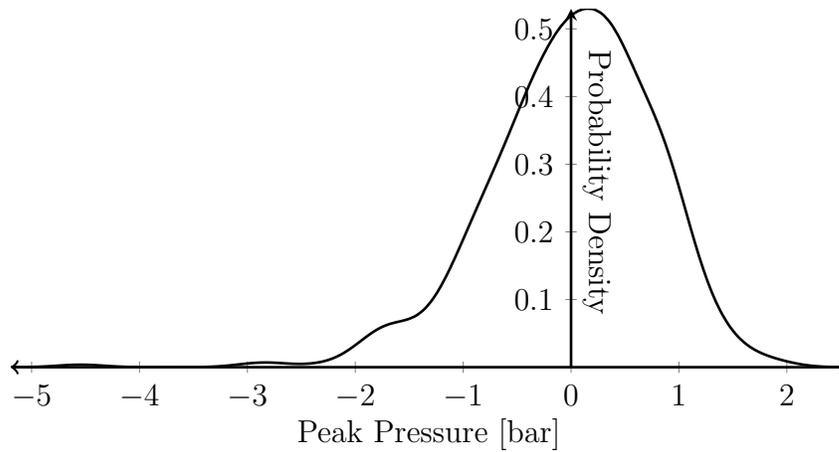
Figure 4.9: Probability density of peak pressure in the presence of cycle-to-cylce variation.

Figure 4.10 shows the closed-loop response of the physics-based model to the same commands applied in Figure 4.7 while experiencing the pressure distribution in Figure 4.9. Overall, the system remains stable with only slight oscillations about the reference position.
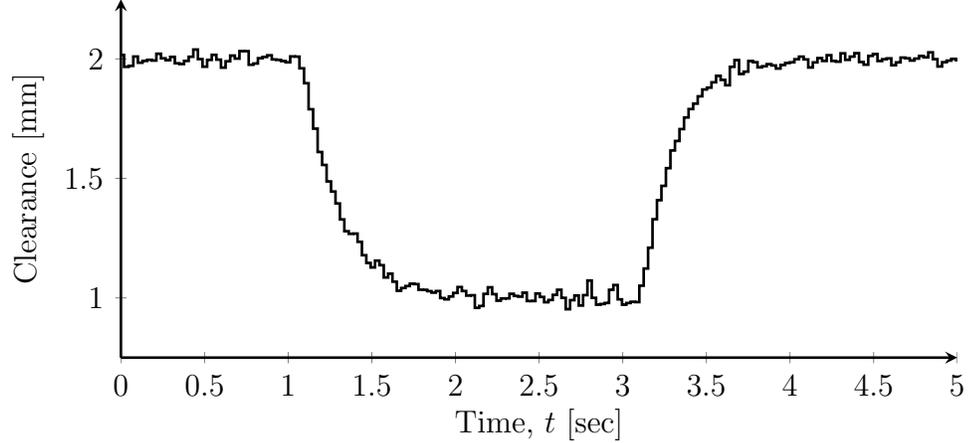
Figure 4.10: Closed-Loop response of the high-fidelity FPE model with the proposed feedback control algorithm in the presence of cycle-to-cycle variation. At $t = 1$ second a step change to the reference from 2 mm to 1 mm drives the FPE to a new equilibrium. At $t = 3$ seconds, the reference changes from 1 mm to 2 mm.

4.9 Reference Governor

In order to sustain safe operation and adequate combustion quality, it is crucial for an FPE to maintain a consistent clearance height [52, 73, 97]. However, as shown by Mikalsen and Roskilly [73], changes in load can result in a violation of desired piston position limitations. Mikalsen and Roskilly attempt to improve FPE behavior by using a pseudo-derivative feedback controller to increase controller response speeds, but only manage to marginally decrease the resulting perturbation to piston position. Their system still violates their self-imposed constraints. A method for constraint management of FPE piston position during a load change does not currently exist. We propose using robust reference governor techniques to manage the hydraulic load of an FPE to prevent constraint violation.

Load or reference governors are a means of constraint management [24, 26, 27, 75, 92, 101]. Following an increase in desired load, at each time step a reference governor predicts and applies the greatest possible load addition to the system that will satisfy the imposed constraints for all future time steps. Reference governor techniques are convenient because they augment rather than replace an existing controller. Recall a

functioning FPE feedback controller already exists as described in Sections 4.2 - 4.7. We implement a reference governor to adjust hydraulic power extraction and enforce constraints, as it is able to augment the nominal controller and can handle parameter uncertainty.

4.9.1   Reference Governors

In continuous-time, the error governor (EG) introduced by Kapasouris et al. is a scalar acting on the error input signal supplied to a compensator [56]. The EG uses supervisory logic to select a gain between zero and one. If the reference or disturbance signal is sufficiently large, the gain is less than one to ensure the controller never receives an input that will result in actuator saturation. Alternatively, if the error is small enough as to not cause saturation, the gain is one and the system acts as designed. The EG technique is applicable to linear systems but generally suffers from long computational time. Gilbert and Tan [28] expand EG concepts by constructing a maximal output admissible set containing all initial controller states for which the controller output with zero error input will remain within the desired, constrained range. Further, the authors show that for a discrete-time formulation, the maximal output admissible set can be approximated using a finite number of linear inequalities. Conveniently, the linear inequalities can be calculated efficiently offline, reducing computational complexity. Further studies augment reference governors to act as a dynamic low pass filter on a reference input with an adjustable bandwidth parameter, rather than a single adjustable gain [23, 24, 27]. More recently, reference governor theory has evolved to include nonlinear systems and Lyapunov function-based admissible set characterizations [25, 26, 60].

Reference governor techniques have been proposed and demonstrated for various applications. Gilbert et. al. demonstrate discrete-time reference governor techniques on a fourth-order linear model of vertical helicopter dynamics with control saturation

[27]. In the automotive field, Kalabić et al. regulate throttle and wastegate commands in a turbocharged gasoline engine using reference and command governors to prevent compressor surge and actuator saturation. The authors create the controller and compute the maximal output admissible set based on linear models and demonstrate performance on a more complex nonlinear engine simulation [55]. For more robust fuel cell operation, Sun and Kolmanovsky use a reference governor to limit oxygen excess ratio and oxygen mass inside the cathode by adjusting current draw. Further, they introduce a method to manage uncertainty by considering model sensitivity. Rather than applying the maximal output admissible set theory, the authors calculate the maximum feasible load step with online simulations and a bisection search algorithm [92]. Vahidi et al. continue fuel cell reference governor research by protecting against compressor surge and choke through attenuation of the load command to the fuel cell. They introduce a step disturbance observer with the reference governor to adjust for unmodeled nonlinearities[101]. Miller et al. constrain the motion of electromagnetically actuated mass-spring damper hardware using a Lyapunov approach to reference governors [75]. Weiss et al. use a reference governor to assist with constraint management during periods of emergency operation of a turbo-fan engine [105]. However, none of the existing results apply to implicit system models of the type treaded in this dissertation.

4.9.2 Algorithm

Suppose f_{cl} is the closed-loop equivalent of (4.1) and describes the FPE behavior while operating with the fuel adjustment control law (4.34),

$$f_{cl}\left(x_{k+1}, x_k, u_{2,k}, \theta\right) = 0. \tag{4.35}$$

In (4.35), the state x_k is the clearance height at each turnaround, $u_{2,k}$ controls work output by specifying the hydraulic power extraction length, and θ is a loss parameter. The control-oriented model described in Section 4.2 approximates closed-loop FPE dynamics as

$$\hat{f}_{cl}\left(x_{k+1}, x_k, u_{2,k}, \hat{\theta}\right) = 0. \tag{4.36}$$

Let $\hat{x}_k$ be an estimate of x_k. Equation (4.36) implicitly describes the evolution of $\hat{x}_k$ as $\hat{F}_{cl}$ where

$$\hat{x}_{k+1} = \hat{F}_{cl}\left(x_k, u_{2,k}, \hat{\theta}\right), \tag{4.37}$$

and $\hat{F}_{cl}$ is unknown. The reference governor enforces the constraints $\hat{x}_k \in X$. Set X is defined as

$$X = \{x : |x_k - x_r| < \mathcal{C}\}, \tag{4.38}$$

where $\mathcal{C}$ is a safety constraint margin. Note that changes in hydraulic load, $u_{2,k}$, may force the piston beyond the imposed constraints. To prevent constraint violation, we implement a reference governor to manage the transition of $u_{2,k}$ to a desired load $u_{2,r}$.

The reference governor attenuates the load command by filtering the desired set-point through the function

$$u_{2,k} = u_{2,k-1} + \beta_k(u_{2,r} - u_{2,k-1}), \tag{4.39}$$

requiring that $\beta_k \in [0,1]$. An algorithm chooses the maximum value for β_k to enforce the constraints. Because the control-oriented model has an implicit relationship, it is difficult to construct a maximal output admissible set to assist with gain selection. Instead, a bisection search method ensures that a projection of piston position remains within the bounds at every time step by selecting

$$\beta_k = \max\left\{\beta \in [0,1] : x(k+n|k, u_{2,k}) \in X; n = 0, \ldots, n_c\right\}, \tag{4.40}$$

where $x(k + n|k, u_{2,k})$ denotes the predicted response n steps ahead from the time instant k with load maintained at a constant level $u_{2,k}$. The prediction horizon is n_c. If the time horizon is sufficiently long and the prediction satisfies all constraints over the time interval $[k, k + n_c]$, they will remain satisfied for any interval $n > n_c$. Typically, n_c is chosen to be comparable to or larger than the discrete settling time of the system[92].

Sun and Kolmanovsky successfully applied a bisection search algorithm to a fuel cell reference governor [92]. The bisection method iteratively simulates the system over the time interval $[k, k + n_c]$ for different values of β. Starting with $\beta = 1$, if at any point a constraint is violated, the algorithm terminates simulation, decreases the candidate gain halfway in the direction of a lower bound, and moves the upper bound. When a simulation concludes at time step $k + n_c$ without any violations, the gain increases halfway towards an upper bound and the lower bound relocates. The bisection search continues until either β converges within a specified tolerance or a particular number of iterations is completed.

Because an explicit description of $\tilde{F}_{cl}$ does not exist, Newton's method, as described in Section 4.5, predicts the response over the time interval $[k, k + n_c]$ based on $\hat{f}_{cl}$.

Figure 4.11 shows the reference governor and system behavior as applied to the control-oriented model and constrained to ± 0.25 mm of a reference clearance, $x_r = 2$ mm. The simulation does not include any model uncertainty. In the results of Figure 4.11, the reference governor optimizes the transition speed and allows the state x_k to 'glide' at the constraint limit. As demonstrated by a single case in Figure 4.11, the bisection search evaluates gain β such that the system satisfies the constraints for all time points. More relaxed constraints would lead to a nearly trivial response where $\beta \simeq 1$ after just a few time steps.

Treating model uncertainty presents another modeling challenge. A number of
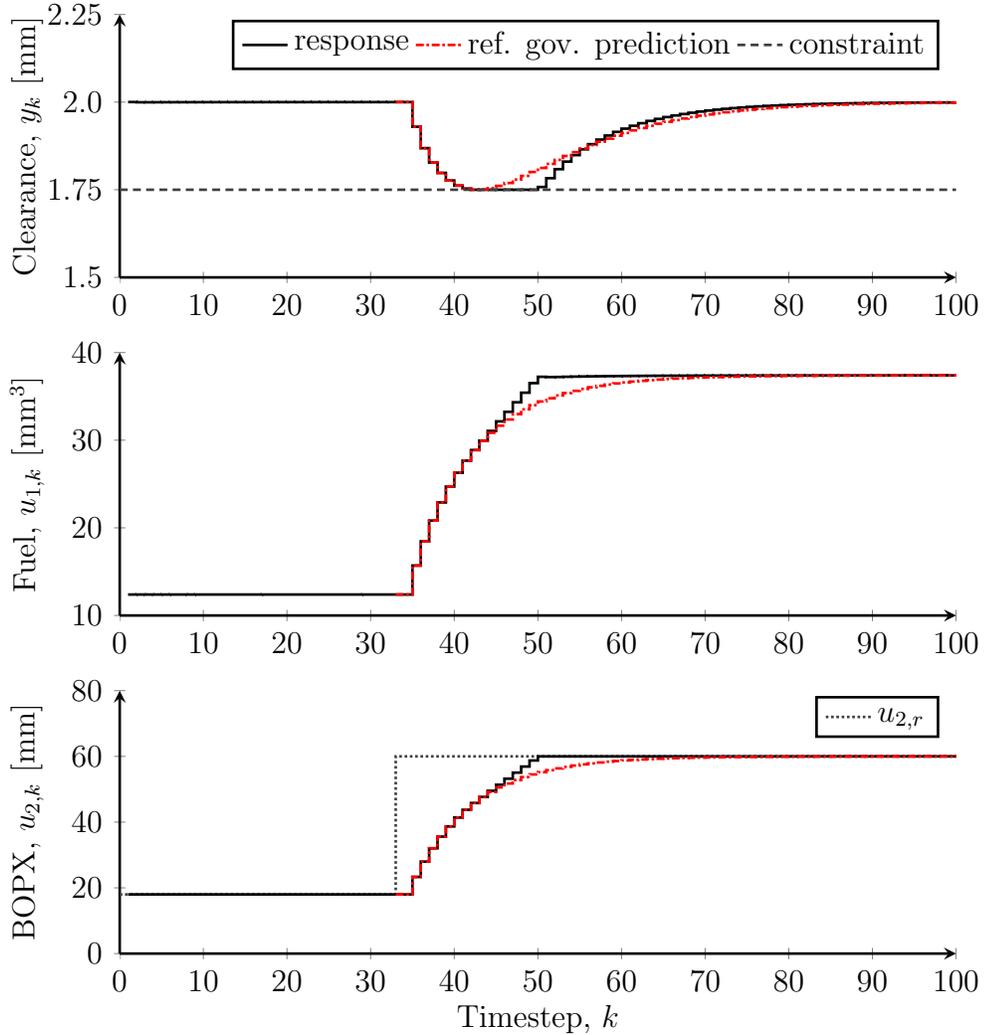
Figure 4.11: Closed-loop response of both the control-oriented model with a reference governor and a reference governor prediction to a step change in desired load, $u_{2,r}$, at timestep $k = 33$. The reference governor prediction is the predicted evolution of y_k with the maximum β satisfying the constraints starting at timestep $k = 33$.

different approaches exist to adjust for uncertainty in a reference governor model. One method, proposed by Vahidi et al. [101], modifies the constraints based on the maximum observed error between the measured and predicted outputs. Here we employ the robust reference governor techniques presented by Sun and Kolmanovsky [92], where existing constraints are tightened based on constrained output sensitivity to the uncertain parameters and parameter bounds. Sensitivity-based adjustments are a convenient approach because the proposed FPE control structure already evaluates

sensitivity functions for the Newton's method root finding algorithm, (4.19), and the nonlinear state feedback gain, (4.26).

In the implementation, we assume the discrepancies between actual and modeled behavior are accounted for as an uncertainty in parameter θ. Supposing the system and model satisfy (4.35) and (4.36), based on a first-order Taylor series expansion, the true state x_k is approximately

$$x_k \approx \hat{x}_k + \left.\frac{\partial \hat{F}_{cl}}{\partial \theta}\right|_{\hat{x}_k,\hat{\theta}} (\theta - \hat{\theta}_k), \tag{4.41}$$

where $\hat{x}_k$ is the nominal prediction and $\frac{\partial \hat{F}_{cl}}{\partial \theta}$ is the model sensitivity with respect to the uncertain parameter θ. Since θ is a scalar parameter, the greatest discrepancy in x_k and $\hat{x}_k$ occurs at $\max\left\{|\theta - \hat{\theta}_k|\right\}$. To reduce and bound the maximum uncertainty in $\hat{\theta}$ we add the open-loop disturbance estimate (4.31). By exploiting (4.41) and inserting a term to protect against higher order terms omitted in (4.41), $\mathcal{M}$, the robust state constraint becomes [92]

$$\tilde{x}_k + \left|\frac{\partial \hat{F}_{cl}}{\partial \theta}\right| \max\left\{|\theta - \hat{\theta}_k|\right\} + \mathcal{M} \max \|\theta - \hat{\theta}_k\|^2 < \mathcal{C}. \tag{4.42}$$

In practice, $\mathcal{M}$ can be calculated analytically using the second-order sensitivity function or adjusted through calibration. This approach is easily extended to handle multidimensional constraints, the details of which are presented by Sun and Kolmanovsky [92].

Figure 4.12 shows the response of the control-oriented model and reference governor to the same input commands applied in Figure 4.11. However, the model in Figure 4.12 experiences uncertainty in parameter $\hat{\theta}$. Without adjusting for the uncertainty, the reference governor is unable to enforce the constraints. By enforcing the more conservative robustness condition (4.42), the robust reference governor success-

fully enforces the constraints at the cost of increased response time.
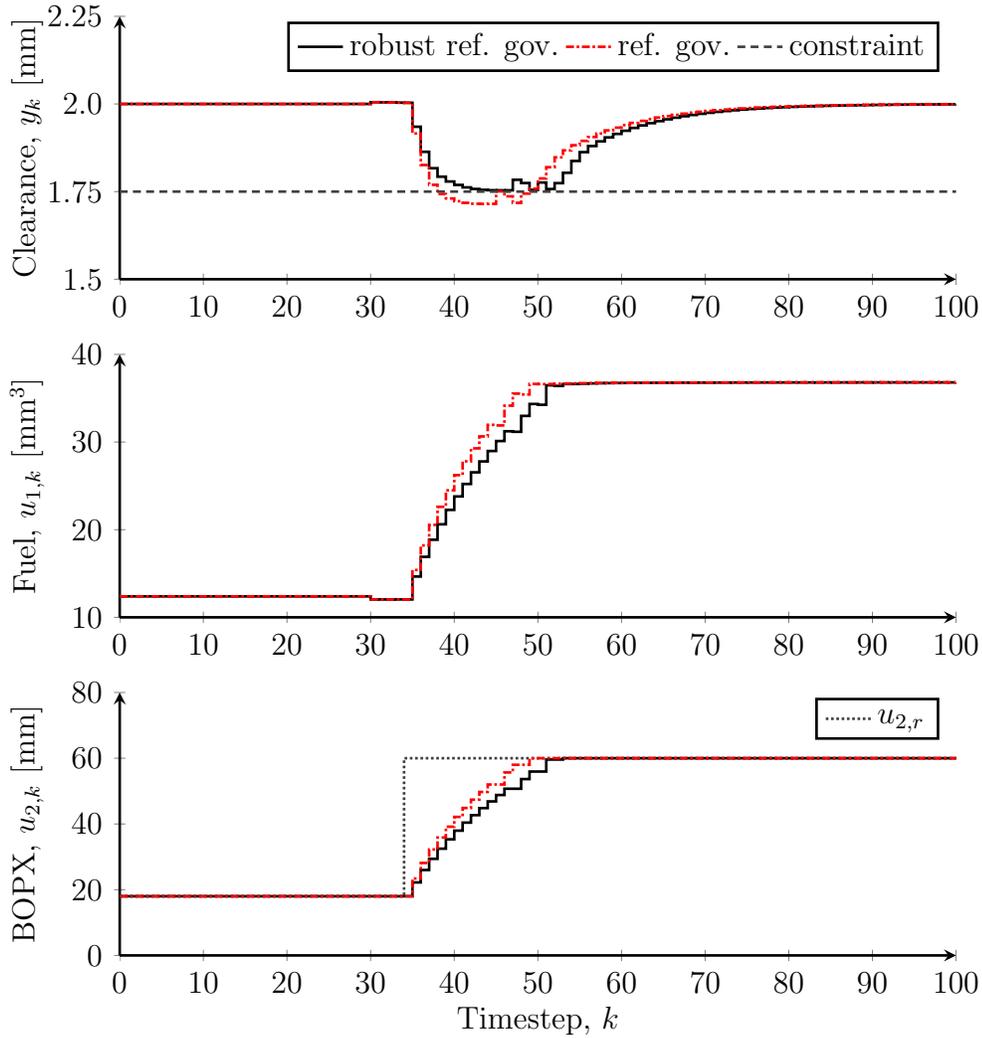
Figure 4.12: Closed-loop response of the control-oriented model to a step change in desired load, $u_{2,r}$, at timestep $k = 33$ with a reference governor, and with a robust reference governor.

4.9.3 Reference Governor Results

In Figure 4.13, the physics-based FPE model responds to changes in load demand, alternating from $u_{2,r} = 18$ mm to $u_{2,r} = 50$ mm. Commanded to a reference of $x_r = 2$mm, the clearance height fluctuates by a magnitude greater than 1 mm when the load change is applied as a step command. This behavior is unacceptable for any

target clearance $x_r \leq 1$mm and would result in collision with the cylinder head. By applying a robust reference governor technique, the controller is able to constrain the FPE to operate within ± 0.5mm of the desired piston turnaround position. Even with the reference governor, $u_{2,k}$ reaches $u_{2,r}$ within 0.25 seconds, making the response time almost negligible from a driver point of view.
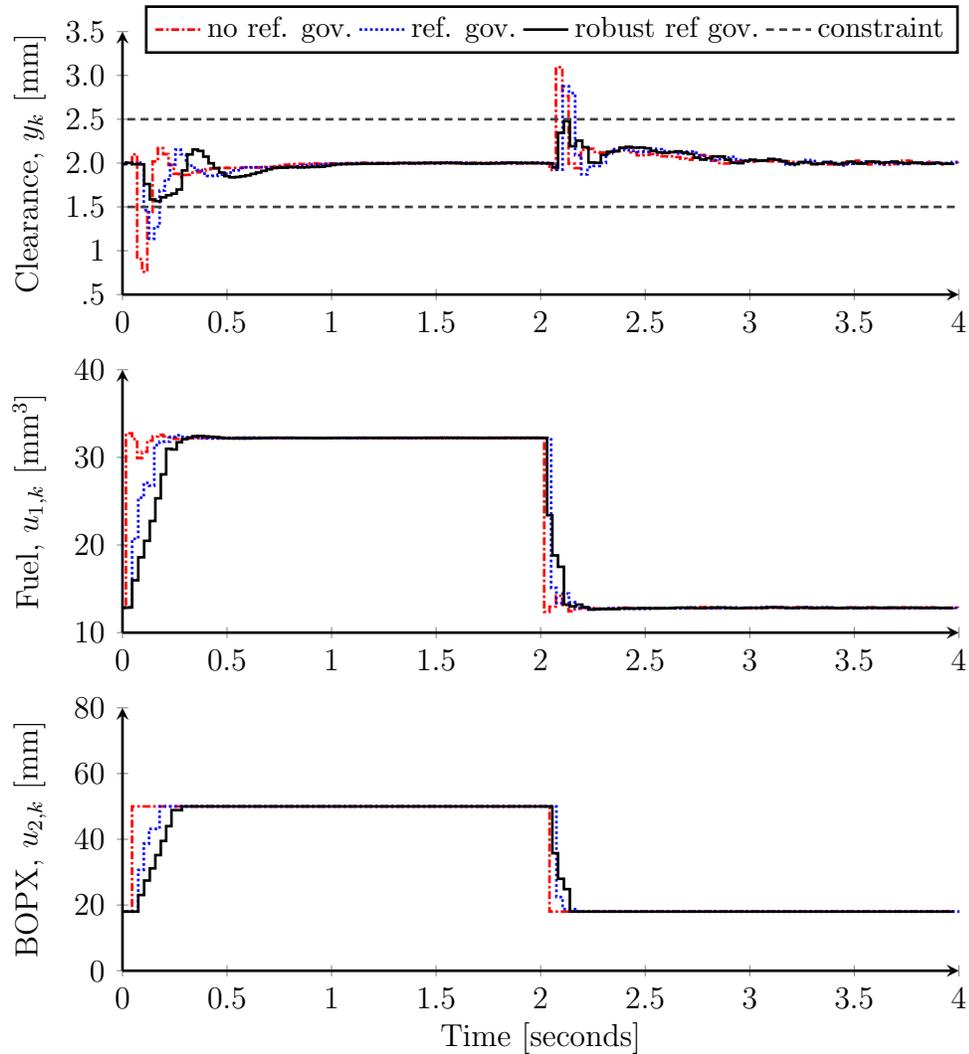
Figure 4.13: Closed-loop response of the high-fidelity model to a step change in desired load, $u_{2,r}$, with a reference governor, with a robust reference governor, and without a reference governor.

4.10   Conclusions

This chapter considered the control of FPE piston clearance height at the end of each stroke and constraint management during a load transition. A simplified, four-stroke Otto cycle model has been introduced that represents engine behavior as an implicit control-oriented dynamic system. By linearizing the control-oriented model, the FPE is predicted to be unstable at high load, high compression ratio conditions. A state feedback control law based on dynamic inversion stabilizes the plant, and a Smith predictor compensates for a single time step delay in output. Newton's method estimates the output at time step k using information from time step $k-1$. To compensate for the effects of uncertainty, an RLS algorithm estimates a work loss parameter. The closed-loop simulated response of the physics-based FPE model shows successful operation and set-point changes.

Without special treatment, load changes perturb the FPE piston position outside specified margins and can cause collisions with the cylinder head. As a solution, a reference governor manages load changes by only applying loads that satisfy the constraints in a prediction of all future time steps. Additional robustness terms tighten the constraints to compensate for model uncertainty. The physics-based FPE model in combination with the proposed feedback control and reference governor demonstrate successful constraint enforcement.

CHAPTER V

FPE, HLE, and Conventional ICE Comparison

In order to compare, evaluate, and improve upon existing hydraulic engine designs, we have constructed physics-based models of both an HLE and an FPE. Each model is based on the framework established in Chapter II. The EPA designed the FPE and HLE as hydraulic power plants for a series HHV. The engines potentially replace a conventional internal combustion engine (ICE) coupled to a pump / motor (P/M). To facilitate a balanced survey, we have therefore modeled a diesel ICE and pump combination.

In order to remove geometry as a variable, each modeled engine contains identically sized components. Every model describes a four-cylinder, four-stroke diesel. Cylinder bore is 79.5 mm, equivalent to the larger diameter cylinders employed on the original, unbalanced FPE and HLE [12]. Where applicable, crank radius is 57.5 mm and stroke length is 115 mm, unchanged from prototype HLE hardware. The resulting HLE and ICE bore-to-stroke ratio is 0.69, producing a displacement of 0.57 liters per cylinder or 2.28 liters cumulatively. When factoring in squish height, piston-bowl volume, and valve-crevice volume, the corresponding HLE and ICE geometric compression ratio is 18.5:1. The FPE possesses matching geometry, but can operate with a stroke length up to 121 mm and can deliver a maximum displacement of 0.6 liters per cylinder or 2.4 liters total. At the same extremes, maximum FPE geometric compression ratio

is 34.5:1. However, by operating with the maximum stroke length, the FPE piston would be in contact with the cylinder head at each turnaround point.

Although we simulate each engine with identical geometry, they are subject to different internal forces and thus require different dynamics models. A Newtons second law force balance describes the FPE dynamics as a single equivalent mass. A crank torque balance captures ICE and HLE dynamics. However, the HLE has one crank apparatus and the ICE consists of four crank arm and bearing sets. In a conventional ICE, the crank-slider interactions induce side loads on the piston that increase both normal and frictional forces. Without a crank, the FPE theoretically does not experience any piston side-loads. While the HLE slider mechanism experiences side-loads, the pistons interact with the crank through a rack and pinion device which is assumed to only transmits forces in the longitudinal direction. Consequently, the HLE and FPE models do not include friction terms corresponding to normal loading of the pistons due to crank dynamics. Apart from the rack and pinion contributions, all other frictional expressions are consistent for each engine.

The HLE, FPE, and ICE simulations assume thermodynamics and heat transfer are identical. Combustion dynamics are for the most part matching, and only differ in time scale. Based on observations by [39, 70, 117] and in Chapter II, the FPE and HLE operate with a significantly reduced combustion duration.

While the HLE and FPE generate hydraulic power with a linear pump according to the expressions in Section 2.3, the ICE requires an additional high-efficiency, bent-axis, hydraulic P/M [35]. A series of model-based performance maps, used in various publications [20, 54], capture P/M performance. The maps, presented in Figure 5.1, deliver P/M efficiency as a function of speed and displacement factor. The displacement factor is a fraction of total possible displacement, similar to the HLE power extraction fraction discussed in Chapter III. The particular pump sizing absorbs maximum displacement near peak engine efficiency at the lowest desirable

124

hydraulic operating pressure.
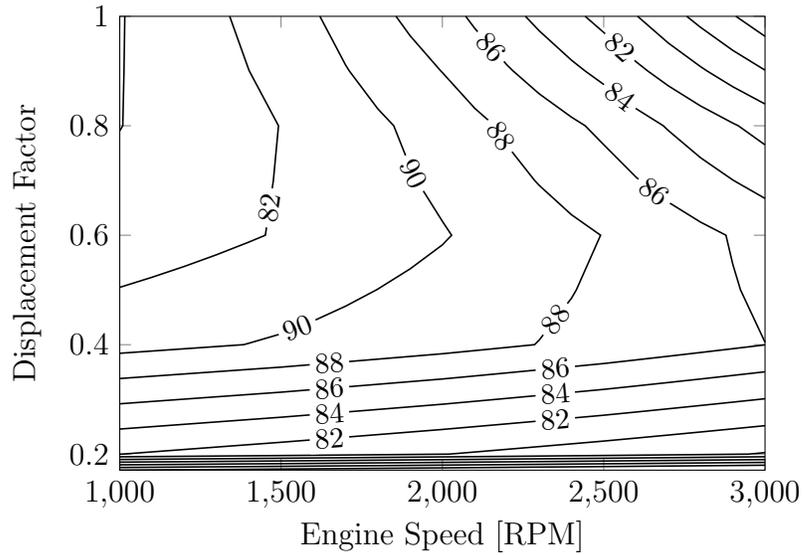
Figure 5.1: Efficiency [%] of hydraulic pumped coupled to ICE. Pump performance is a function of engine speed [RPM] and displacement factor. Displacement factor is the fraction of total displacement available to the pump.

In this section we leverage the FPE, HLE, and ICE models to compare a variety of performance trends. Primarily, we present each engines behavior as a function of engine speed and load. brake mean effective pressure (BMEP) describes load and revolutions per minute (RPM) describes engine speed. However, FPE operating frequency is fixed for a particular load and compression ratio [2, 68]. To convey more meaningful results, we instead portray FPE behavior as a function of clearance height and hydraulic load. When appropriate, the units 'RPM equivalent' describe FPE oscillation frequency. In a conventional engine, one revolution corresponds to two strokes of the piston. Similarly, RPM equivalent conveys the number of times an FPE completes two strokes within one minute. Also keep in mind that a mean effective pressure (MEP) term is an estimate of cycle work or energy normalized by engine displacement volume. While we consider the displacement identical for each engine in this study, normalizing by displacement volume allows for easy comparison to other engines. For each performance map, the extremum seeking algorithm, discussed in

Section 3.3, optimizes the injection timing and intake valve closure position at each considered condition. Other valve timing remains constant. The models use the control algorithms discussed in Chapters III and IV to manage fuel quantity and maintain a speed or clearance height set-point at a specific hydraulic load.

5.1 Piston Travel and Combustion Interactions

In order to better interpret the following modeling results, it is critical to understand the interaction between FPE, HLE, and ICE piston travel and combustion duration. Piston dwell describes the period of time during which a piston inhabits a position near TDC or BDC. A long TDC dwell signifies that a piston lingers near the cylinder head for an extended duration. Vise versa, a short TDC dwell indicates a brief stay at low volume. It follows that a piston with a short TDC dwell experiences higher velocities and accelerations near TDC than a piston with long TDC dwell. As illustrated in Figure 1.3, an FPE possesses a short dwell duration at TDC and BDC compared to both the HLE and ICE. With the addition of a crank, Figure 1.3 shows BDC and TDC dwell are not symmetric. Thus, the ICE experiences shorter TDC dwell and longer BDC dwell. As discussed previously in Section 2.4 and depicted in Figure 2.10 and Figure 2.11 due to the unique crank mechanism, HLE cylinders 1 and 4 have a short TDC dwell and long BDC dwell whereas HLE cylinders 2 and 3 have a long TDC dwell and short BDC dwell.

Combustion duration expresses the time interval necessary for combustion to complete after ignition. A short combustion duration implies a fast burn rate. Of the three engines considered, the FPE has the shortest combustion duration, roughly 1-2 ms according to [39, 70, 117]. Based on preliminary test results, the HLE combustion duration is approximately 2-3 ms. By altering $D(t)$ in (2.26), the modeling architecture presented in Chapter II scales combustion duration. Incorporating burn duration allows us to be consistent and as fair as possible in comparing these engines.

Combustion duration and TDC dwell time are somewhat at odds. As a datum, consider that constant volume combustion can occur at TDC if one of two perquisites is satisfied: either the combustion is instantaneous or the piston stops at TDC for the entire heat release event. Finite combustion durations and TDC dwell times decrease pressure and temperature peaks (and often indicated work) by forcing a portion of the heat release to occur during the expansion stroke.

5.2   Cylinder Pressure

Figure 5.2 shows a pressure volume (PV) diagram of each engine. The data show that the FPE experiences the highest peak pressure. Although the piston does not dwell for long periods near TDC, short FPE combustion durations result in the rapid pressure rise and high peak. The ICE exhibits the lowest peak pressure in Figure 5.2 because it possesses the longest combustion duration. All HLE cylinders present similar combustion durations, however cylinders 2 and 3 experience a longer TDC dwell duration. As a consequence, HLE cylinders 2 and 4 have a higher pressure peak than cylinders 1 and 4.

Figure 5.2 also highlights differences in exhaust behavior. The Otto cycle illustrates that an ideal exhaust event consists of a constant volume pressure drop or constant volume heat rejection. Because HLE cylinders 2 and 3 as well as the FPE possess a short BDC dwell duration, the piston moves further as pressure drops during exhaust. Some work is potentially lost as the blowdown diverges from an ideal, constant volume process.

Peak pressure behavior, available in Figure 5.3, follows from the same logic discussed above regarding the PV diagram. Short combustion duration provides the FPE with the highest peak pressures and long TDC dwell increases the peak pressure in HLE cylinders 2 and 3. Figure 5.3 also suggests that ICE and HLE peak pressures are a predominately a function of load. Higher loads require increased fuel to maintain

127
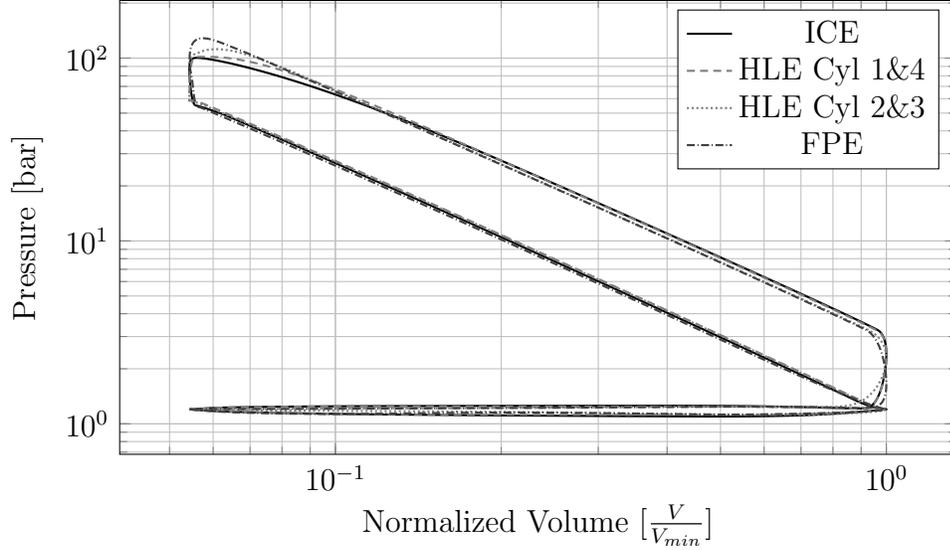
Figure 5.2: Pressure volume diagram of a complete engine cycle for the FPE, ICE, HLE cylinders 2 & 3, and HLE cylinders 1 & 4. Each engine is operating with an 18.4:1 compression ratio, at roughly 1000 RPM or RPM equivalent, and injected with 30 mm^3 of fuel.

a given speed and translate to a greater energy addition and higher peak pressures. Engine speed has a secondary impact on the ICE and HLE trends in Figure 5.3 by influencing combustion duration and heat loss. Free-piston engine peak pressure behavior is equally dependent on clearance height and hydraulic load. As FPE piston clearance decreases, the volume during combustion decreases and the compression ratio increases. Higher compression ratios result in an increased TDC pressure prior to combustion. Variations in combustion volume and pressure prior to combustion compound to give FPE clearance a significant impact on peak pressure behavior.

Note that conventional diesel engines generally use turbochargers to boost intake manifold pressures and increase power density. Elevated intake pressures increase the mass of air induced in cylinder at IVC and produce higher pressures at TDC, both prior to and following combustion. As simulated, the FPE, HLE, and ICE do not include turbochargers. By introducing a turbo, the engines would likely exhibit higher peak pressures than in Figure 5.3 and perhaps different trends. Peak pressures in excess of 200 bar can damage engine components. While the current peak pressure
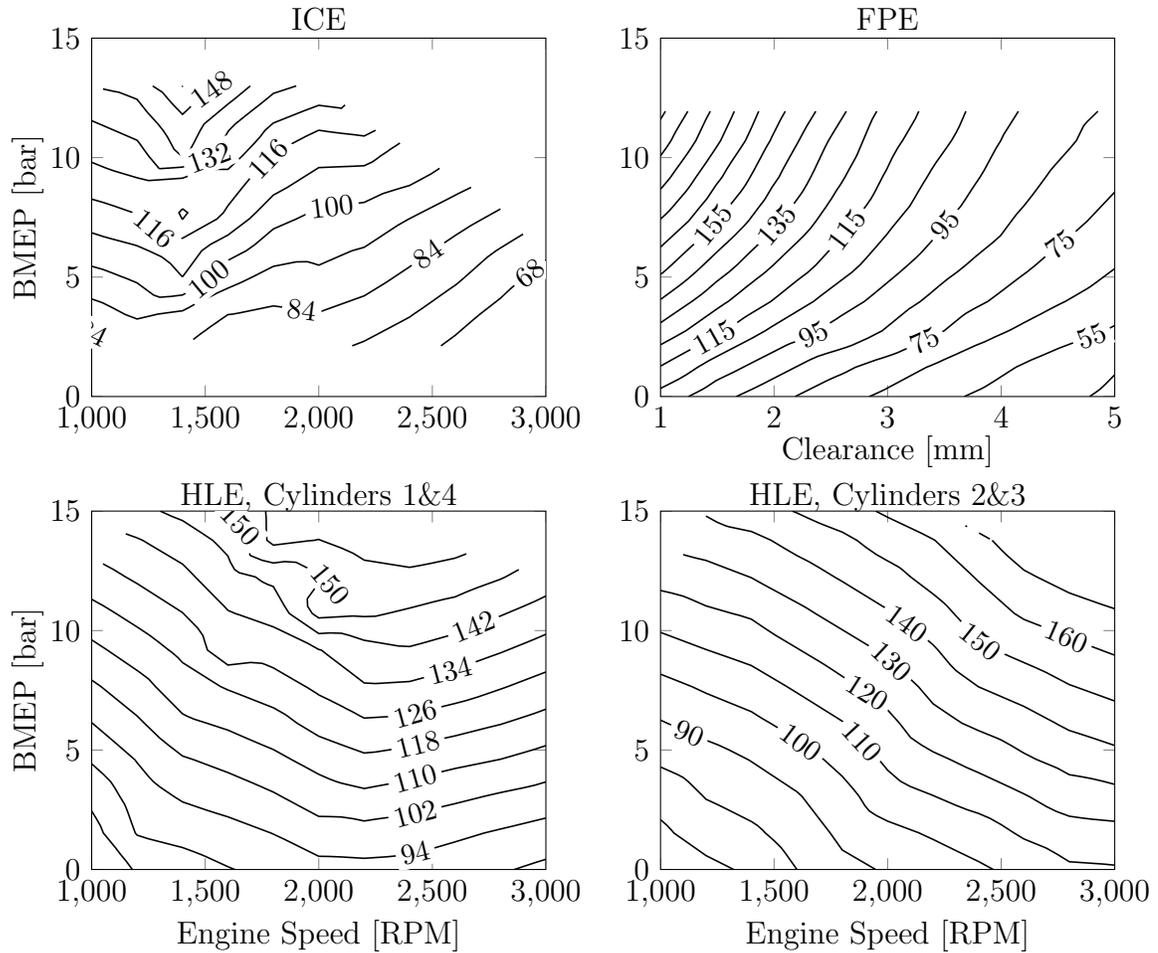
Figure 5.3: Peak pressure [bar] of the HLE, FPE, and ICE. The HLE and ICE behavior is a function of engine speed [RPM] and load. The FPE performance is a function of clearance height [mm] and load. Load is the useful hydraulic work per cycle normalized by the displacement volume, denoted as BMEP [bar].

data is under 200 bar, the addition of a turbo may boost FPE and HLE in-cylinders pressures above the suggested range.

5.3 Peak Temperature and Exhaust Temperature

Figure 5.4shows trends in peak cylinder temperature. Peak temperatures can significantly impact heat loss because they occur at a high surface-area-to-volume ratio. Although not considered in this study, high peak temperatures are also indicative of NOx emissions. The behavior of each engine, presented in Figure 5.4, is primarily

load driven. Higher loads demand increased fueling, which in turn indicates a greater energy addition and higher peak temperatures. Due to heat transfer factors discussed in Section 5.5, FPE clearance volume has a reduced influence on the peak temperature performance of Figure 5.4. As with the peak pressure trends in Section 5.2, peak temperature data shows that the FPE and ICE experience the highest and lowest peak temperatures, respectively. Likewise, FPE and ICE behavior is the result of combustion duration and piston dwell. Long ICE combustion durations lead to low peak temperatures and short FPE combustion durations produce high peak temperatures. The HLE cylinders 2 and 3 exhibit higher peak pressures in Figure 5.4 than HLE cylinders 1 and 4 due to a longer TDC dwell duration. Dwell has an additional impact on temperature through heat transfer, discussed in Section 5.5.

Figure 5.5 is a plot of exhaust gas temperature. Exhaust temperature is an indication of unused energy available in the exhaust gases that can potentially be utilized for turbocharging. A multitude of parameters impact exhaust temperature, including injection timing, combustion duration, expansion ratio, indicated efficiency, heat loss, and EVO timing. Although it is difficult to attribute exhaust temperature characteristics to any one parameter, it is apparent that there is slightly less exhaust energy available in the FPE.

Also keep in mind that, as we show later, the FPE has a higher efficiency than the HLE or ICE and requires a decreased quantity of fuel at a given load. Likewise, the HLE is more efficient than the ICE and requires less fuel.
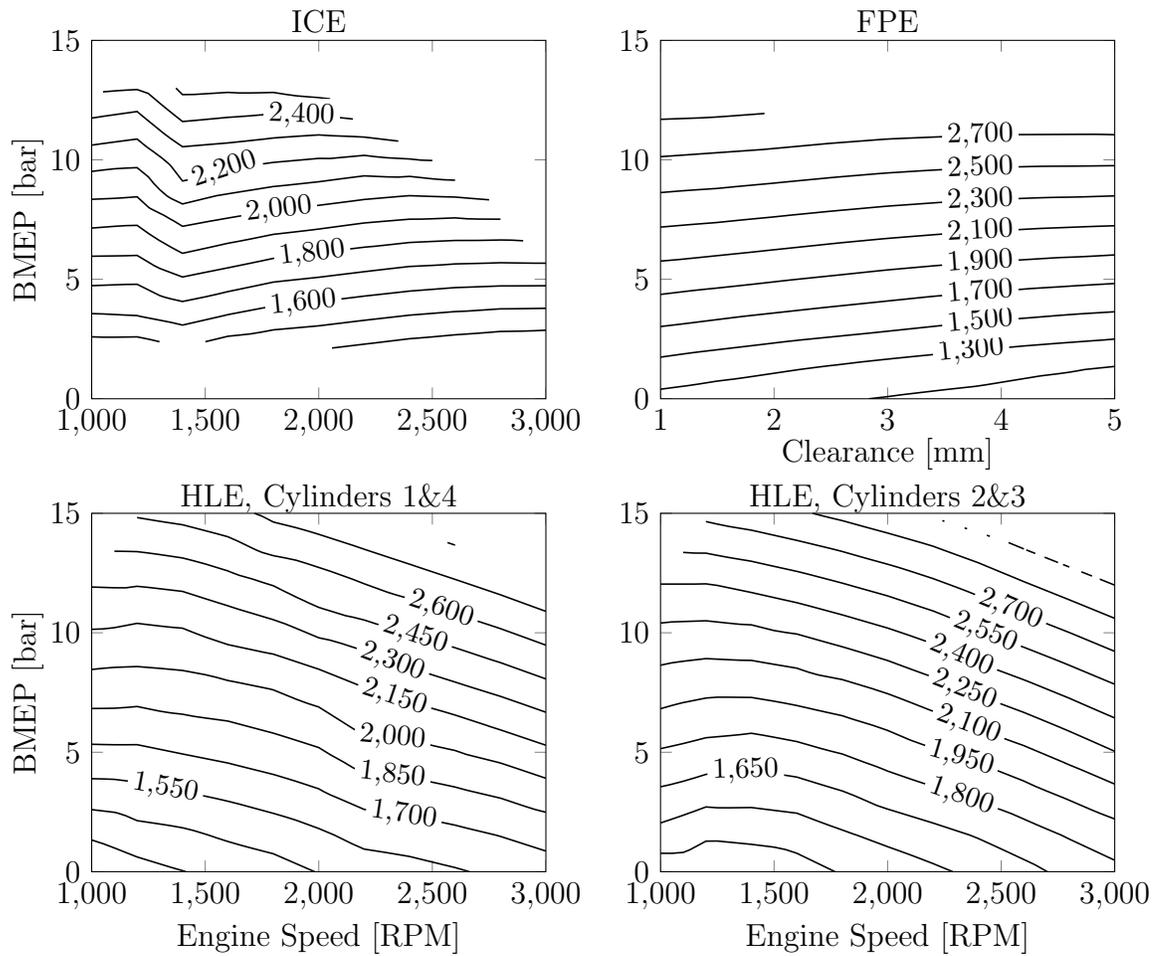
Figure 5.4: Peak temperature [K] of the HLE, FPE, and ICE. The HLE and ICE behavior is a function of engine speed [RPM] and load. The FPE performance is a function of clearance height [mm] and load. Load is the useful hydraulic work per cycle normalized by the displacement volume, denoted as BMEP [bar].
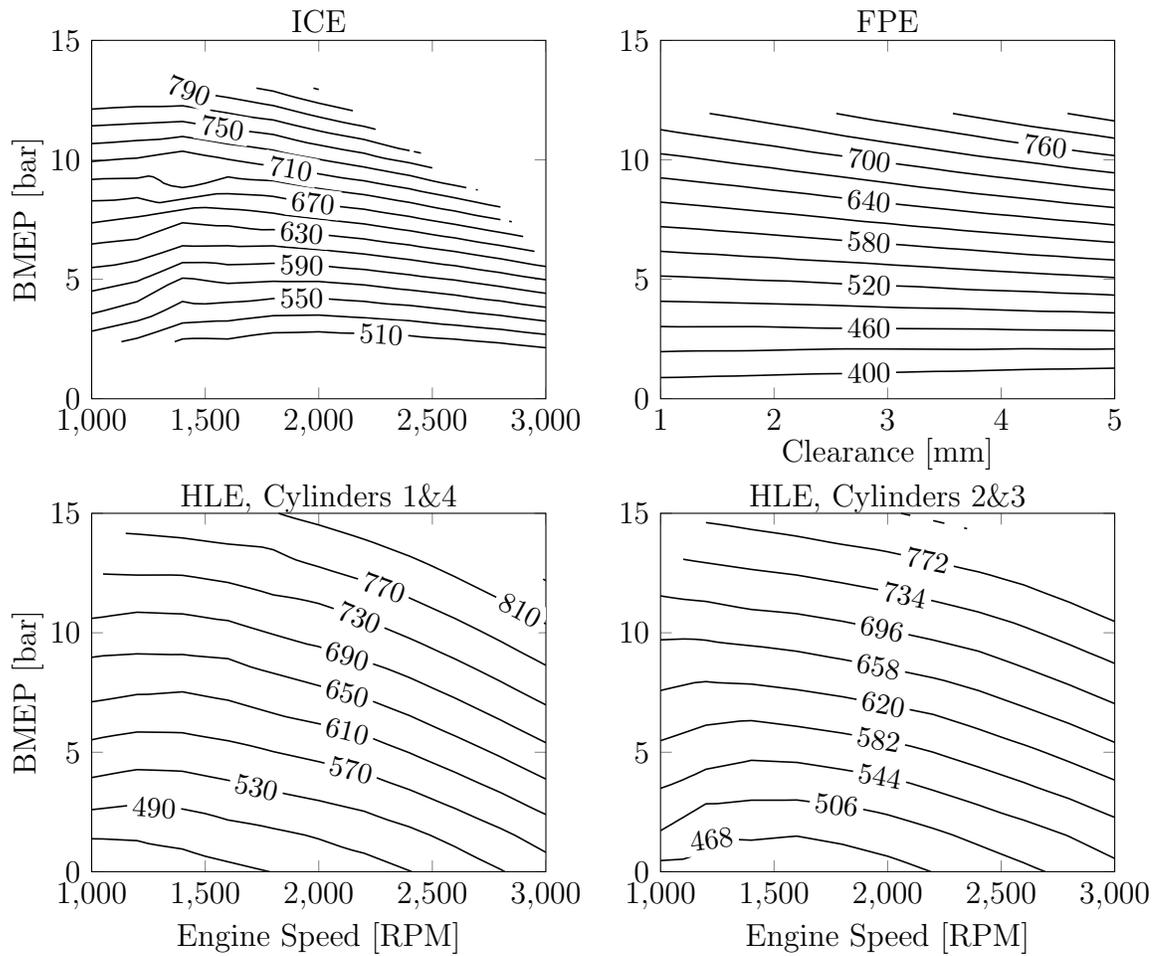
Figure 5.5: Exhaust temperature [K] of the HLE, FPE, and ICE. The HLE and ICE behavior is a function of engine speed [RPM] and load. The FPE performance is a function of clearance height [mm] and load. Load is the useful hydraulic work per cycle normalized by the displacement volume, denoted as BMEP [bar].

5.4 Engine Friction and Mechanical Efficiency

Friction mean effective pressure (FMEP), shown for each engine in Figure 5.6, is a measurement of friction work per cycle normalized by the displaced volume. The estimated FMEP considers the losses associated with both engine and hydraulic pumping friction.
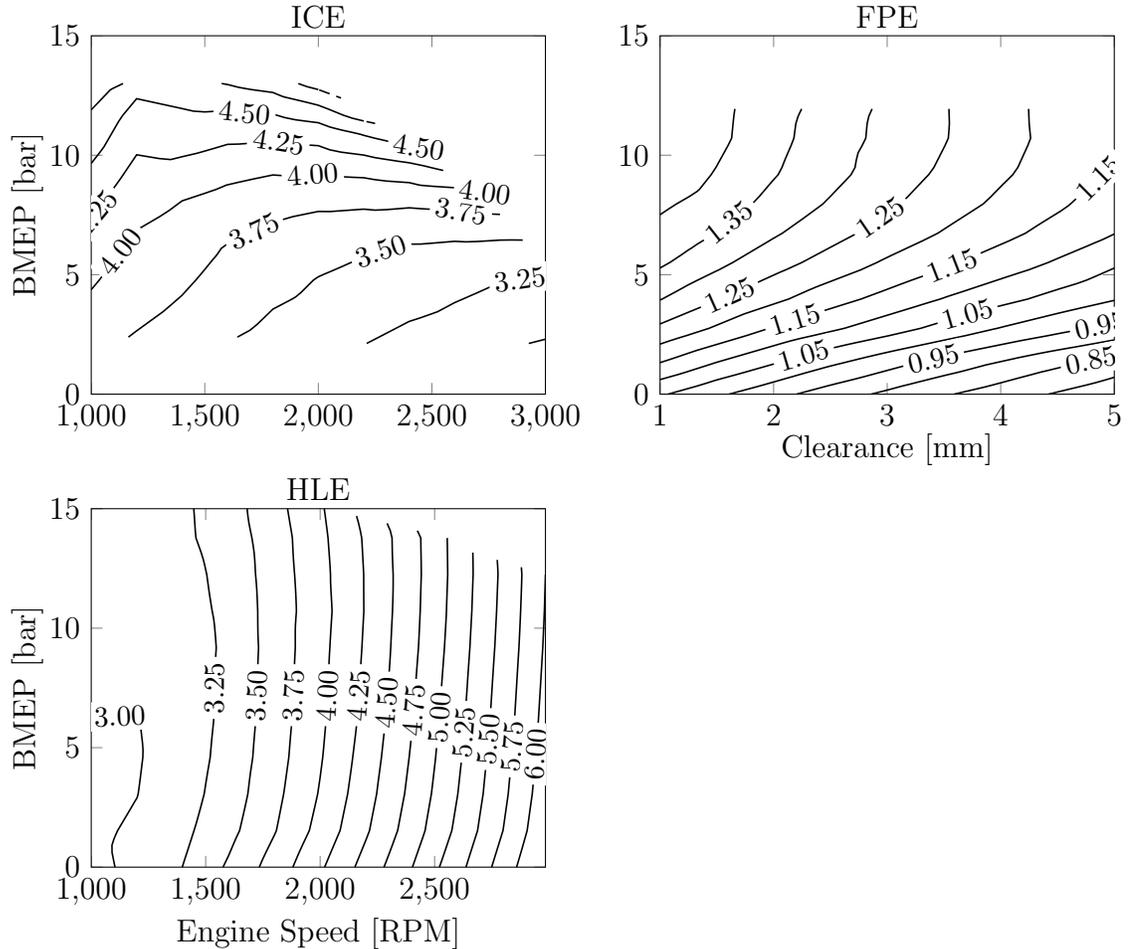
Figure 5.6: FMEP [bar] of the HLE, FPE, and ICE. The HLE and ICE behavior is a function of engine speed [RPM] and load. The FPE performance is a function of clearance height [mm] and load. Load is the useful hydraulic work per cycle normalized by the displacement volume, denoted as BMEP [bar].

According to Heywood, motoring FMEP can range from 2-4 bar for a diesel engine [41]. The data presented in Figure 5.6 correspond to firing operation and consequently portrays greater overall FMEP. The dominant factor contributing to FPE and ICE

friction appears to be cylinder pressure, as the FMEP plots follow roughly the same trends as the peak in-cylinder pressures presented by Figure 5.3. Recalling (2.9) from Section 2.1.2.1, greater cylinder pressures increase piston ring normal forces and drag against the cylinder wall. It follows that for the FPE, higher compression ratios produce an increase in friction due to elevations in pressure. Likewise, a higher load demand calls for increased fueling which causes a rise in pressure and friction. Additionally, ICE bearing loads increase with pressure.

Engine speed is another factor contributing to friction, where a higher relative velocity between two contacting surfaces generally leads to increased friction. In fact, as a result of large piston assembly mass, HLE friction is primarily a function of engine speed in Figure 5.6. Recall from Section 2.1 that we consolidate all of the oscillating components into one large equivalent mass term in (2.4). The equivalent mass of the piston assemblies is 36 kg (80 lbs). For perspective, the HLE is a single-cylinder engine with a 36 kg piston from the cranks point of view. With each stroke the HLE crank and connecting rod must decelerate and reverse direction of the 36 kg piston. As piston mass increases, the amount of kinetic energy the piston possesses at a given velocity increases linearly. Similarly, piston kinetic energy increases with the square of velocity. With an increase in kinetic energy, the amount of work necessary to change piston velocity increases. Consequently, the HLE crank bearing experiences remarkably high loads at high engine speeds and exhibits the speed dependence implied in Figure 5.6.

To further elaborate on HLE friction behavior, recall that Figure 2.15 from Section 2.4 shows the increase in bearing loads when increasing HLE engine speed from 1800 RPM and 2800 RPM. Essentially, the HLE piston assembly was originally an FPE and has a propensity to behave like one, with a natural operating frequency and the FPE piston velocity profile shown in Figure 1.3. However, the crank constrains the HLE piston assembly to perform similar to an ICE. Again referring to Figure 1.3,

the ICE piston velocity is noticeably different than the FPE. The HLE crank does work on the piston to change its velocity profile from FPE to ICE, resulting in higher bearing loads and the friction trends of Figure 5.6.

Figure 5.7 and Figure 5.8 further explore the impact of piston mass on HLE friction. Each plot shows the change in mechanical efficiency due to variations in piston mass and rotational moment of inertia of the crank. At low speed, Figure 5.8 demonstrates that high piston mass can be somewhat desirable as mechanical efficiency decreases slightly with decreasing mass. In this low speed case, piston inertia provides compression work rather than the crank, decreasing bearing load and friction. However, the influence of piston mass at low engine speeds is minimal compared to the impact of piston mass at high engine speeds provided in Figure 5.7. At high engine speeds, higher mass significantly reduces mechanical efficiency. The crank must provide work to change direction of a heavy piston, increasing bearing load and friction. In both cases, flywheel inertia does not drastically influence mechanical efficiency.
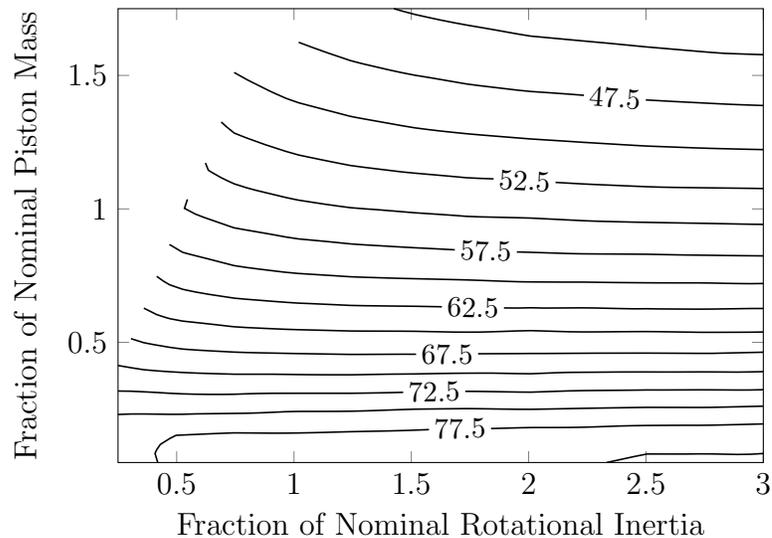
Figure 5.7: Mechanical Efficiency [%] of the FPE as a function of fraction of nominal piston mass and fraction of nominal rotational inertial at 3000 RPM.

Referring back to Figure 5.6, the FPE has low friction relative to an ICE as predicted by various institutions [2, 12, 68]. In fact, the FPE experiences the lowest

135
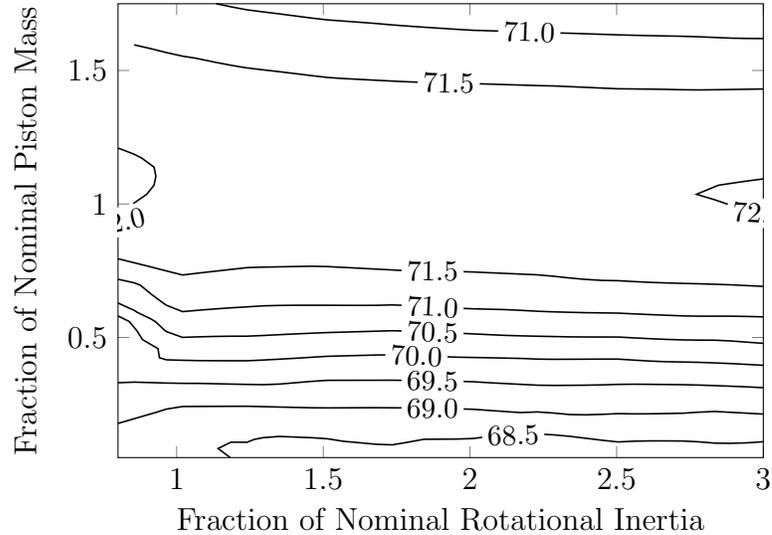
Figure 5.8: Mechanical Efficiency [%] of the FPE as a function of fraction of nominal piston mass and fraction of nominal rotational inertial at 1000 RPM.

overall FMEP, ranging from 0.8 - 1.4 bar. In Figure 5.6, the ICE suffers the highest relative friction at lower engine speeds due to an abundance of moving parts. Additionally, the ICE cranks apply side-loads to each piston, increasing normal forces and friction. Since the HLE crank is separated from the pistons by the rack and pinion apparatus, the HLE pistons do not experience side-loads from the crank. However, the HLE crank creates a side-load on the slider mechanism. The slider, advantageously, is not subject to the same packaging constrains as a standard piston and is designed to reduce friction. In addition, oil is applied more directly to the slider because there are no concerns about additional hydrocarbons in the combustion chamber.

Figure 5.9 shows the mechanical efficiency of each engine. Mechanical efficiency conveys the fraction of energy transferred through the mechanical components and delivered to the load. Alternatively, mechanical efficiency is also the difference between final work output and indicated work, normalized by the indicated work. Figure 5.9 illustrates that mechanical energy is largely a function load, even for the HLE,. In effect, the fraction of usable work increases faster than friction increases. Intuitively, the mechanical efficiency in Figure 5.9 approaches zero as the engine approaches idle

136

condition (zero load). At idle, all energy is used to overcome friction or heat transfer losses and mechanical efficiency is zero. However, based on Figure 5.9, HLE engine speed has an increased influence on mechanical efficiency at higher magnitudes. Amplified engine speed influence is due to large HLE piston mass.
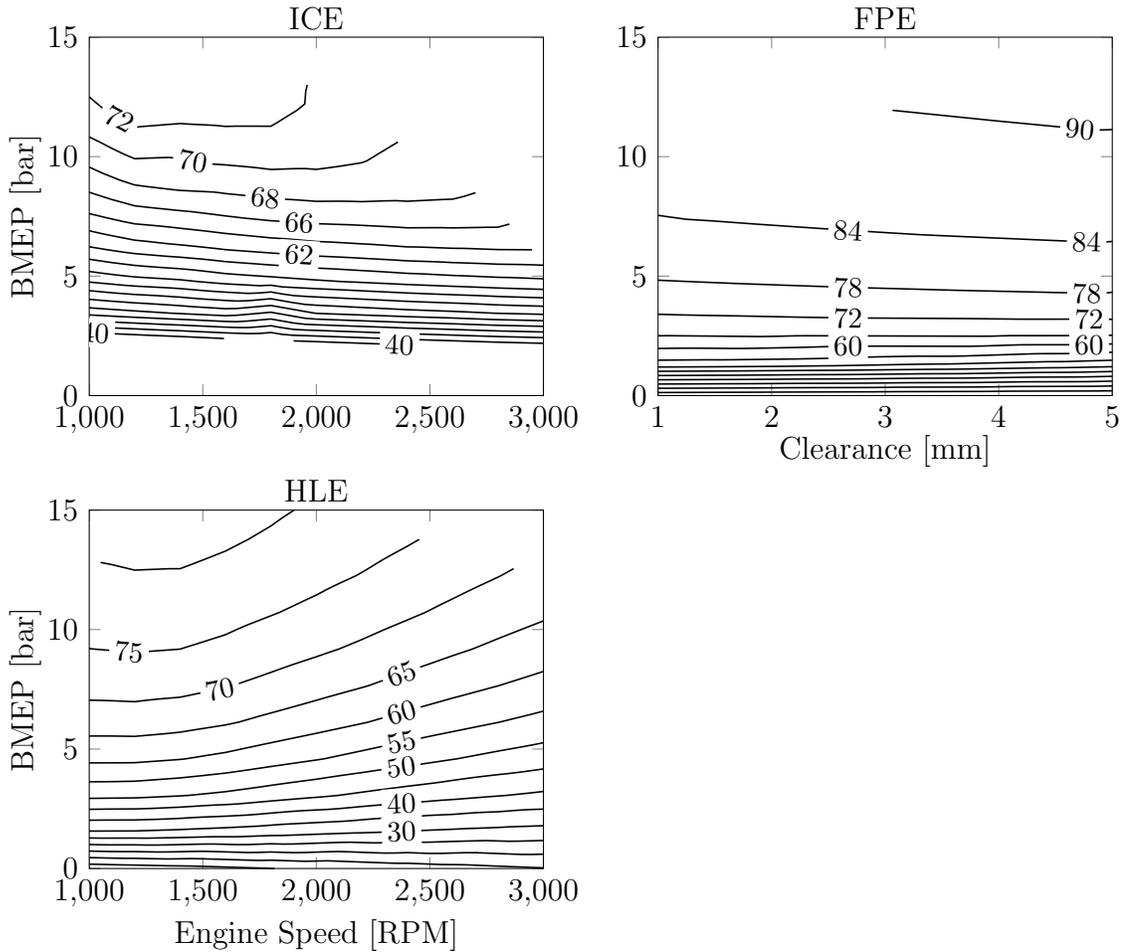
Figure 5.9: Mechanical Efficiency [%] of the HLE, FPE, and ICE. The HLE and ICE behavior is a function of engine speed [RPM] and load. The FPE performance is a function of clearance height [mm] and load. Load is the useful hydraulic work per cycle normalized by the displacement volume, denoted as BMEP [bar].

A few factors potentially affect friction accuracy and trends. The FPE and HLE models do not consider friction losses associated with the interaction between the rack and pinion gears. Additionally, we neglect FPE and HLE piston side-loads. In practice, the pinion exerts some secondary motion onto to the pistons that produces

137

some small side-load. Lastly, the FPE is subject to parasitic losses associate with hydraulic valve actuation not captured by the model.

5.5 Heat Loss

Heat loss is provided in Figure 5.10 as an MEP-type measurement. Specifically, we define QMEP as the heat transfer per cycle in Joules normalized by the total engine displacement. In this sense, QMEP is an indication of absolute heat loss. Each engine in Figure 5.10 presents only a slightly different QMEP, although the magnitudes are similar. For all engines, high in-cylinder surface-area-to-volume ratios near TDC promote elevated heat transfer rates. By dwelling for longer durations near TDC, HLE cylinders 2 and 3 undergo more heat loss. As a result, the HLE experiences a marginally higher QMEP in Figure 5.10, compounded by higher peak temperatures (shown in Figure 5.4). Equally, the FPE is only momentarily close to the turnaround point and shows a lower overall QMEP in Figure 5.10, even with fast combustion and higher peak temperatures. Additionally, because heat transfer is a function of temperature differential, Figure 5.10 follows roughly the same trends as peak temperature shown in Figure 5.4.

Figure 5.11 plots heat transfer as a percentage of the total injected fuel energy. While the QMEP in Figure 5.10 is predominantly dependent on load, normalizing by fuel energy introduces the consequence of other processes like friction. As a result, HLE and ICE heat transfer percentage is principally a function of engine speed in Figure 5.11. Overall heat transfer percentage decreases as engine speed escalates because smaller cycle durations provide less time for heat exchange. Once again, HLE cylinders 2 and 3 experience greater heat transfer than cylinders 1 and 2 due to piston dynamics. FPE heat loss percentage is both a function of load and compression ratio. As clearance volume decreases, higher surface-area-to-volume ratios lead to amplified heat loss.
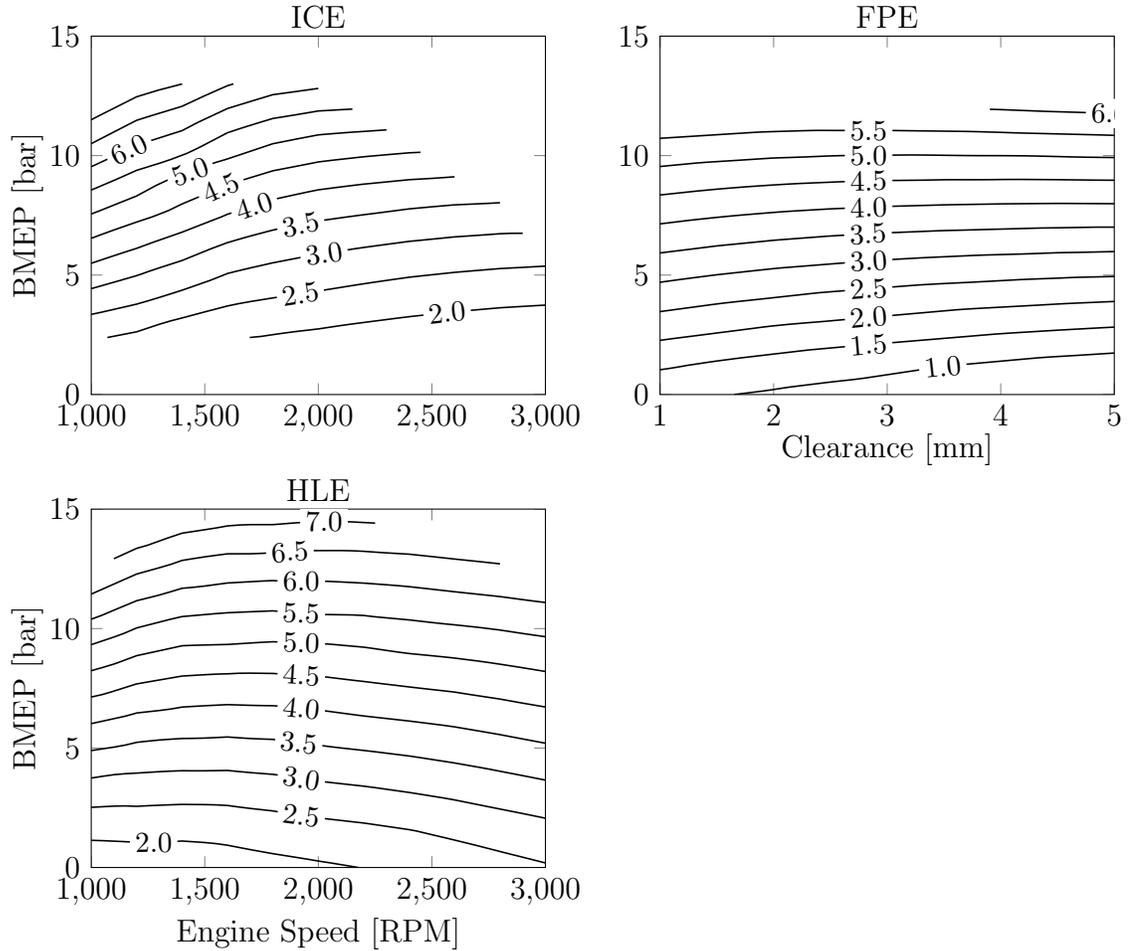
Figure 5.10: Heat transfer per cycle normalized by displacement [bar] of the HLE, FPE, and ICE. The HLE and ICE behavior is a function of engine speed [RPM] and load. The FPE performance is a function of clearance height [mm] and load. Load is the useful hydraulic work per cycle normalized by the displacement volume, denoted as BMEP [bar].

Given that FPE mechanical efficiency is relatively high in Figure 5.9, heat loss accounts for a comparatively larger fraction of FPE fuel energy in Figure 5.11 in contrast with the other engines. However absolute FPE heat loss, shown in Figure 5.10, is slightly lower than the HLE or ICE exhibit. Therefore, looking at fractional heat loss yields an incomplete picture of heat loss behavior, and absolute FPE heat loss must be considered.

Regarding accuracy, note that Hohenberg's heat transfer correlation is an empirical relationship established through careful observation of conventional engine behav-
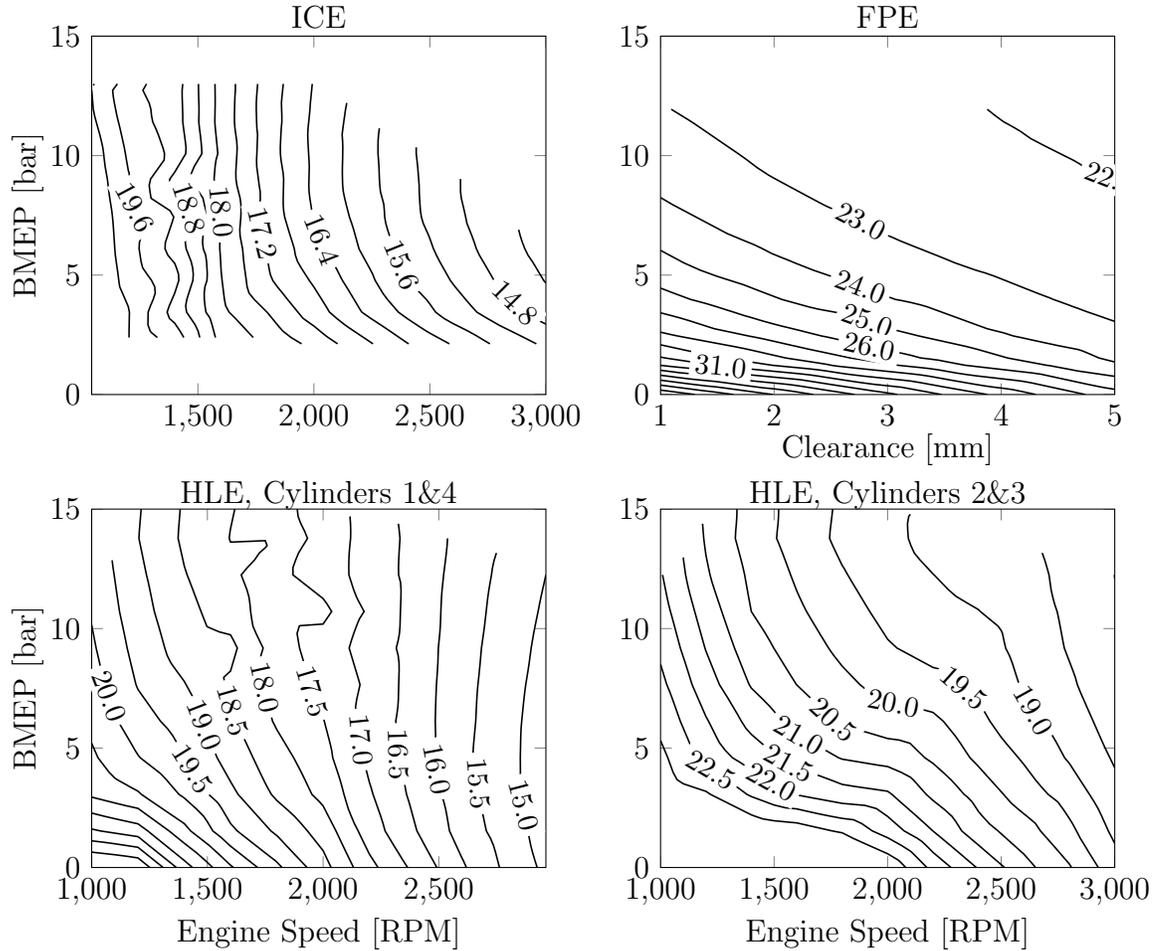
Figure 5.11: Heat transfer as a fraction of fuel energy [%] of the HLE, FPE, and ICE. The HLE and ICE behavior is a function of engine speed [RPM] and load. The FPE performance is a function of clearance height [mm] and load. Load is the useful hydraulic work per cycle normalized by the displacement volume, denoted as BMEP [bar].

ior [47]. While the correlation may capture the general behavior of heat transfer in each engine, it is not intended for application with FPE or HLE-like piston dynamic or combustion and may therefore introduce some error.

5.6   Indicated Performance

Net indicated mean effective pressure (IMEP) is the indicated work calculated from the pressure-volume history over a single cycle, normalized by the displaced vol-

ume. In each case, the IMEP shown in Figure 5.12 is almost exclusively a function of load. However, as friction builds with speed, HLE IMEP increases. Because the FPE exhibits lower friction and heat transfer than the HLE and ICE, the corresponding IMEP is lower.
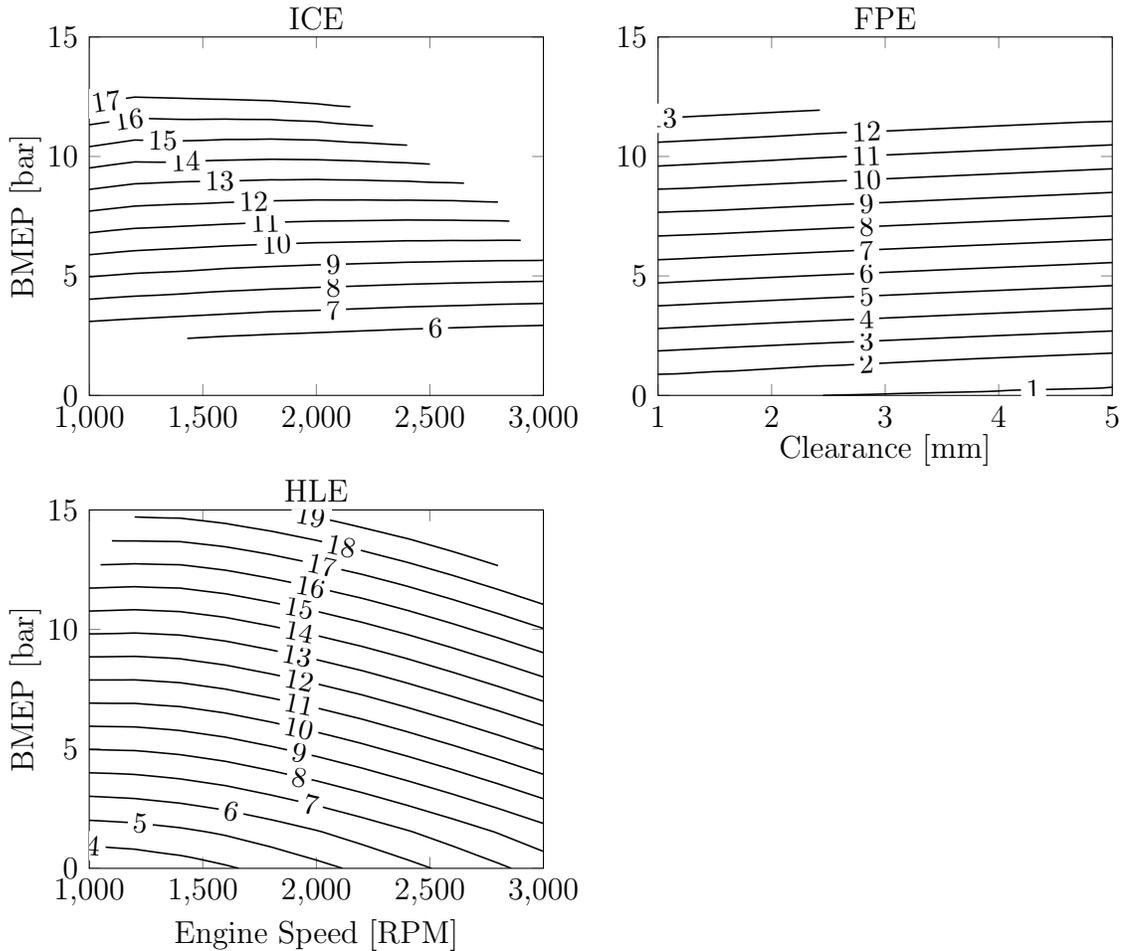
Figure 5.12: IMEP [bar] of the HLE, FPE, and ICE. The HLE and ICE behavior is a function of engine speed [RPM] and load. The FPE performance is a function of clearance height [mm] and load. Load is the useful hydraulic work per cycle normalized by the displacement volume, denoted as BMEP [bar].

Figure 5.13 shows the net indicated efficiency of each engine, i.e. the indicated work as a fraction of fuel energy. Elevated heat transfer percentages (see Figure 5.11) rapidly decrease the FPE indicated efficiency presented in Figure 5.13 at low load, negating potential advantages of higher compression ratios. However, higher load

141

reductions in TDC clearance height lead to clear benefits to indicated efficiency in Figure 5.13.

As expected, the ICE and HLE cylinders 1 and 4 exhibit similar indicated efficiency behavior in Figure 5.13. They experience similar piston velocity profiles, although somewhat different combustion duration. Overall, HLE cylinders 2 and 3 exhibit lower indicated efficiencies in Figure 5.13 because longer TDC dwell increases heat loss.
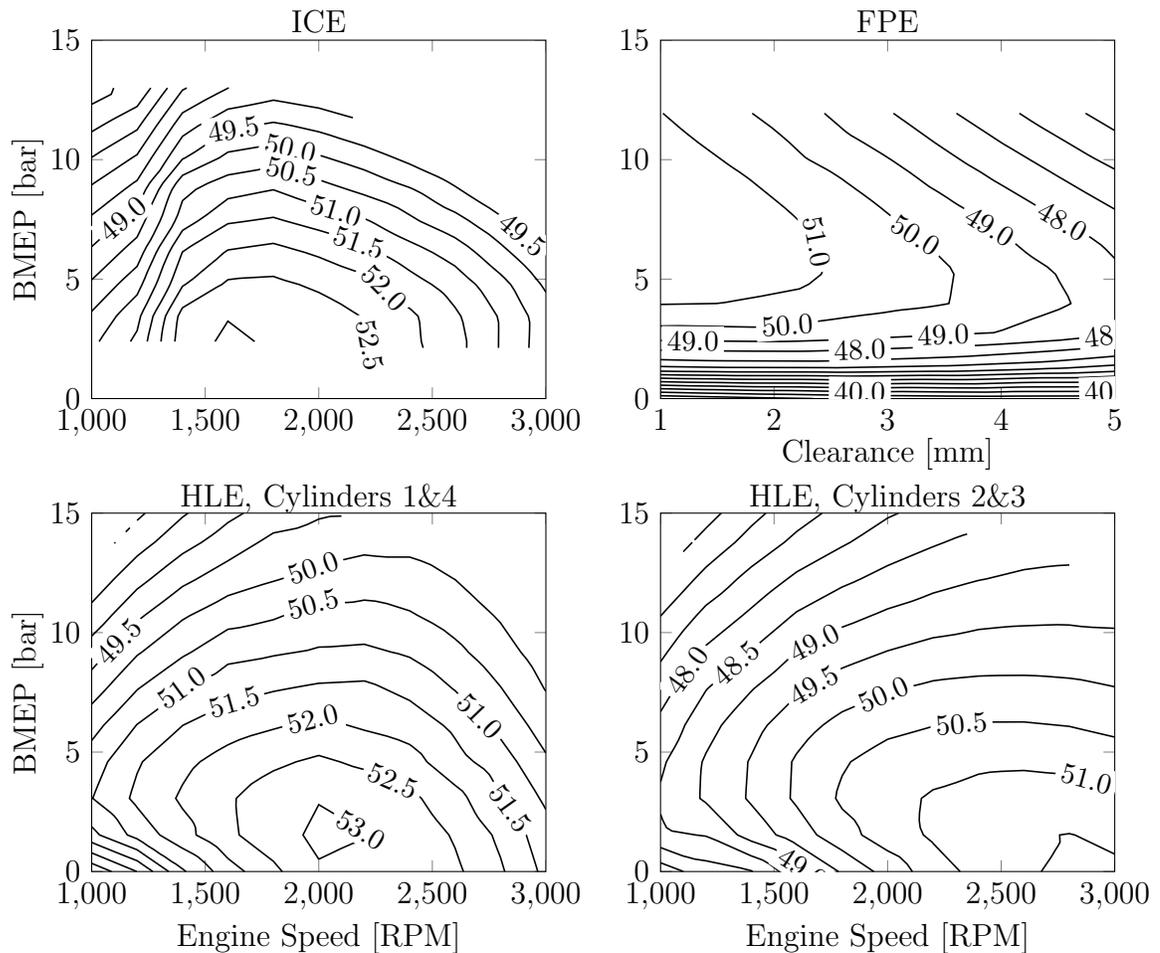
Figure 5.13: Indicated Efficiency [%] of the HLE, FPE, and ICE. The HLE and ICE behavior is a function of engine speed [RPM] and load. The FPE performance is a function of clearance height [mm] and load. Load is the useful hydraulic work per cycle normalized by the displacement volume, denoted as BMEP [bar].

5.7 Combustion Duration and Injection Timing

To investigate the HLE and FPE sensitivity to injection timing and combustion duration, a series of physics-based simulations evaluated indicated efficiency. The models parametrically altered the start of injection (SOI) and $D(t)$ from (2.26). Both engines operate at 15 kW, near 1000 RPM or RPM equivalent, and with an 18.4:1 compression ratio. Because it is not a novel concept, we do not consider ICE behavior. Figure 5.14 contains the resulting data. As presented, combustion duration is the interval of time in milliseconds corresponding to 10-90% fuel consumption. Start of injection occurs at some distance in millimeters before TDC.
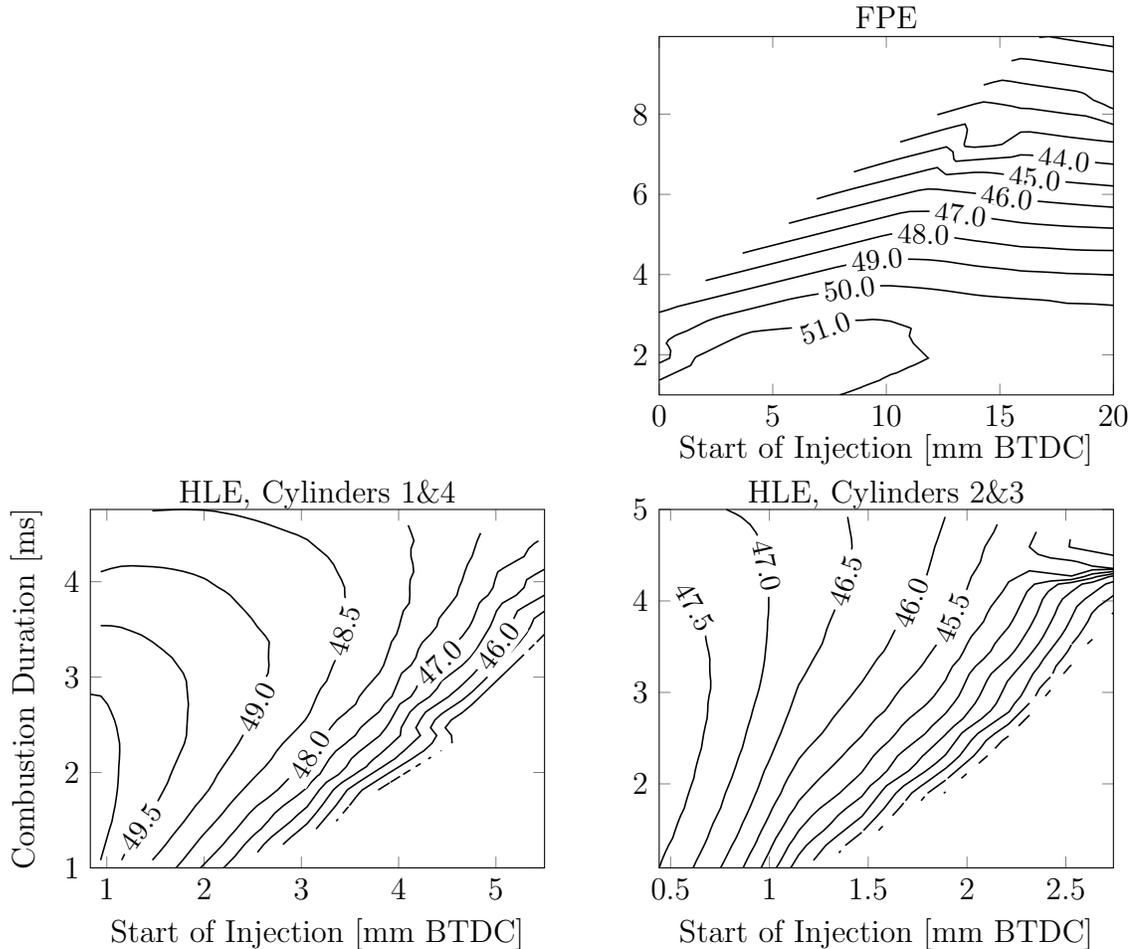
Figure 5.14: Indicated Efficiency [%] of the HLE and FPE as a function of combustion duration [ms] and start of injection [mm Before Top Dead Center (BTDC)].

Figure 5.14 shows that as injection timing approaches TDC for HLE cylinders 2 and 3, it has a greater impact on indicated efficiency than combustion duration. Otherwise stated, the indicated efficiency is more sensitive to injection timing at these conditions. Because HLE cylinders 2 and 3 have a long TDC dwell, for injections near TDC there is sufficient time available for combustion to complete before expansion. However, as injection timing advances there is more time for heat transfer. The increased heat transfer causes thermal efficiencies to drop and results in an increase in sensitivity to combustion duration in Figure 5.14.

In Figure 5.14, HLE cylinders 1 and 4 are more sensitive to combustion duration than cylinders 2 and 3 due to a shorter TDC dwell. For an SOI close to TDC, longer combustion durations in HLE cylinders 1 and 4 cannot produce the appropriate pressure rise before expansion. The resulting less than constant volume combustion decreases indicated efficiency. Injection timing impact on HLE cylinders 1 and 4 in Figure 5.14 is similar to SOI impact on HLE cylinders 2 and 3, but on a larger scale due to higher TDC piston velocities.

Free-piston engine thermal efficiency in Figure 5.14 is not particularly sensitive to injection timing. Van Blarigan et al. noted similar behavior, stating that efficiency did not seem to suffer from compression after combustion [102]. With a brief TDC dwell, the FPE piston occupies a high surface-area-to-volume position for a short duration. As a result, hot combustion gasses have less opportunity for heat transfer. Keep in mind, however, that advanced combustion may not be desirable from a practical perspective as higher pressures resulting from early injection may increase friction and damage components. In contrast, the FPE is very sensitive to combustion duration. Without the appropriate period of time at low volume, longer combustion durations diminish peak pressures, prolong the burn further into the expansion stroke, and hinder a constant volume process.

5.8   Hydraulic Conversion Efficiency and BSFC

Hydraulic conversion efficiency, conveyed for each engine in Figure 5.15, expresses the fraction of fuel energy contributing to useful hydraulic work. The crank constrained engines display fundamentally similar behavior in Figure 5.15, wherein friction accounts for the largest discrepancies. Of the three hydraulic power plants, the ICE exhibits the lowest efficiency due to increased friction. Optimal HLE efficiency conditions occur at slightly lower engine speeds than the ICE. As the piston velocity rises, high oscillating mass degrades the HLE performance and causes the discrepancy. Because free-piston friction is minimal and absolute heat loss is lower, the FPE possess the highest comparative hydraulic conversion efficiencies of the three engines in Figure 5.15. However, the FPE compression ratio is unexpectedly insignificant, particularly at low load and low clearance. At these conditions, high surface-area-to-volume ratios ensure higher heat transfer percentages dominate, as alluded to in Figure 5.11. Additionally, Figure 5.9 shows that load is the primary mechanism contributing to mechanical efficiency, further reducing the impact of compression ratio. The anticipated advantages of larger compression ratios instead surface at high load in Figure 5.15.

brake specific fuel consumption (BSFC) is the fuel injection rate per unit power. Decreasing BSFC magnitudes correspond to better behavior. By normalizing with power, BSFC is a convenient performance parameter for comparing multiple engines. By definition, BSFC trends, available in Figure 5.16, are somewhat inverse compared to the hydraulic conversion efficiency (Figure 5.15) ; an increase in hydraulic conversion efficiency generally indicates a decrease in BSFC. As a result, the same trends follow from the discussion above. The ICE and HLE have a similar BSFC range and behavior while the FPE has overall lower values due to decreased friction and heat transfer that are largely dependent on load.
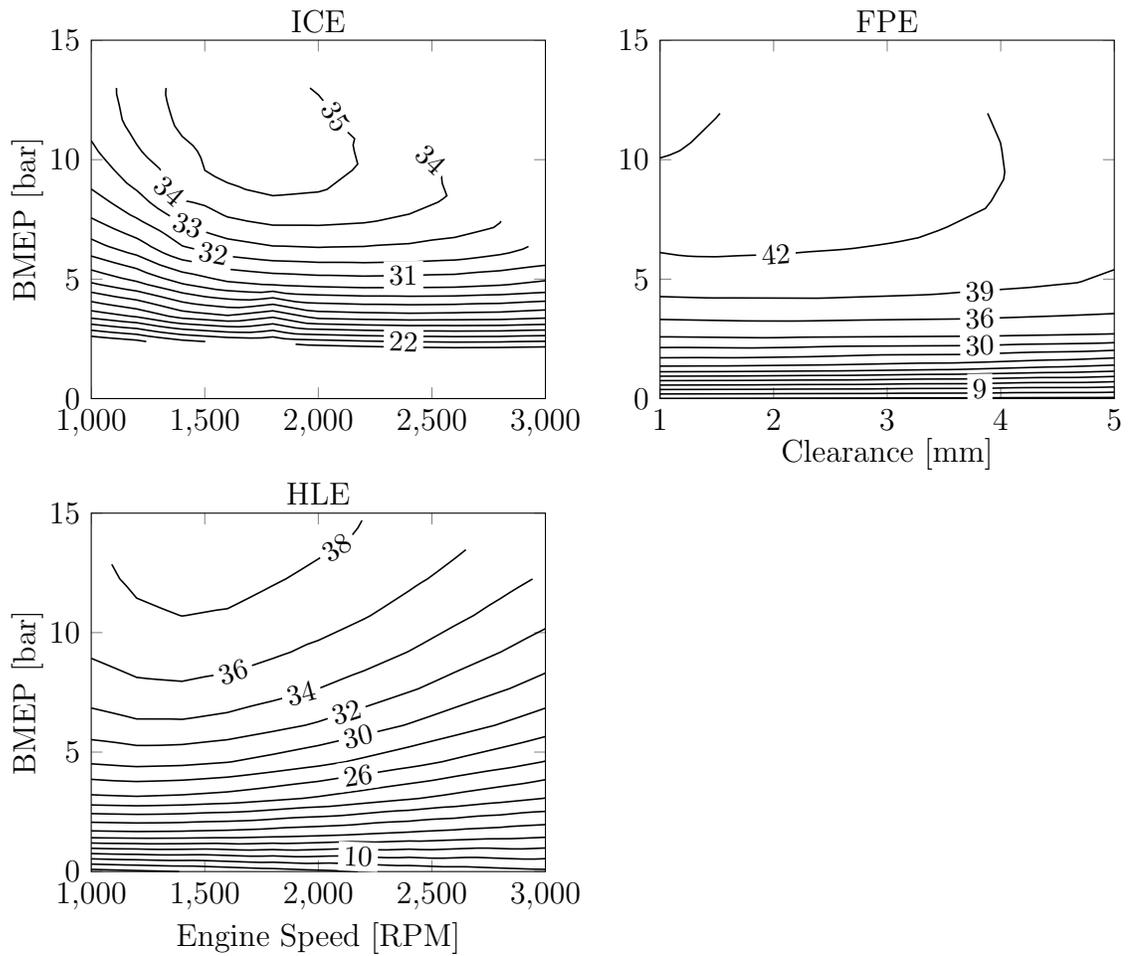
Figure 5.15: Hydraulic Conversion Efficiency [%] of the HLE, FPE, and ICE. The HLE and ICE behavior is a function of engine speed [RPM] and load. The FPE performance is a function of clearance height [mm] and load. Load is the useful hydraulic work per cycle normalized by the displacement volume, denoted as BMEP [bar].
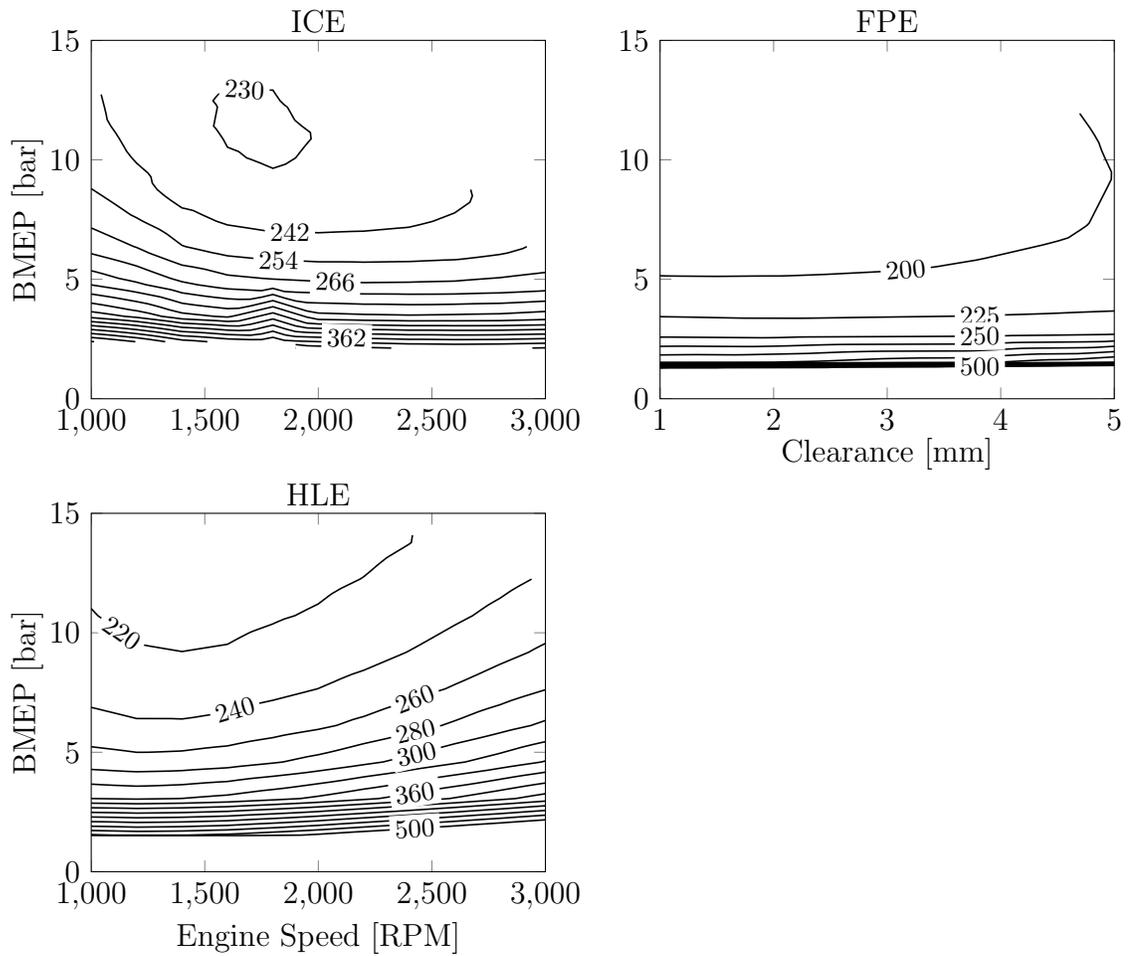
Figure 5.16: BSFC $\left[\frac{g}{kWh}\right]$ of the HLE, FPE, and ICE. The HLE and ICE behavior is a function of engine speed [RPM] and load. The FPE performance is a function of clearance height [mm] and load. Load is the useful hydraulic work per cycle normalized by the displacement volume, denoted as BMEP [bar].

5.9   Power and Minimum BSFC Path

Figure 5.17 shows hydraulic power output maps superimposed on the BSFC plots from Figure 5.16. Trends in HLE and FPE power are similar because both engines are crank constrained, and as such, power increases with both load and speed. In contrast, FPE operating frequencies are virtually constant, bounded between 720 and 1160 RPM equivalent as shown in Figure 5.18. Several institutions documented analogous behavior [1, 68]. Accordingly, the FPE power range is severely limited when weighed against HLE and ICE output and is a distinct disadvantage to operating without a crank.

By comparing the BSFC and power curves, Figure 5.17 also traces the lowest possible BSFC path at each power level. The HLE minimum BSFC line in Figure 5.17 tends to operate at the minimum speed corresponding to a particular power. By operating a lower speed, the HLE reduces friction associated with a large oscillating piston mass. In Figure 5.17 the ICE exhibits its peak performance at slightly higher speeds than the HLE and follows a minimum BSFC path more balanced between speed and load.

Unexpectedly, the FPE minimum BSFC line in Figure 5.17 does not run exclusively at high compression ratios. As Figure 5.18 shows, FPE frequency increases as clearance ratios decreases. Consequently, the small changes in speed slightly increase FPE power as clearance decreases. Were the frequency constant, FPE power would be exclusively load dependent and the best BSFC line would fall at low clearance. Instead, the combination of frequency, heat loss, and friction produces the minimum BSFC path from Figure 5.18. The FPE minimum BSFC line lingers at high compression ratios at near peak power but operates across the entire clearance height range as load decreases.

Although the FPE has a narrow power range, additional measures can increase both engine speed and power output. The natural frequency of an FPE is a function
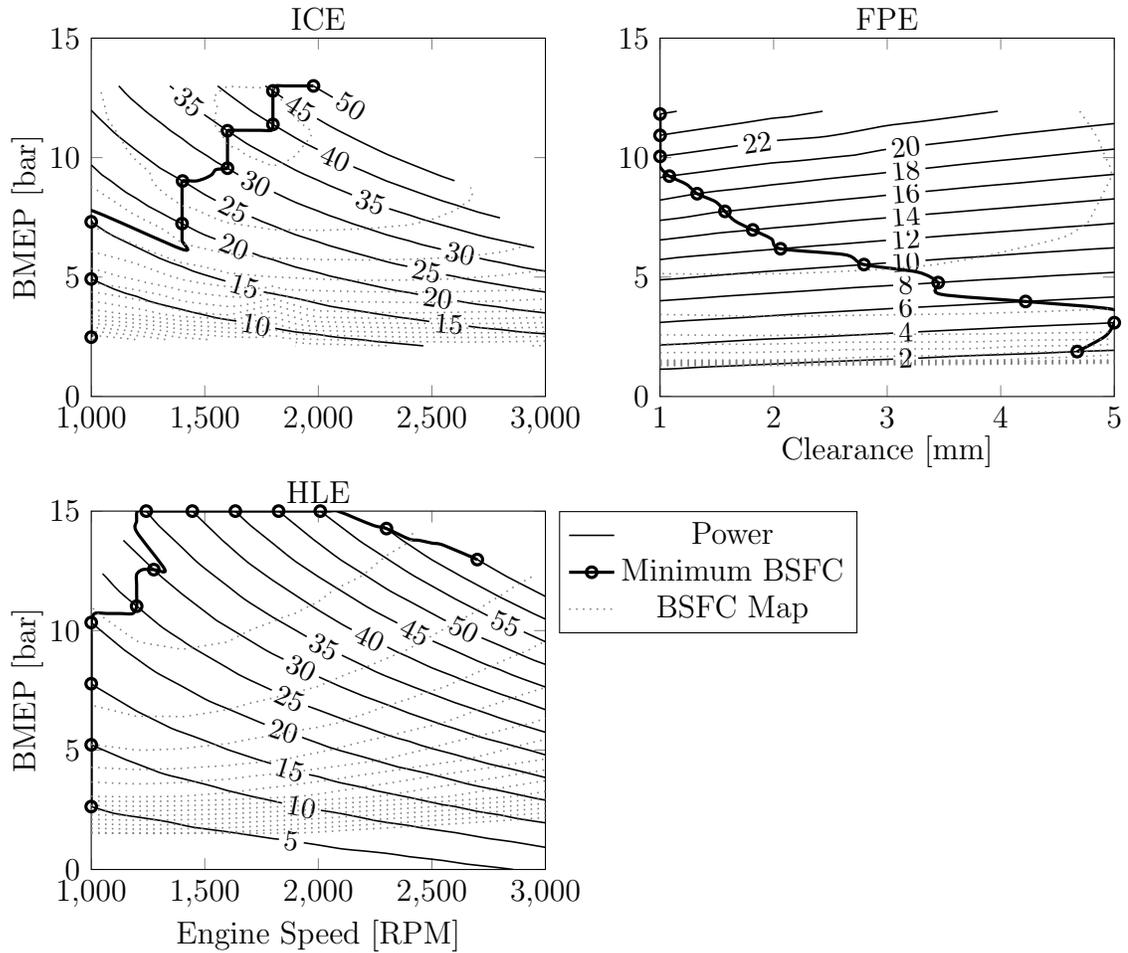
Figure 5.17: Power [kW] and lowest BSFC line of the HLE, FPE, and ICE. The HLE and ICE behavior is a function of engine speed [RPM] and load. The FPE performance is a function of clearance height [mm] and load. Load is the useful hydraulic work per cycle normalized by the displacement volume, denoted as BMEP [bar].

of piston mass, working pressure (intake pressure), friction, compression ratio, gas properties, and load. Load and compression ratio actuators are required to meet a certain power demand and will not significantly extend the current power range of the engine. Likewise, improvements to damping and friction are not necessarily available. However, more advanced design and manufacturing could reduce piston mass. As shown in Figure 5.19, a 50% decrease in piston assembly mass will result in roughly a 30% increase in operating frequency.

Intake pressure and gas properties are also available as actuators to adjust FPE
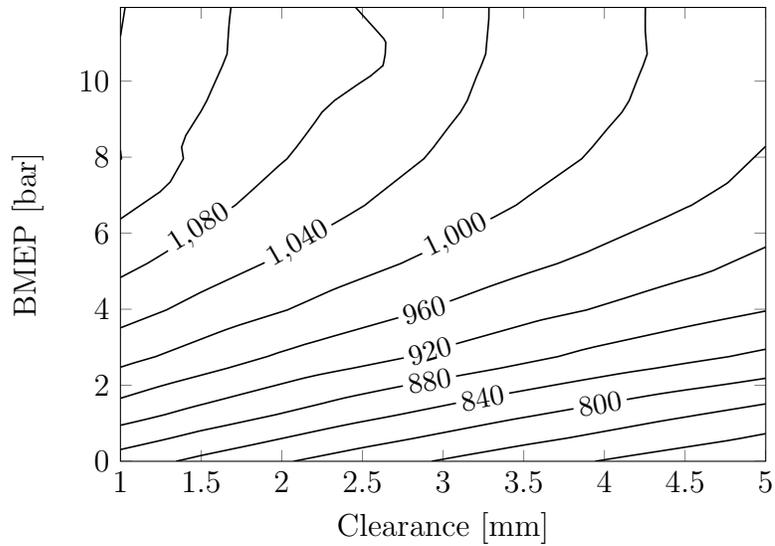
Figure 5.18: FPE Operating Speed [RPM Equivalent] as a function of clearance height [mm] and load. Every two strokes, an FPE completes the equivalent of a conventional engine's revolution. The RPM equivalent is the number of equivalent revolutions completed in one minute. Load is the useful hydraulic work per cycle normalized by the displacement volume, denoted as BMEP [bar].
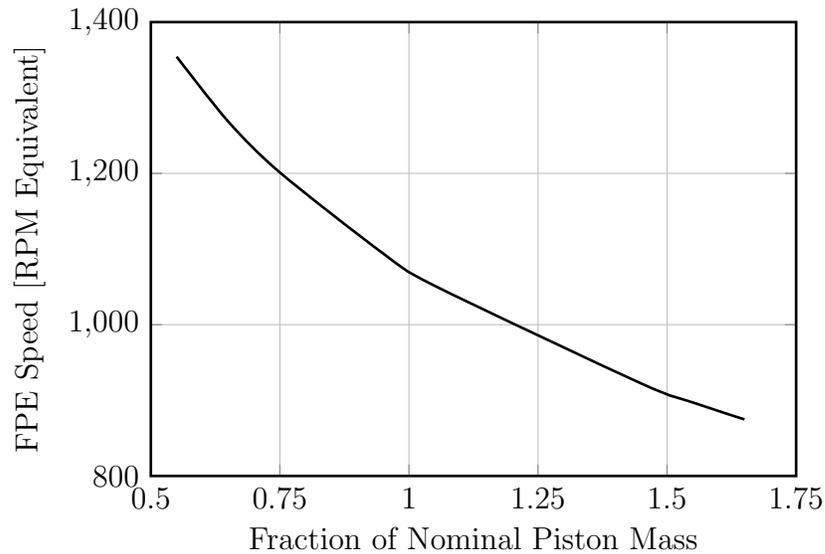
Figure 5.19: FPE Operating Speed [RPM Equivalent] as a function of fraction of nominal piston mass. Every two strokes, an FPE completes the equivalent of a conventional engine's revolution. The RPM equivalent is the number of equivalent revolutions completed in one minute.

power. Turbochargers expand hot exhaust gasses and use the mechanical work to compress atmospheric air to higher pressures prior to entering the intake manifold.

Higher intake pressures enable the cylinder to capture more air during induction, increasing power density. As an added benefit, elevated cylinder pressures also increase FPE operating frequency, further improving power. While the two-fold turbocharger benefit is attractive, intake and exhaust manifold transients resulting from turbine dynamics will present an additional controls challenge.

exhaust gas recirculation (EGR) is the process of inserting exhaust products into the intake stream, often to reduce combustion temperatures and NOx emmisions. Essentially, EGR decreases a mixtures ratio of specific heats, γ. Decreasing γ lowers FPE oscillation frequency. By extension, EGR may be undesirable because power output drops. It will be important to keep the negative impacts of EGR in mind when considering FPE emissions.

5.10   Comparison of Performance Parameters along Minimum BSFC Path

Figure 5.20 compares the hydraulic conversion efficiency, BSFC, and heat transfer percentages of each engine along minimum BSFC conditions. While frictional advantages provide the FPE with higher relative efficiency and lower BSFC, uncontrollable operating frequencies limit maximum FPE power. The HLE appears to be a suitable balance between power output and hydraulic efficiency. As predicted in Section 5.5, the ICE and HLE cylinders 1 and 4 operate with similar heat transfer percentages in Figure 5.20 due to nearly identical piston dynamics about TDC. However, HLE cylinders 3 and 4 suffer higher heat losses than cylinders 1 and 2 in Figure 5.20 as a result of longer durations with high surface-area-to-volume ratios. The FPE presents the highest heat transfer percentage in Figure 5.20, but recall from Section 5.5 that the absolute magnitude of energy lost to the cylinder walls is similar for all engines. Higher FPE heat loss percentages occur because the overall system is more efficient.
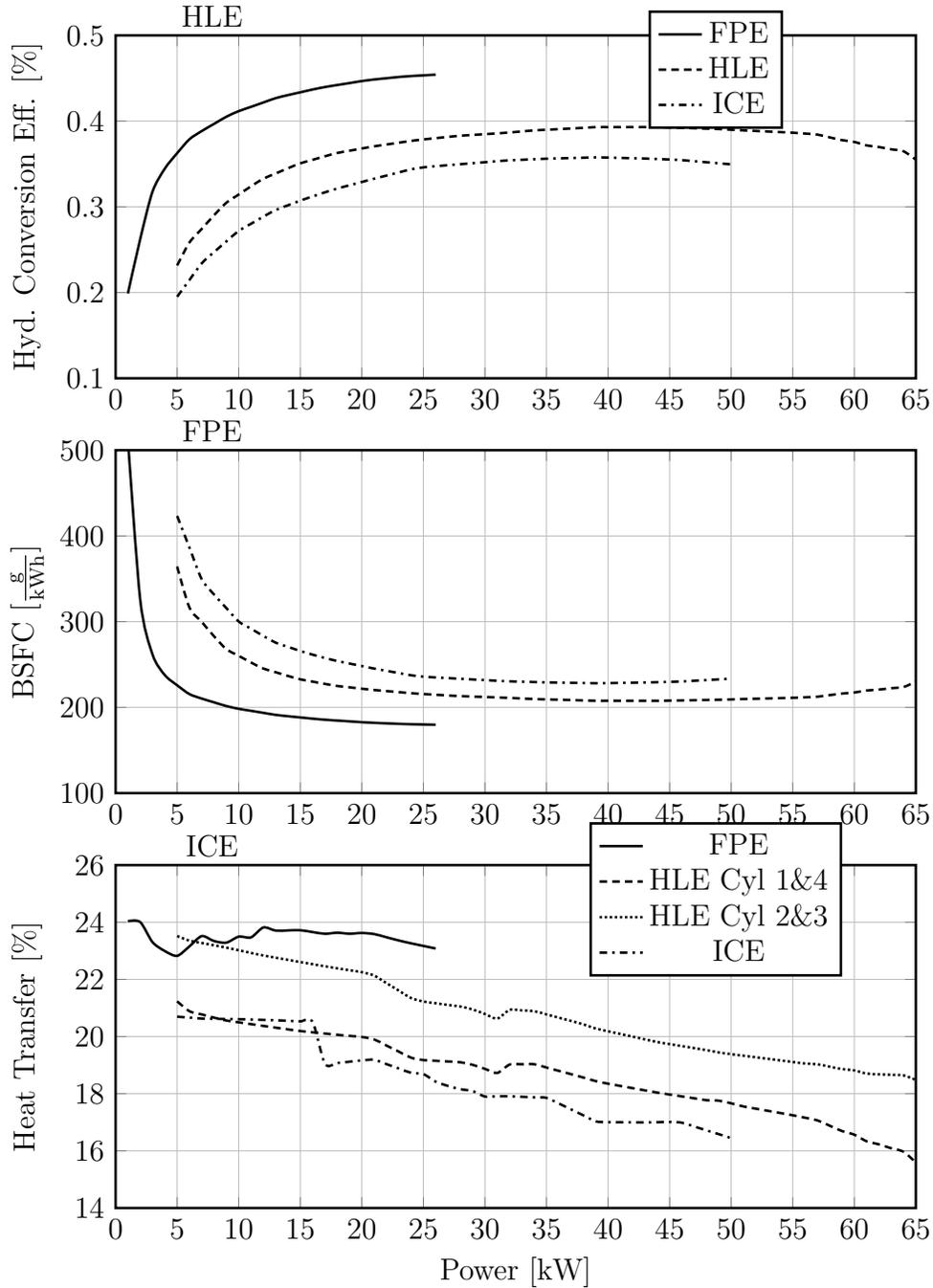
Figure 5.20: Comparison of hydraulic conversion efficiency [%], BSFC [$\frac{g}{kWh}$], and Heat Transfer [%] along the minimum BSFC path. This figure presents heat transfer as a percentage of total fuel energy for each HLE cylinder because they perform differently.

5.11 BSFC Breakdown

Figure 5.21 contains a breakdown of each engine's BSFC along the minimum BSFC line plotted in Figures 5.20 and 5.17. The subplots divide BSFC into fractions

describing fuel energy contribution to useful work, fuel energy lost through friction, fuel energy lost as heat transfer, and fuel energy available in the exhaust. Keep in mind that indicated efficiency is approximately the friction plus useful work fractions over the whole, while hydraulic conversion efficiency is the useful work fraction over the whole.

As depicted in Figures 5.20, the FPE presents the best BSFC performance. Figure 5.21 clearly demonstrates that FPE friction is minute relative to the other modeled engines, giving it a distinct advantage. Interestingly, FPE exhaust energy is also comparatively low, corroborated by the low exhaust gas temperatures in Figure 5.5. However, the absolute heat transfer of each engine is roughly the same, see Figure 5.10 and Section 5.5. As a result FPE heat loss percentage is larger than both the HLE and ICE, shown by Figure 5.11. By combining the frictional losses and useful work in Figure 5.21, it is apparent that HLE, FPE, and ICE indicated efficiencies are more or less 50%, agreeing with Figure 5.13. The only real improvement moving from ICE to HLE in Figure 5.21 is friction. The HLE experiences low mid-power friction, but as the speed increases toward higher power levels, friction increases due to issues with excessive piston mass discussed in Section 5.4.
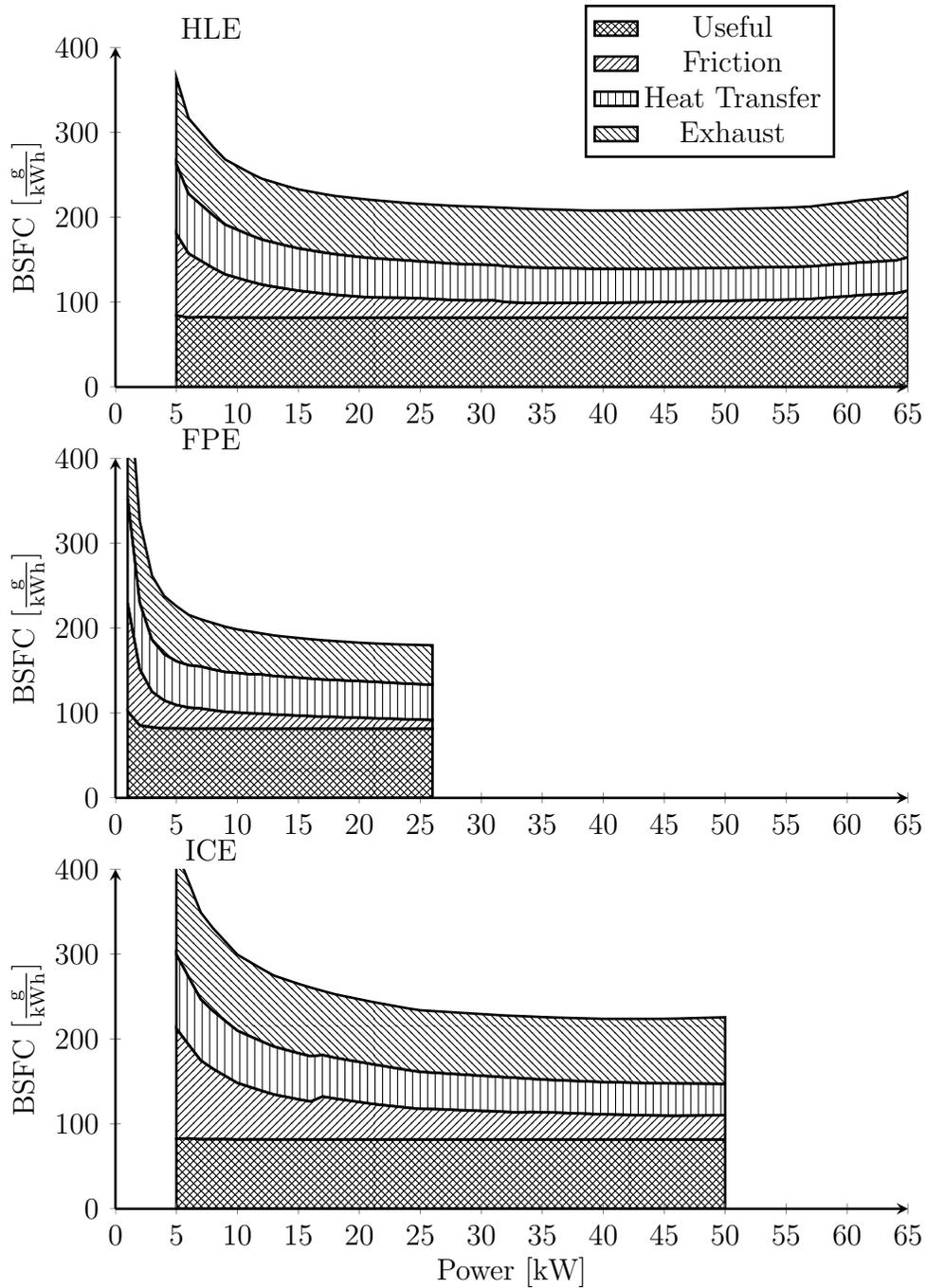
Figure 5.21: Breakdown of HLE, FPE, and ICE BSFC [$\frac{g}{kWh}$] energy content as a function of power [kW] along the minimum BSFC line.

5.12 Beginning of Power Extraction

With current prototype hardware, high pumping chamber pressures prevent FPE and HLE hydraulic power extraction (PX) from terminating before a turnaround

point. As a result, PX is confined to the end of a stroke. It may be advantageous for future hardware iterations to have some additional freedom in PX scheduling. Figure 5.22 explores the potential benefits of advancing the PX window toward TDC rather than BDC while using a 50% hydraulic stroke length at 2000 RPM. Even considering multiple accumulator pressures, Figure 5.22 indicates there is no apparent thermal advantage moving the PX window. While a higher fidelity hydraulics model or experimental testing could potentially show otherwise, it is unnecessary to research and implement a new mechanism to alter PX. However, providing the end of PX as well as the beginning of PX as actuators may assist with controls accuracy and robustness.
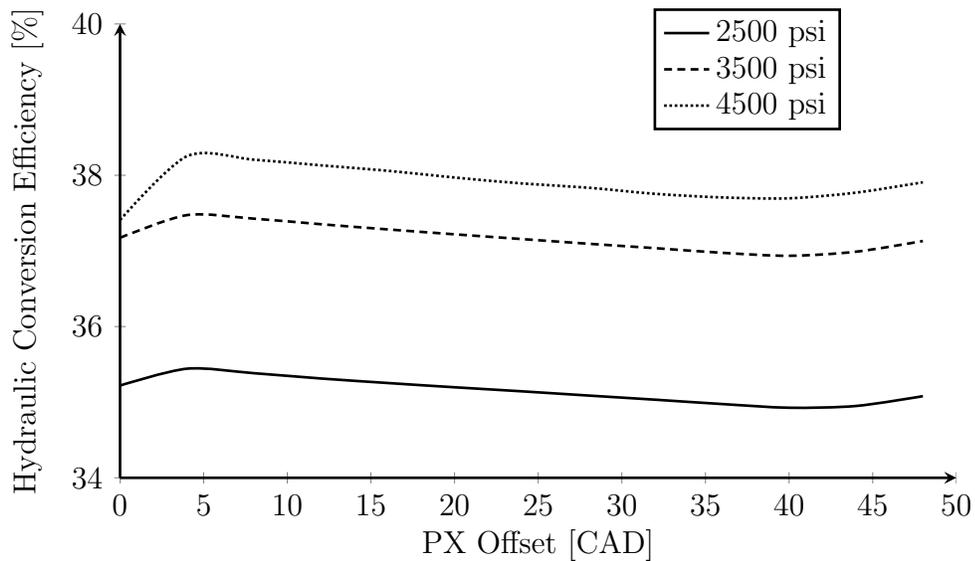
Figure 5.22: Hydraulic Conversion Efficiency [%] of the HLE as a function of EOPX and BOPX offset [CAD] with constant hydraulic power take-off.

5.13   Conclusions

Using the physics-based modeling framework discussed in Chapter II, this chapter compares an FPE, HLE, and ICE in context of hydraulic power generation. While each engine exhibits a similar magnitude of heat loss, the FPE experiences less than

half the friction losses of an HLE or FPE. However, the FPE is confined to a severely low power range as a result of limited engine speeds. Because heat transfer increases as clearance decreases, minimum FPE BSFC performance at a fixed power output does not necessarily occur at the highest compression ratio. The HLE also has the advantage over the ICE with respects to friction, although HLE performance suffers at high speed due high piston assembly mass. Overall, however, the HLE demonstrates the desirable combination of low friction and high power. The HLE has fewer moving parts and no piston side loads, and therefore exhibits lower friction than a conventional engine in our simulations. Further, by possessing a crank, the HLE is able to increase frequency and achieves a higher hydraulic power output than the FPE.

To remark on model accuracy, Hohenbergs heat transfer model [47] and Watsons heat release [104] model are empirical formulas derived from observation of conventional engines. While the relations are a good and necessary place to start, they do not necessarily capture the true behavior of an HLE and FPE.

CHAPTER VI

Conclusions

This dissertation has addressed several modeling and control problems for a free-piston engine (FPE) and its derivates us as the hydraulic linear engine (HLE). The EPA has developed a new engine for application in a series hydraulic hybrid vehicle, the HLE. The HLE is built on FPE principles, but possess a single crank as a safety mechanism to constrain piston motion. The crank does not transmit power to a load. Rather, a linear hydraulic pump extracts work directly from the oscillating piston motion. One of the objectives of this dissertation was to compare and evaluate the performance of the HLE and FPE compared to a conventional internal combustion engine (ICE). To this end, we described the tools developed to enable and evaluate HLE and FPE operation.

In Chapter II we developed a physics-based modeling framework to describe the behavior of an HLE, FPE, and a conventional ICE. An HLE simulations suggest discrepancies in cylinder-to-cylinder performance; the differences are partially due to cylinder bore variations and are partially the result of incongruent piston velocities approaching TDC and BDC. Although a production scale HLE may possess balanced geometry, asymmetric piston velocities are unavoidable, create heat transfer dispari-ties, and necessitate an active approach to cylinder-balancing.

Chapter III describes an adaptive control method to estimate and adjust for dif-

ferences in cylinder behavior. Using recursive least square techniques and an energy balance to create a control-oriented model, the controller ensures that an estimate of rotation kinetic energy tracks a set point. The algorithm successfully reduces variations in sampled engine speed as much as 99% on the physics-based model. As an added bonus, the proposed methods enable the engine to function with different loads and conditions in each cylinder and potentially allows unique operating modes. Differences in cylinder behavior also require that each cylinder be optimized individual. We leverage the adaptive cylinder balancing controller to use an extremum-seeking-type algorithm for optimization of injection timing for each cylinder individually. A physics-based HLE simulation demonstrates parameter convergence and BSFC improvement.

In order to enable FPE operation and evaluate an HLE performance comparison, Chapter IV proposes a method of FPE fuel and load control. The most significant issue preventing a useful FPE is robust and reliable control of TDC piston position. We create a discrete, control-oriented model by sampling the clearance height at each turnaround and using the same energy balance principles employed for HLE control. A model linearization provides information regarding FPE stability and sensitivity. At high loads and compression ratios, the FPE has a pole outside the unit disc and is open-loop unstable. Suppose the FPE is at equilibrium with constant fuel and load when a disturbance increases the compression ratio. Physically, instability occurs because the additional energy put into the system through an increase in efficiency is greater than the additional energy either lost to friction or extracted as useful work. As a result, the following stroke will have a greater compression ratio and the effect will cascade until collusions with the cylinder head. To stabilize the FPE, feedback control is crucial. Additionally, an FPE sensitivity reveals that as compression ratio increases, fuel as an actuator loses control authority over TDC position. Since the control-oriented model is nonlinear and without an explicit solution, we linearize

the system about an operating point and use dynamic inversion with linear quadratic techniques to place closed-loop poles inside the unit disc. A smith predictor solves for current sates using Newtons method to adjust for a single time step delay and enable state feedback. As demonstrated with a physics-based model, the proposed controller stabilizes the FPE and tracks clearance set points. However, abrupt load changes can cause the piston to travel outside a safe operating range. To constrain piston motion, we use reference governor techniques to manage load transitions. The algorithm calculates the maximum possible increase in load that will maintain an acceptable piston trajectory for all future time steps. When implemented on the physics-based model, the resulting reference governor maintains the reference clearance within $\pm$ 0.5 mm of a nominal set point during a load change.

With FPE and HLE control established, Chapter V uses the physics-based modeling framework to compare FPE, HLE, and ICE performance under similar conditions with identical geometry. Each engine exhibits a similar magnitude of heat loss. However, FPE friction is comparatively low without a crank. Hydraulic linear engine friction increases drastically at high speeds because a large oscillating mass increases bearing loads. Indicated efficiencies show only marginal improvements in FPE behavior with increasing compression ratio because rapid combustion results in increased heat transfer. Further, the FPE has low power range relative to the HLE and ICE due to engine speed limitations. By breaking down BSFC losses across the best BSFC lines, friction has the biggest impact on the modeled performance of each engine.

6.1   Comments on FPE and HLE Design

Chapters II - V highlight several opportunities to improve HLE and FPE design.

The current HLE prototype possesses a high mass oscillating piston assembly of 36 kg (80 lbs). The large piston mass applies high loads to the crank bearing, connecting rod, and flywheel. Previously, engine speed fluctuations have occasionally damaged

the HLE prototype. Further, high bearing loads lead to high frictional losses. Large piston mass is a liability of the HLE design, detrimental to both robustness and friction. Future HLE hardware iterations should decrease oscillating inertia while also improving mechanical strength of the flywheel, connecting rod, and crank.

While manufacturing identical cylinder bores may be ideal from a cost perspective, an adaptive cylinder balancing algorithm will always be necessary for an HLE to adjust for heat loss discrepancies due to crank dynamics. Additionally, there is no apparent efficiency advantage to altering the HLE end of power extraction position. However, HLE controls may benefit from an additional actuator.

As FPE compression ratio increases, fuel control authority decreases. As a result, turnaround position is less sensitive to fuel and combustion-based disturbances at high compression ratios. Ensuring the highest possible compression ratio before the piston could possibly impact the cylinder head reduces the possibility of collision. In order to improve FPE safety and robustness, it is important to incorporate the smallest possible cylinder bowl or to remove it entirely.

This dissertation definitively shows that feedback control is necessary to achieve stable FPE operation; open-loop calibration is not sufficient at high load. Two alterations will improve FPE power by accelerating operating frequency: a decrease in oscillating mass and an increase in intake pressure. To this end, including a turbocharger will increase power output by both increasing intake pressure and enabling higher fueling.

The FPE is particularly sensitive to combustion duration wherein a longer burn leads to decreased thermal efficiency. Future iterations of FPE design should incorporate fast combustion schemes like HCCI and avoid long strategies like split injection that decrease the burn rate.

6.2 Future Work

This dissertation underscores numerous opportunities for additional investigation.

6.2.1 HLE and FPE Experimentation

Because the HLE is a novel design, the concept is virtually unexplored. Additional research is necessary to understand the benefits offered by the HLE and to properly optimize the system. Experimentation is crucial to characterizing combustion, heat transfer, and other losses. As the results in Section 2.4 indicate, any additional HLE testing with the current hardware configuration should focus around low rotational velocities in a mid to high load range to minimize crank stress.

Like the HLE, FPE combustion and heat transfer are not well understood and require additional experimental observation. Additionally, the potential benefits of forced induction with an FPE warrant further investigation. As it was outside the scope of this dissertation, further studies are necessary to address vehicle emissions requirements.

6.2.2 Physics-Based HLE and FPE Model Improvement

Simulations are helpful in exploring operating conditions not easily or cost effectively investigated with experimentation. However, models are only as accurate as the individual components. The current generation of HLE and FPE simulations is dependent on models created through empirical observation of conventional engines. New heat loss, friction, and combustion correlations based on experimental FPE and HLE data are necessary to better simulate FPE and HLE behavior.

For an HHV application, hydraulic transmission losses, viscous losses, and pressure waves also warrant inclusion into future physics-based FPE and HLE models. It would also be informative to incorporate accumulator dynamics, vehicle dynamics, and road loads into the system. By introducing a number of drive cycles, a more

accurate comparison to conventional hybrid technology can be made.

6.2.3 HLE and FPE Control

As in any application, improved HLE and FPE control-oriented and physics-based models will assist with control development and validation. Foremost, an improved model is necessary to capture the behavior of loss parameter θ in Chapters III and IV. A more accurate estimate of θ would enhance the behavior of both the feedback control law and the FPE reference governor by reducing overall model uncertainty. Future investigations should correlate θ to clearance, load, and speed. For an FPE control-oriented model, the use of a pressure limited heat addition phase rather than constant volume combustion may also improve estimation accuracy.

For both FPE and HLE operation, it would be interesting to taking advantage of truly separate and individual cylinder control. As a hypothetical example, by adjusting fuel and load to each cylinder independently, an HLE or FPE could expand the load range of HCCI by operating most cylinders at low load with HCCI and one at high load with more conventional combustion. The adaptive cylinder balancing structure can also adjust for cylinder-to-cylinder variations in an FPE, where any difference in performance can lead to more severe consequences.

In a series configuration, the engine is removed from road loads. It may be possible to use the proposed HLE and FPE control structures to estimate on-line losses. By applying parameter learning techniques, a controller could intelligently update open-loop fuel maps using on-line results from the adaptive control algorithms presented in this paper.

By linearizing the FPE model, we introduce error into the system. Deriving a Lyapunov control function does not require linearization and as a result may be more accurate. As an additional benefit, a Lyapunov-based control law would facilitate the creation of an output maximal admissible set and reduce the on-line computational

intensity of a reference governor. Additionally, reference governor techniques can be used as saturation protection for various actuators on the HLE and FPE.

An HLE or FPE supervisory controller is necessary to facilitate a vehicle level study over various drive cycles. Because the energy storage of a hydraulic accumulator is small, stochastic methods would be helpful to appropriately utilize each engine. It would also be useful to incorporate FPE clearance control into the supervisory controller to ensure power demand is smooth, reduces disturbances, and helps maintain an appropriate clearance.

The stability analysis in Chapter IV is specifically for a four-stroke, dual-piston FPE. After altering the geometry, incorporating a scavenging process, and adding a bounce chamber, the same framework can easily comment on the stability of other FPE configurations.

To enable FPE turbocharging, it is crucial to explore the robust control of clearance height in the presence of intake and exhaust pressure transients. Because intake pressures also change FPE frequency, a controller can utilize a variable geometry turbo to manage engine speed and power.

While the proposed reference governor method is an effective means of maximizing β, the combination of a Newton-type solver with a bisection search has a potentially high computational cost. Before application on FPE hardware, an additional study is necessary to investigate computational latency and algorithms that are more efficient. Other root finding methods may also improve computation time or accuracy.

BIBLIOGRAPHY

BIBLIOGRAPHY

[1] PAJ Achten. A Review of Free Piston Engine Concepts. *SAE Paper 941776*, 1994.

[2] PAJ Achten, JPJ van den Oever, Jeroen Potma, and GEM Vael. Horsepower with brains: The design of the Chiron free piston engine. *SAE Paper 2000-01-2545*, 2000.

[3] US Energy Information Administration. Annual energy outlook 2011 with projections to 2035. *DOE/EIA-0383(2011)*, 2011.

[4] US Environmental Protection Agency. Clean automotive technology 2006 progress report. *EPA-420-R-06-008*, 2006.

[5] H.T. Aichlmayr. *Design Considerations , Modeling , and Analysis of Micro-Homogeneous Charge Compression Ignition Combustion Free-Piston Engines.* PhD thesis, The University of Minnesota, 2002.

[6] Dennis N. Assanis and John B. Heywood. Development and use of a computer simulation of the turbocompounded diesel system for engine performance and component heat transfer studies. *SAE Paper 860329*, 1986.

[7] CM Atkinson and Sorin Petreanu. Numerical simulation of a two-stroke liner engine-alternator combination. *SAE Paper 1999-01-0921*, 1999.

[8] Norman H. Beachley and Frank J. Fronczak. Design of a Free-Piston Engine-Pump. *SAE Paper 921740*, 1992.

[9] Miriam Bergman and Valeri I Golovitchev. CFD Modeling of a Two-Stroke Free Piston Energy Converter using Detailed Chemistry. *SAE Paper 2005-24-074*, 2005.

[10] R. Bitmead. Persistence of excitation conditions and the convergence of adaptive schemes. *IEEE Transactions on Information Theory*, 30(2):183–191, March 1984.

[11] A. T. Braun and P. H. Schweitzer. The Braun Linear Engine. *SAE Paper 730185*, 1973.

[12] Matthew Brusstar and Charles L Gray Jr. Design , Development and Testing of Multi-Cylinder Hydraulic Free-Piston Engines Reprinted From : Advanced Hybrid Vehicle Powertrains 2005. *SAE Paper 2005-01-1167*, 2005.

[13] A. Cameron. *Basic Lubrication Theory*. Ellis Horwood Ltd, 3rd editio edition, 1981.

[14] D. F. Caris and E. E. Nelson. A New Look at High Compression Engines. *SAE Transactions*, 67:112–124, 1959.

[15] C Carlson and L Peng. Air charging system for an opposed piston opposed cylinder free piston engine. *US Patent 6,957,632*, 2005.

[16] Douglas Carter and Edward Wechner. The Free Piston Power Pack : Sustainable Power for Hybrid Electric Vehicles. *SAE Paper 2003-01-3277*, 2003.

[17] Chia-Jui Chiang, Jing-Long Yang, Shao-Ya Lan, Tsung-Wei Shei, Wen-Shu Chiang, and Bo-Liang Chen. Dynamic modeling of SI/HCCI free-piston engine generators. In *2011 6th IEEE Conference on Industrial Electronics and Applications*, pages 1615–1620. Ieee, June 2011.

[18] Nigel N. Clark and Subhash Nandkumar. Fundamental Analysis of a Linear Two-Cylinder Internal Combustion Engine. *SAE Paper 982692*, (724), 1998.

[19] Z. S. Filipi and D. N. Assanis. A Nonlinear, Transient, Single-Cylinder Diesel Engine Simulation for Predictions of Instantaneous Engine Speed and Torque. *Journal of Engineering for Gas Turbines and Power*, 123(4):951, 2001.

[20] Zoran Filipi and Y. J. Kim. Hydraulic Hybrid Propulsion for Heavy Vehicles: Combining the Simulation and Engine-In-the-Loop Techniques to Maximize the Fuel Economy and Emission Benefits. In *Oil & Gas Science and Technology Revue de lInstitut Français du Pétrole*, volume 65, pages 155–178, September 2009.

[21] Jakob Fredriksson, Miriam Bergman, Valeri I Golovitchev, and Ingemar Denbratt. Modeling the Effect of Injection Schedule Change on Free Piston Engine Operation. *SAE Paper 2006-01-0449*, 2006.

[22] Jakob Fredriksson and Ingemar Denbratt. Simulation of a Two-Stroke Free Piston Engine. *SAE 2004-01-1871*, 2004.

[23] Elmer G. Gilbert and Ilya Kolmanovsky. Nonlinear control of discrete-time linear systems with state and control constraints: a reference governor with global convergence properties. *Proceedings of 1994 33rd IEEE Conference on Decision and Control*, pages 144–149, 1994.

[24] Elmer G. Gilbert and Ilya Kolmanovsky. Discrete-time reference governors for systems with state and control constraints and disturbance inputs. In *Proceedings of the 34th IEEE Conference on Decision and Control*, number December, pages 1189–1194, 1995.

[25] Elmer G. Gilbert and Ilya Kolmanovsky. Set-point control of nonlinear systems with state and control constraints: A Lyapunov-function, Reference-Governor approach. In *Proceedings of the 38th Conference on Decisions and Control*, volume 2507, 1999.

[26] Elmer G. Gilbert and Ilya Kolmanovsky. Nonlinear tracking control in the presence of state and control constraints: a generalized reference governor. *Automatica*, 38(12):2063–2073, December 2002.

[27] Elmer G. Gilbert, Ilya Kolmanovsky, and Kok Tin Tan. Discrete-time reference governors and the nonlinear control of systems with state and control constraints. *International Journal of Robust and Nonlinear Control*, 5(5):487–504, 1995.

[28] Elmer G Gilbert and Kok Tin Tan. Linear Systems with State and Control Constraints : The Theory and Application of Maximal Output Admissible Sets. *IEEE Transactions on Automatic Control*, 36(9):1008–1020, September 1991.

[29] Scott Goldsborough and Peter Van Blarigan. A Numerical Study of a Free Piston IC Engine Operating on Homogeneous Charge Compression Ignition Combustion. *SAE Paper 1999-01-0619*, 1999.

[30] Scott Goldsborough and Peter Van Blarigan. Optimizing the Scavenging System for a Two-Stroke Cycle , Free Piston Engine for High Efficiency and Low Emissions : A Computational Approach. *SAE Paper 2003-01-0001*, 2003.

[31] G. C. Goodwin and K. S. Sin. *Adaptive Filtering Prediction and Control*. Prentice-Hall, 1984.

[32] Charles L Gray Jr. Fully-controlled, free-piston engine. *US Patent 6,582,204*, 2003.

[33] Charles L Gray Jr. Fully-controlled, free-piston engine. *US Patent 6,652,247*, 2003.

[34] Charles L Gray Jr. QUASI FREE PISTON ENGINE. *US Patent 8,104,436*, 2011.

[35] Charles L Gray Jr, AJ Moskalik, MJ Brusstar, DK Gill, K Fuqua, and CD Moffat. High-efficiency, large angle, variable displacement hydraulic pump/motor. *US Patent 7,014,429*, 2006.

[36] JW Grizzle, KL Dobbins, and JA Cook. Individual cylinder air-fuel ratio control with a single EGO sensor. *IEEE Transactions on Vehicular Technology*, 40(1):280–286, February 1991.

[37] Feng Guo, Ying Huang, Chang Lu Zhao, Jia Liu, and Zhen Yu Zhang. Study on Operation Control Strategy of Single Piston Hydraulic Free-Piston Diesel Engine. *Applied Mechanics and Materials*, 128-129:1044–1049, October 2011.

[38] Feng Guo, Chang-lu Zhao, Ying Huang, and Jia Liu. Study on Piston Motion Control Strategy of Single Piston Hydraulic Free-piston Engine. In *2012 Second International Conference on Intelligent System Design and Engineering Application*, pages 1140–1143. Ieee, January 2012.

[39] Feng Guo, Chang-lu Zhao, Ying Huang, and Wei Wu. Experimental Study on Hydraulic Free-Piston Diesel Engine. *2011 International Conference on Computer Distributed Control and Intelligent Environmental Monitoring*, pages 786–792, February 2011.

[40] Rohit Gupta, Ilya V Kolmanovsky, Yan Wang, and Dimitar P Filev. Onboard learning-based fuel consumption optimization in series hybrid electric vehicles. In *American Control Conference (ACC)*, pages 1308–1313, 2012.

[41] J. Heywood. *Internal Combustion Engine Fundamentals*. McGraw Hill, 1988.

[42] A Hibi and Y Hu. A Prime Mover Consists of a Free Piston Internal Combustion Hydraulic Power Generator and a Hydraulic Motor. *SAE Paper 930313*, 1993.

[43] A Hibi and T Ito. Fundamental test results of a hydraulic free piston. *Proceedings of the Institution of Mechanical Engineers, Part D: Journal of Automobile Engineering*, 218(May):1149–1157, 2004.

[44] P Hofbauer. Internal combustion engine with a single crankshaft and having opposed cylinders with opposed pistons. *US Patent 6,170,443*, 2001.

[45] P HOFBAUER. OPPOSED PISTON OPPOSED CYLINDER FREE PISTON ENGINE. *U.S. Patent 6,953,010*, 2005.

[46] P Hofbauer, L Peng, A Tusinean, and K Fuqua. Air scavenging for an opposed piston opposed cylinder free piston engine. *US Patent 6,941,904*, 2005.

[47] Gunter F. Hohenberg. Advanced approaches for heat transfer calculations. *SAE Paper 790825*, 1979.

[48] J. Hu, W. Wu, S. Yuan, and C. Jing. On-off motion of a hydraulic free-piston engine. *Proceedings of the Institution of Mechanical Engineers, Part D: Journal of Automobile Engineering*, 227(3):323–333, August 2012.

[49] Jibin Hu, Wei Wu, Shihua Yuan, and Chongbo Jing. Mathematical modelling of a hydraulic free-piston engine considering hydraulic valve dynamics. *Energy*, 36(10):6234–6242, October 2011.

[50] Ling Huang. An Opposed-Piston Free-Piston Linear Generator Development for HEV. *SAE Paper 2012-01-1021*, 2012.

[51] Tor Arne Johansen, Olav Egeland, Erling Aa. Johannessen, and Rolf Kvamsdal. Free-piston diesel engine dynamics and control. *Proceedings of the 2001 American Control Conference*, 6:4579–4584, 2001.

[52] Tor Arne Johansen, Olav Egeland, Erling Aa. Johannessen, and Rolf Kvamsdal. Free-piston diesel engine timing and control-toward electronic cam-and crankshaft. *Control Systems Technology*, 10(2):177–190, 2002.

[53] Tor Arne Johansen, Olav Egeland, Erling Aa. Johannessen, and Rolf Kvamsdal. Dynamics and control of a free-piston diesel engine. *TRANSACTIONS-AMERICAN SOCIETY OF MECHANICAL ENGINEERS JOURNAL OF DYNAMIC SYSTEMS MEASUREMENT AND CONTROL*, 125(3):468–474, 2003.

[54] Rajit Johri and Zoran Filipi. Low-cost pathway to ultra efficient city car: Series hydraulic hybrid system with optimized supervisory control. *SAE Paper 2009-24-0065*, 2009.

[55] Uros Kalabic, Ilya Kolmanovsky, Julia Buckland, and Elmer Gilbert. Reference and extended command governors for control of turbocharged gasoline engines based on linear models. *2011 IEEE International Conference on Control Applications (CCA)*, pages 319–325, September 2011.

[56] Petros Kapasouris, Michael Athans, and Gunter Stein. Design of feedback control systems for stable plants with saturating actuators. In *Proceedings of the 27th Conference on Decision and Control*, number December, 1988.

[57] Hassan K. Khalil. *Nonlinear Systems*. Prentice Hall, vol. 3 edition, 2002.

[58] Nick J Killingsworth, Salvador M Aceves, Daniel L Flowers, and Miroslav Krsti. Extremum Seeking Tuning of an Experimental HCCI Engine Combustion Timing Controller. In *Proceedings of the 2007 American Control Conference*, pages 3665–3670, 2007.

[59] A. P. Kleemann, J.C. Dabadie, and S. Henriot. Computational Design Studies for a Free Piston Engine Prototype. *SAE Paper 2004-01-2928*, 2004.

[60] Ilya Kolmanovsky and Jing Sun. Parameter governors for discrete-time nonlinear systems with pointwise-in-time state and control constraints. *Automatica*, 42(5):841–848, May 2006.

[61] D. A. Kouremenos, C. D. Rakopoulos, and K. G. Kotsos. A stochasticexperimental investigation of the cyclic pressure variation in a di singlecylinder diesel engine. *International Journal of Energy Research*, 16:865–877, 1992.

[62] Martti Larmi, Sten Isaksson, Seppo Tikkanen, and Mika Lammila. Performance Simulation of a Compression Ignition Free Piston Engine. *SAE Paper2001-01-0280*, 2001.

[63] Ke Li, Ali Sadighi, and Zongxuan Sun. Motion control of a hydraulic free-piston engine. In *American Control Conference (ACC)*, 2012.

[64] Ke Li, Wilson Santiago, and ZX Sun. Modeling of a two-stroke free-piston engine with hcci combustion. In *Proceedings of ASME Dynamic Systems and Control Conference*, 2010.

[65] Ke Li and Zongxuan Sun. Modeling and control of a hydraulic free piston engine with HCCI combustion. In *Proceedings of the 52nd National Conference on Fluid Power*, 2011.

[66] Ke Li and Zongxuan Sun. Stability Analysis of a Hydraulic Free Piston Engine With HCCI Combustion. *ASME 2011 Dynamic Systems and Control Conference and Bath/ASME Symposium on Fluid Power and Motion Control, Volume 2*, pages 655–662, 2011.

[67] Q Li, J Xiao, and Z Huang. PARAMETRIC STUDY OF A FREE PISTON LINEAR ALTERNATOR. *International Journal of Automotive Technology*, 11(1):111–117, 2010.

[68] R. Mikalsen and a.P. Roskilly. A review of free-piston engine history and applications. *Applied Thermal Engineering*, 27(14-15):2339–2352, October 2007.

[69] R. Mikalsen and a.P. Roskilly. The design and simulation of a two-stroke free-piston compression ignition engine for electrical power generation. *Applied Thermal Engineering*, 28(5-6):589–600, April 2008.

[70] R. Mikalsen and a.P. Roskilly. A computational study of free-piston diesel engine combustion. *Applied Energy*, 86(7-8):1136–1143, July 2009.

[71] R. Mikalsen and a.P. Roskilly. Coupled dynamicmultidimensional modelling of free-piston engine combustion. *Applied Energy*, 86(1):89–95, January 2009.

[72] R. Mikalsen and a.P. Roskilly. The control of a free-piston engine generator. Part 1: Fundamental analyses. *Applied Energy*, 87(4):1273–1280, April 2010.

[73] R. Mikalsen and a.P. Roskilly. The control of a free-piston engine generator. Part 2: Engine dynamics and piston motion control. *Applied Energy*, 87(4):1281–1287, April 2010.

[74] R. Mikalsen, E. Jones, and a.P. Roskilly. Predictive piston motion control in a free-piston internal combustion engine. *Applied Energy*, 87(5):1722–1728, May 2010.

[75] Robert H. Miller, Ilya Kolmanovsky, Elmer G. Gilbert, and Peter D. Washabaugh. Control of Constrained Nonlinear Systems . *Control System Magazine*, pages 23–32, 2000.

[76] M. Morari and E. Zafiriou. *Robust Process Control*. Prentice-Hall, Englewood Cliffs, NJ, 1989.

[77] National Research Counsel. *Review of the Research Program of the Partnership for a New Generation of Vehicles*. National Academy Press, seventh re edition, 2001.

[78] F Ostman and HT Toivonen. Adaptive cylinder balancing of internal combustion engines. *IEEE Transactions on Control Systems Technology*, 19(4):782–791, July 2011.

[79] R. P. Pescara. Motor Compressor Apparatus. *US Patent 1,657,641*, 1928.

[80] Sorin Petreanu. *CONCEPTUAL ANALYSIS OF A FOUR-STROKE LINEAR*. PhD thesis, , 2001.

[81] D. Popovic, M. Jankovic, S. Magner, and A. R. Teel. Extremum seeking methods for optimization of variable cam timing engine operation. *IEEE Transactions on Control Systems Technology*, 14(3):398–407, May 2006.

[82] C.D Rakopoulos, D.C Rakopoulos, E.G Giakoumis, and D.C Kyritsis. Validation and sensitivity analysis of a two zone Diesel engine model for combustion and emissions prediction. *Energy Conversion and Management*, 45(9-10):1471–1495, June 2004.

[83] Hao Ling Ren, Hai Bo Xie, and Hua Yong Yang. Dynamic Analysis of the Single Piston Hydraulic Free Piston Engine. *Applied Mechanics and Materials*, 48-49:455–460, February 2011.

[84] Sohair F. Rezeka and Naeim A. Henein. A New Approach to Evaluate Instantaneous Friction and Its Components in Internal Combustion Engines. *SAE Paper 840179*, 1984.

[85] Ali Sadighi, Ke Li, and Zongxuan Sun. A Comparative Study of Permanent Magnet Linear Alternator and Hydraulic Free-Piston Engines. *ASME 2011 Dynamic Systems and Control Conference and Bath/ASME Symposium on Fluid Power and Motion Control, Volume 1*, pages 137–144, 2011.

[86] Yan Shi and Si Qin Chang. Research on Design and Testing of a Novel Power Source for Hybrid Vehicles. *Applied Mechanics and Materials*, 29-32:2285–2289, August 2010.

[87] Ehab Shoukry, Samuel Taylor, Nigel N. Clark, and Parviz Famouri. Numerical Simulation for Parametric Study of a Two-Stroke Direct Injection Linear Engine Reprinted From : Engine Modeling Techniques : SI and Diesel. *SAE Paper 2002-01-1739*, (724), 2002.

[88] Jean-Jacques E. Slotine and Weiping Li. *Applied Nonlinear Control*. Prentice-Hall, 1991.

[89] O. J. Smith. A Controller to Overcome Dead Time. *ISA J.*, 6:28–33, 1959.

171

[90] JHE Somhorst and PAJ Achten. The Combustion Process in a DI-Diesel Hydraulic Free Piston Engine. *SAE Paper 960032*, 1996.

[91] J. C. Spall. Stochastic optimization, stochastic approximation and simulated annealing. *Wiley Encyclopedia of Electrical and Electronics Engineering*, 1999.

[92] Jing Sun and Ilya Kolmanovsky. Load governor for fuel cell oxygen starvation protection: a robust nonlinear reference governor approach. *IEEE Transactions on Control Systems Technology*, 13(6):911–920, November 2005.

[93] A. R. Teel. Lyapunov methods in nonsmooth optimization. Part II: Persistently exciting finite differences. In *Proceedings of the 39th IEEE Conference on Decision and Control*, pages 118–123, 2000.

[94] Chun Lai Tian, Hui Hua Feng, and Zheng Xing Zuo. Oscillation Characteristic of Single Free Piston Engine Generator. *Advanced Materials Research*, 383-390:1873–1878, November 2011.

[95] Chun Lai Tian, Hui Hua Feng, and Zheng Xing Zuo. Load Following Controller for Single Free-Piston Generator. *Applied Mechanics and Materials*, 157-158:617–621, February 2012.

[96] Seppo Tikkanen, Mika Lammila, Mika Herranen, and Matti Vilenius. First Cycles of the Dual Hydraulic Free Piston Engine. *SAE Paper 2000-01-2546*, 2000.

[97] Seppo Tikkanen and Matti Vilenius. Control of dual hydraulic free piston engine. *International Journal of Vehicle Autonomous Systems*, 4(1), 2006.

[98] Csaba Tóth-Nagy. *Linear Engine Development for Series Hybrid Electric Vehicles*. PhD thesis, West Virginia University, 2004.

[99] Csaba Tóth-Nagy and Nigel N. Clark. The Linear Engine in 2004. *SAE 2005-01-2140*, 2005.

[100] A. F. Underwood. The GMR 4-4 Hyprex Engine - A Concept of the Free-Piston Engine for Automotive Use. *SAE Paper 570032*, 1957.

[101] Ardalan Vahidi, Ilya Kolmanovsky, and Anna Stefanopoulou. Constraint Handling in a Fuel Cell System: A Fast Reference Governor Approach. *IEEE Transactions on Control Systems Technology*, 15(1):86–98, January 2007.

[102] Peter Van Blarigan, Nicholas Paradiso, and Scott Goldsborough. Homogeneous Charge Compression Ignition with a Free Piston : A New Approach to Ideal Otto Cycle Performance. *SAE Paper 982484*, (724), 1998.

[103] M. J. van Nieuwstadt and I. V. Kolmanovsky. Detecting and Correcting Cylinder Imbalance in Direct Injection Engines. *Journal of Dynamic Systems, Measurement, and Control*, 123(September):413–424, 2001.

[104] N. Watson, A. D. Pilley, and M. Marzouk. A Combustion Correlation for Diesel Engine Simulation. *SAE Paper 800029*, 1980.

[105] Avishai Weiss, Ilya Kolmanovsky, and Walter Merrill. Incorporating Risk into Control Design for Emergency Operation of Turbo-Fan Engines. *Infotech@Aerospace*, (March):1–13, 2011.

[106] Benjamin E. Wylie, Victor Lyle Streeter, and Lisheng Suo. *Fluid Transients in Systems*. Prentice-Hall, 1993.

[107] Bi Zhong Xia, Gang Su, Hai Bo Xie, and Hua Yong Yang. Analysis on Energy-Flow of a Bipropellant-Powered Hydraulic Free Piston Engine. *Applied Mechanics and Materials*, 121-126:3102–3106, October 2011.

[108] Bi Zhong Xia, Gang Su, Hai Bo Xie, and Hua Yong Yang. Study on the Starting Process Driven by Accumulator of a Hydraulic Free Piston Engine. *Applied Mechanics and Materials*, 121-126:3092–3096, October 2011.

[109] Jin Xiao, Qingfeng Li, and Zhen Huang. Motion characteristic of a free piston linear engine. *Applied Energy*, 87(4):1288–1294, April 2010.

[110] Shuaiqing Xu, Yang Wang, Tao Zhu, Tao Xu, and Chengjun Tao. Numerical analysis of two-stroke free piston engine operating on HCCI combustion. *Applied Energy*, 88(11):3712–3725, November 2011.

[111] Zhaoping Xu and Siqin Chang. Prototype testing and analysis of a novel internal combustion linear generator integrated power system. *Applied Energy*, 87(4):1342–1348, April 2010.

[112] Shihua Yuan and Wei Wu. Simulation study of a two-stroke Single Piston Hydraulic Free Piston Engine. *2008 Asia Simulation Conference 7th International Conference on System Simulation and Scientific Computing*, pages 1244–1249, 2008.

[113] Kevin Zaseck, Matthew Brusstar, and Dennis Assanis. Design and Modeling of a Novel Internal Combustion Engine with Direct Hydraulic Power Take-off. *SAE Paper 2013-01-1733*, 2013.

[114] Kevin Zaseck, Ilya Kolmanovsky, and Matthew Brusstar. Adaptive Control Approach for Cylinder Balancing in a Hydraulic Linear Engine. In *American Control Conference (ACC)*, 2013.

[115] Kevin Zaseck, Ilya Kolmanovsky, and Matthew Brusstar. Extremum Seeking Algorithm to Optimize Fuel Injection in a Hydraulic Linear. *Proceedings of the 7th IFAC Symposium on Advances in Automotive Control2*, 2013.

[116] Zhenfeng Zhao, Fujun Zhang, Ying Huang, and Changlu Zhao. An experimental study of the cycle stability of hydraulic free-piston engines. *Applied Thermal Engineering*, 54(2):365–371, May 2013.

[117] Zhenfeng Zhao, Fujun Zhang, Ying Huang, Changlu Zhao, and Feng Guo. An experimental study of the hydraulic free piston engine. *Applied Energy*, 99:226–233, November 2012.

[118] Zhenfeng Zhao, Fujun Zhang, Changlu Zhao, and Yu Chen. Modeling and Simulation of a Hydraulic Free Piston Diesel Engine. *SAE Paper 2008-01-1528*, 2008.

[119] Y H Zweiri, J F Whidborne, and L D Seneviratne. Dynamic simulation of a single-cylinder diesel engine including dynamometer modelling and friction. *Proceedings of the Institution of Mechanical Engineers, Part D: Journal of Automobile Engineering*, 213(4):391–402, January 1999.

[120] Y. H. Zweiri, J. F. Whidborne, and L. D. Seneviratne. Instantaneous friction components model for transient engine operation. *Proceedings of the Institution of Mechanical Engineers, Part D: Journal of Automobile Engineering*, 214(D):809–824, 2000.